Development of Epicardial Devices for the Support of Cardiac Function in Patients with Myocardial Infarction and Heart Failure

Dissertation

der Mathematisch-Naturwissenschaftlichen Fakultät

der Eberhard-Karls Universität Tübingen

zur Erlangung des Grades eines

Doktors der Naturwissenschaften

(Dr. rer. nat.)

vorgelegt von

Björn Hofmann

aus Gotha

Tübingen

2020

Gedruckt mit Genehmigung der Mathematisch-Naturwissenschaftlichen Fakultät der Eberhard-Karls Universität Tübingen.

Tag der mündlichen Qualifikation:	17.06.2020
Dekan:	Prof. Dr. Wolfgang Rosenstiel
1. Berichterstatter:	Prof. Dr. Katja Schenke-Layland
2. Berichterstatter:	Prof. Dr. Garry Duffy

So eine Arbeit wird eigentlich nie fertig,

man muss sie für fertig erklären,

wenn man nach der Zeit und den Umständen

das Möglichste getan hat.

(Johann Wolfgang von Goethe)

Table of content

Abstract

The administration of biomaterial-based therapies to the infarcted ventricle wall by currently available approaches is often associated with several issues impairing the final performance of the applied therapeutic agents. As the epicardium has been identified as region with vast regenerative potential, it is supposed to represent a reasonable target for the support of the weakened myocardium after a myocardial infarct. However, targeted local delivery of biomaterial-based therapies to the dynamic epicardial heart surface in a non-surgical procedure represents a remarkable challenge due to limitations imposed by the biomaterials and regenerative agents, especially in case of stem cell technologies. Hence, this PhD thesis aims to address current limitations for the delivery of biomaterials to well-defined regions on the epicardium by developing novel advanced application strategies for biomaterial-based therapies to the epicardial heart surface. These novel delivery devices intend to provide the opportunity to better exploit the potential of applied therapeutic agents and reduce application associated deleterious effects.

Both developed devices SPREADS and EpiPAD have successfully shown its capacity to accomplish the atraumatic site-specific administration of a hydrogel- and patch-based biomaterial to the epicardial heart surface via a minimal-invasive, closed chest intervention, respectively. Pre-clinical efficacy assessment of SPREADS demonstrated a significant improvement in %LVEF 14 days post-treatment when clinical gold standard treatment (GS) was compared to treatment groups GS + SPREADS + Gel with and without cells ($p \leq 0.001$). Obtained results suggest that neither the infarct quality nor the vascularisation was the mechanism of action involved in the determined improvement of cardiac function. Since SPREADS is potentially compatible with a myriad of new or previously developed biomaterial hydrogels, it represents a unique opportunity to conquer translational obstacles accompanied with the delivery of hydrogels to the heart. EpiPAD's inflatable pad may moreover offer the potential to additionally provide acute assistance to the infarcted ventricle wall by epicardial augmentation. Thus, EpiPAD may enable in a multimodal approach apart from biological support additionally active mechanical support to the weakened myocardium.

Zusammenfassung

Die finale Effizienz von Biomaterial-basierten Therapien zur Behandlung des Herzens nach einem Infarkt ist zumeist beeinträchtigt durch verschiedene mit aktuellen Verabreichungsmethoden verbundenen Einschränkungen. Das Epikard stellt auf Grund dessen enormen regenerativen Potentials ein plausibles Ziel für die Behandlung des geschwächten Myokards nach einem Infarkt dar. Allerdings ist die zielgerichtete lokale Applikation von Biomaterial-basierten Therapeutika in einem nicht-chirurgischen Eingriff auf die dynamische epikardiale Herzoberfläche eine außerordentliche Herausforderung wegen der durch die Biomaterialien und Therapeutika bedingten Einschränkungen, speziell bei Stammzell-basierten Strategien. Ziel dieser Arbeit war es daher, aktuelle Einschränkungen für die Verabreichung von Biomaterial-basierten Therapeutika zu definierten Bereichen auf der epikardialen Herzoberfläche durch die Entwicklung neuartiger Applikationsstrategien zu beheben. Mittels dieser neuen Applikationssysteme soll das Potential der verabreichten Therapeutika besser ausgeschöpft sowie applikationsbedingte Komplikationen reduziert werden können.

Beide entwickelten Implantate SPREADS und EpiPAD haben jeweils erfolgreich unter Beweis gestellt, minimal-invasiv bei geschlossen Brustkorb Hydrogel- beziehungsweise Patch-basierte Biomaterialien in einem atraumatischen Eingriff zielgerichtet auf die epikardiale Herzoberfläche applizieren zu können. In vorklinischen Versuchen konnte eine signifikante Verbesserung der %LVEF 14 Tage nach Verabreichung von SPREADS mit einem azellulären beziehungsweise zellulären Hydrogel im Vergleich zum klinischen Goldstandard erzielt werden ($p \leq 0.001$). Die Ergebnisse deuten darauf hin, dass die Verbesserung der Herzleistung weder durch Veränderungen des Infarktgewebes noch durch Vaskularisation hervorgerufen wurde. SPREADS‘ potenzielle Kompatibilität mit einer Vielzahl von neu sowie bereits entwickelten Hydrogelen bietet zudem die einzigartige Gelegenheit, Applikations-assoziierte Hürden bei der Translation von kardialen Hydrogelen in die Klinik zu überwinden. EpiPAD’s inflatierbares Kissen bietet weiterhin die Möglichkeit, die infarzierte Herzwand durch epikardiale Augmentation akut zu unterstützen. Folglich könnte EpiPAD neben der biologischen Unterstützung in einem multimodalen Ansatz das geschwächte Myokardium zudem aktiv mechanisch entlasten.

Abbreviations

A	apical
ACCF	American College of Cardiology Foundation
ACE	Angiotensin-converting enzyme
ADSCs	adipose derived stem cells
AHA	American Heart Association
AM	adjacent myocardium
AMCARE	Advanced Materials for CArdiac Regeneration
ARB	Angiotensin II receptor blocker
AV	atrioventricular
B	basal
BEAT	Biventricular Epicardial Augmentation Technology
BSA	Bovine Serum Albumin
BZ	border zone
c-ADSCs	cardiopoietic adipose derived stem cells
C-CURE	Cardiopoietic stem Cell therapy in heart failURE
CEs	cholesterol esters
CHDs	coronary heart diseases
CHF	congestive heart failure
CMs	cardiomyocytes
CO	cardiac output
CO_2	carbon dioxide
$CoCl_2$	cobalt chloride
CRT	cardiac resynchronisation therapy
CT	computed tomography
CVDs	cardiovascular diseases

DAB	3,3'-diaminobenzidine
DABCO	1,4-diazabicyclo[2,2,2]octane
DAMPs	danger associated molecular patterns
DCC	Direct Cardiac Compression
DI	deionized
DMSO	dimethyl sulfoxide
DNA	deoxyribonucleic acid
ECG	electrocardiography
ECM	extracellular matrix
EDV	end diastolic volume
EF	ejection fraction
EpiPAD	Epicardial Patch Administration Device
ESV	end systolic volume
FDA	Food and Drug Administration
FS	fractional shortening
GAGs	glycosaminoglycans
GFs	growth factors
GS	gold standard
H&E	Haematoxylin and Eosin
H_2O_2	hydrogen peroxide
HA	hyaluronic acid
HaCaT	human keratinocyte cell line
HF	heart failure
HR	heart rate
HRP	horse radish peroxidase
ICD	implantable cardioverter defibrillator

ICD-10	International Classification of Diseases, 10th Revision
iCFs	immortalised cardiac fibroblasts
IL	interleukin
IZ	infarct zone
LA	left atrium
LAD	the left anterior descending
LDI	lysine diisocyanate
LOX	lysyl oxidase
LV	left ventricle
LVADs	Left Ventricular Assist Devices
LVEDd	left ventricular end diastolic diameter
LVEDP	left ventricle end-diastolic pressure
LVEDV	left ventricle end diastolic volume
LVEF	left ventricular ejection fraction
LVESd	left ventricular end systolic diameter
m_0	initial mass
MAP	mean arterial pressure
MI	myocardial infarction
Mi with i = 1-3	mid ventricular
MMPs	matrix metalloproteinases
m_t	mass at time *t*
NHANES	National Health and Nutrition Examination Survey
NYHA	New York Heart Association
P	intraventricular pressure
Pal-HA	palmitoyl-hyaluronan
PBS	phosphate buffered saline

PCI	percutaneous coronary intervention
PEG	polyethylene glycol
PET	polyethylene terephthalate
PEU	poly(ester urethane)
PEUU	poly(ester urethane urea)
PH	*h*ydroxyphen*yl*
PLA-co-PCL	poly(L-lactide-co-ε-caprolactone)
PMMA	poly(methyl methacrylate)
PRRs	pattern recognition receptors
PTFE	polytetrafluoroethylene
PU	polyurethane
Q	swelling ratio
R	curvature radius of the ventricle
RA	right atrium
RAAS	Renin-Angiotensin-Aldosterone system
RCSI	*Royal College of Surgeons in Ireland*
RGD	arginylglycylaspartic acid
ROS	reactive oxygen species
RV	right ventricle
SA	sinoatrial
SEM	scanning electron microscopy
SNS	sympathetic nervous system
SPREADS	Surface PRone EpicArdial Delivery System
SV	stroke volume
t	time
T	tension in the myocardial wall

TAHs	Total Artificial Hearts
TGF	transforming growth factor
TNF	tissue necrosis factor
$t_{Ventricle}$	thickness of the ventricular wall
VADs	Ventricular Assist Devices
VEGF	vascular endothelial growth factor
W_t	weight loss at time t

List of Figures

List of Tables

Publication and Patents

Paper

1. Eimear B. Dolan* and **Björn Hofmann***, M. Hamman de Vaal, Gabriella Bellavia, Stefania Straino, Lenka Kovarova, …, Katja Schenke-Layland, Peter Dockery, Bruce P. Murphy, Helena M. Kelly, Stephen Wildhirt, Garry P. Duffy. *A bioresorbable biomaterial carrier and passive stabilization device to improve heart function post-myocardial infarction.* Materials science and engineering: C, 2019. **103**: p. 109751. **(Accepted 14th May 2019)**

   *both authors contributed equally to this work and are co-first authors

Patents

2. Maier, A, **Hofmann, B**, de Vaal, M H, Wildhirt, S M. *Herzunterstützungsvorrichtung mit strukturierter Oberfläche.* DE102018200974 A1, 2019.
3. Wildhirt, S M, de Vaal, M H, **Hofmann, B**, Maier, A. *Collapsible myocardial patch.* CN109718196A, 2019.
4. Wildhirt, S M, de Vaal, M H, **Hofmann, B**, Maier, A. *Collapsible myocardial patch.* EP 3476385 A1, 2019.
5. Wildhirt, S M, Maier, A, Muller, K W, **Hofmann, B**. *Implantierbare Vorrichtung zur ortsgenauen Zuführung und Applikation von Substanzen in das Perikard oder auf die Herzoberfläche.* EP 3348235 A1, 2018.
6. Wildhirt, S M, Maier, A, Muller, K W, **Hofmann, B**. *Implantable device for precise supply and application of substances to the pericardial sac or the surface of the heart.* EP 3115023 B1, 2017.
7. Wildhirt, S M, Maier, A, Muller, K W, **Hofmann, B**. *Implantable device for the locationally accurate delivery and administration of substances into the pericardium or onto the surface of the heart.* US 2017/0007403 A1, 2017.
8. Wildhirt, S M, Muller, K W, Maier, A, **Hofmann, B**. *Implantierbare Vorrichtung zur ortsgenauen Zuführung und Applikation von Substanzen in das Perikard oder auf die Herzoberfläche.* DE 10 2015 212 699 A1, 2017.

Contributions

The following Table outlines my contribution to the published manuscript with the title *A bioresorbable biomaterial carrier and passive stabilization device to improve heart function post-myocardial infarction* and to all patents as specified in the previous chapter.

Nr	**Published Yes/No**	**Author position**	**Scientific ideas %**	**Data generation %**	**Analysis & interpretation %**	**Paper writing %**
1	Yes	1*	40	40	40	40
2	Yes	2	30	70	80	10
3	Yes	3	40	85	90	10
4	Yes	3	40	85	90	10
5	Yes	4	40	75	80	15
6	Yes	4	40	75	80	15
7	Yes	4	40	75	80	15
8	Yes	4	40	75	80	15

*both authors contributed equally to this work and are co-first authors

1 Introduction

This PhD thesis deals with the controlled application of biomaterial-based therapies to the weakened myocardium after a myocardial infarct to encourage the damaged tissue to regenerate instead of remodelling into non-contractile scar tissue. The research focuses on the development of novel advanced administration strategies with the purpose to facilitate targeted local delivery of hydrogel- and patch-based biomaterials to the epicardial heart surface in a minimal-invasive, closed chest approach, respectively. These novel delivery devices aim to overcome application associated issues of previous administration strategies for biomaterial-based therapies providing the opportunity to better exploit the therapeutic potential of applied regenerative therapeutics.

The following section will first provide an overview of the anatomy and physiology of the heart. Subsequently, a brief introduction regarding cardiovascular diseases (CVDs) with focus on myocardial infarction (MI) and its potential progression to ischemic heart failure (HF) will be given. Finally, the research aims and the outline for this thesis will be described.

1.1 Anatomy and Physiology of the Heart

The physiological function of all organs is maintained by the cardiovascular system, an elaborated network of blood vessels permeating the human body with a total length of approximately 60,000 miles [1]. The blood vessels including arteries, arterioles, capillaries, venules and veins allow blood to circulate to all parts of the body with the objective of performing two essential functions: nutrient and oxygen supply of cells on the one hand and the removal of metabolites such as carbon dioxide and other waste products from cells on the other hand. The required driving force to move blood though this circulatory network is provided by the heart as central motor of the cardiovascular system [1-3].

The cone-shaped heart with size of a human fist is located between the lungs within the medial cavity of the thorax called mediastinum, inferior to the sternal angle and superior to the diaphragm (see Figure 1.1) [1, 2, 4]. In sagittal direction, the heart lies anterior to the vertebral column and posterior to the sternum. Based on the

apex orientation towards the left hip and the direction of the flat base towards the right shoulder [2], approximately two-thirds of the heart mass are situated left of the midsternal line given by the breastbone and one-third to its right [1, 2].

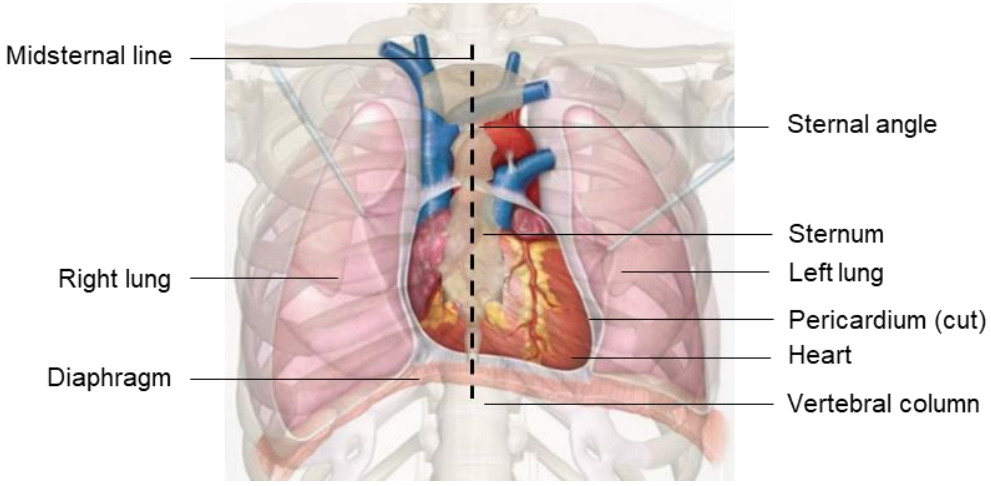

Figure 1.1: Schematic representation showing the relative position of the heart in the thorax regarding the surrounding organs and bones. Adapted from Marieb and Keller [2], Barclay [5]. Reprinted with permission of Pearson Education, Inc., New York, New York [2].

The attachment of the heart to the surrounding body structures is implemented by the outer fibrous layer of the so-called pericardium, a double-walled protecting sac encapsulating the heart and roots of the major blood vessels [1, 2, 4, 6]. The inner serous layer of the pericardium is further divided into an outer parietal layer lining the internal surface of the fibrous pericardium and an inner visceral layer, also known as epicardium, that is firmly attached to the heart forming the outer layer to the heart wall. A thin film of the lubricating pericardial fluid in the pericardial space generated between the parietal and visceral layer allows the beating heart to move almost frictionless within the fibrous pericardium [1, 2, 4].

The human heart is composed of four chambers, the right and left atrium lying superior to the corresponding ventricle (see Figure 1.2). Both the atria and the ventricles are internally separated by the interatrial and interventricular septum, respectively [2]. The rough path of the interventricular septum on the heart surface can also be followed by coronary blood vessels running along the anterior interventricular sulcus (anterior interventricular artery and great cardiac vein) and the continuing posterior interventricular sulcus with the posterior interventricular artery and middle cardiac vein. The border between the atria and ventricles is externally

visible by the coronary sulcus (atrioventricular groove) including the circumflex and right coronary arteries [1, 2, 4].

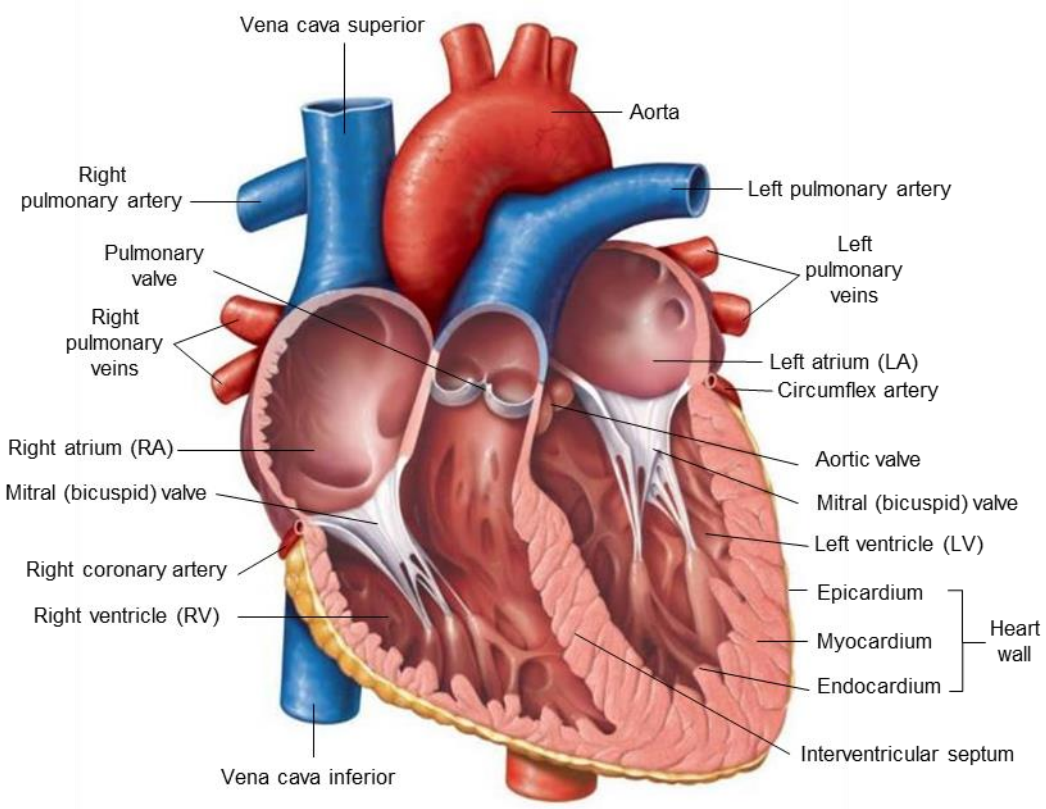

Figure 1.2: Schematic frontal section of the heart showing the four heart chambers, blood vessels, the layers of the heart wall and heart valves preventing backflow of the blood. All blood vessels carrying oxygenated and deoxygenated blood are shown in red and blue, respectively. Reprinted with permission of Pearson Education, Inc., New York, New York [2].

The heart pumps deoxygenated blood via the pulmonary circuit to the lungs for gas exchange and oxygen-rich blood via the systemic circuit to all body tissues as schematically illustrated in Figure 1.3 [2]. Based on the unique architecture of the heart (see Figure 1.2), each blood circuit is individually supplied by its respective heart chamber. Deoxygenated and carbon dioxide-rich blood returning from the body tissues enters the right atrium via the superior and inferior venae cavae. The blood passes the tricuspid valve into the right ventricle, which ejects the blood in the pulmonary circuit [1, 2, 4]. After exchanging carbon dioxide (CO_2) and oxygen in the lungs, the oxygen-rich blood is returned to the left atrium via pulmonary veins and passes via the mitral (bicuspid) valve into the left ventricle. The left ventricle pumps the blood back into the aorta. From there smaller systemic arteries carry the blood to the organs and tissue for gas and nutrient exchange. The systemic

veins return the deoxygenated and with metabolites enriched blood again back to the right atrium before the next cycle starts [1, 2, 4].

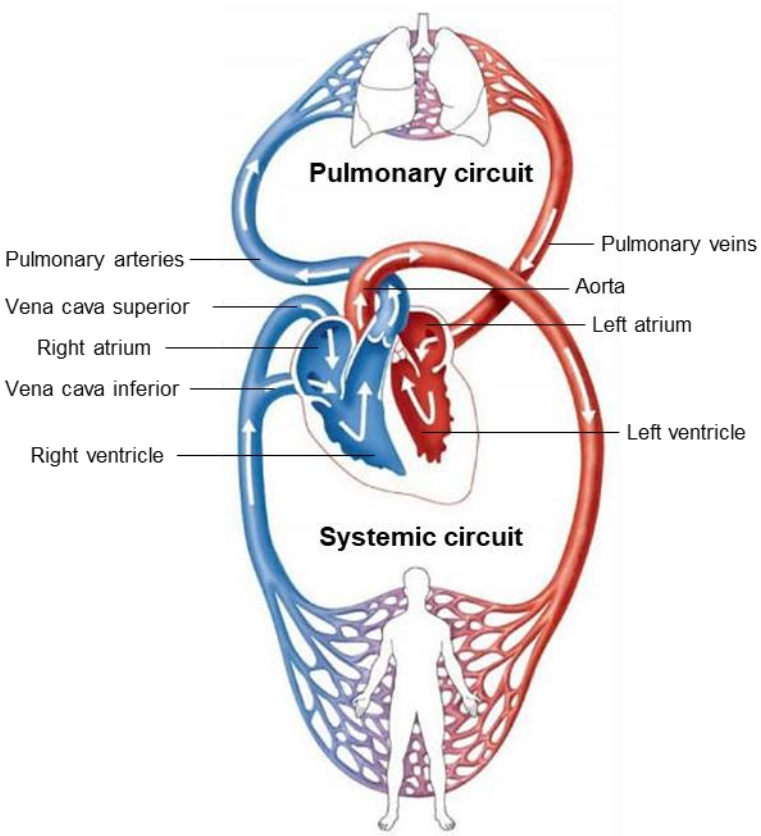

Figure 1.3: Schematic illustration of the cardiovascular system with the heart as central motor showing the blood supply to all body organs via the systemic circuit and the blood flow through the lungs for gas exchange via the pulmonary circuit. Oxygen-poor and CO_2-rich blood is shown in blue. Oxygenated and CO_2-poor blood is represented in red. The direction of the blood flow through the respective circulation system and the several heart chambers is illuminated by the white arrows. The actual number of two pulmonary arteries and four pulmonary veins is for simplicity reasons reduced to one, respectively. Reprinted with permission of Pearson Education, Inc., New York, New York [2].

The blood flow from the atria to the ventricles and out into the respective arteries in only one direction is implemented by a system of four one-way valves [1, 2]. Each valve opens and closes in response to pressure changes between its adjacent sides. The atrioventricular tricuspid and mitral (bicuspid) valves separate the ventricles from the atria. Analogously, the pulmonary and aortic valves serve a similar function preventing blood backflow in the respective ventricle from the associated arteries [1, 2]. These valves are opened to let blood pass when the associated ventricle contracts and the corresponding intraventricular pressure rises above the pressure in following vasculature. As the ventricles relax, the backflowing blood fills the cusps of each valve and forces them to close [1, 2, 4]. Both the

inner lumen of each heart chamber and the fibrous skeleton of each heart valve are covered with a protective layer called endocardium, which is composed of endothelial cells resting on a thin layer of connective tissue. The smooth surface of the endocardium facilitates a uniform blood flow and reduces the formation of blood cloths [1, 2].

In order to keep the heart continuously pumping blood though the body, a separate coronary circulation system consisting of coronary arteries, cardiac veins and the coronary sinus supply the heart with the needed blood [1, 2]. The right and left coronary artery provide oxygenated blood to the heart. Both coronary arteries exit the aorta above the aortic valve and encircle the heart in the coronary sulcus (atrioventricular groove) indicating the external border between atria and their respective ventricles. Both arteries divide into two major branches continuing in respective grooves on the outside of the heart muscle before branching in smaller vessels and capillaries that transport blood to the muscle fibres [1, 2]. The oxygen-poor blood is mainly collected by several cardiac veins that join to the coronary sinus circulating the blood back into the right atrium. Several anterior cardiac veins also transport the blood directly back into the right atrium [1, 2].

The pumping motion of the heart is generated by the synchronized contraction of cardiomyocytes (heart muscle cells) that are located in the middle muscular layer of the heart wall called myocardium [3]. The cardiomyocytes (CMs) are integrated within the extracellular matrix (ECM), a network of protein and non-protein components that are produced by cardiac fibroblasts [6, 7]. Most of the ECM comprises collagen type I (approximately 85 %) and collagen type III (approximately 11 %) that form the structural continuum around the cardiomyocytes. Collagen type I mainly provides the structural support determining the stiffness and resistance to deformation. In contrast, collagen type III accounts for elasticity [6, 8]. Together, these two types of collagen jointly tether the branching CMs [2, 8] by their unique assembly of helical structures [6] arranged in spiral or circular bundles [2]. Other structural components such as elastin and glycosaminoglycans (GAGs) provide a high degree of compliance to the myocardium and render the required viscoelastic properties of the heart wall, respectively. GAGs also bind bioactive substances such as growth factors (GFs), requisite for the signal transmission between cells.

Fibronectin and laminin as adhesive proteins do not directly influence the mechanical integrity of the myocardium but support cell adhesion and migration [6].

The coordinated rhythmic relaxation and contraction of the heart is created by the intrinsic conduction system ensuring the heart beats as one unit [1, 2, 4]. One heart cycle refers to the consecutive diastolic and systolic phases of the ventricles during which the ventricles are relaxed and contract, respectively. The diastole begins at the sinoatrial (SA) node, which is also known as pacemaker of the heart and forces the heart to beat typically 75 times per minute [2]. During the end of the diastolic phase, electrical impulses generated by the SA node force the two atria to contract promoting the blood flow into the relaxed ventricles. After passing the atrioventricular (AV) node, the electrical impulse follows the AV bundle (also called His bundle), which splits into the right and left bundle brunch along the interventricular septum towards the apex. From there, the electrical depolarisation wave continues via the Purkinje fibres completing the pathway to the apex before spreading superiorly into the ventricular heart walls to depolarize the CMs of both ventricles. Immediately following this depolarization wave, the ventricles contract to eject blood into the respective arteries before the ventricles relax again and a new cardiac cycle starts. [1, 2, 4].

The amount of blood each ventricle ejects during the systolic phase is characterized by the stroke volume (SV), which describes the difference between the end diastolic volume (EDV) and the end systolic volume (ESV), as shown in the following equation [1, 2].

$$SV = EDV - ESV \tag{1.1}$$

According to Marieb and Keller [2], an average healthy heart pumps approximately 70 mL with each heart beat based on a normal EDV of 120 mL and average ESV of 50 mL. This corresponds to nearly 60 % of the blood the ventricles contain, which is described by the ejection fraction (EF).

$$EF = \frac{SV}{EDV} \tag{1.2}$$

The cardiac output (CO) as product of SV and heart rate (HR) reflects the amount of blood ejected by each ventricle per time.

$$CO = SV \cdot HR \tag{1.3}$$

Based on the heart rate of 75 beats/min for a healthy heart at rest, the average CO for an adult is 5.25 L/min.

The amount of blood ejected during the contraction of each ventricle is controlled by a sophisticated, autonomous mechanism called Frank-Starling mechanism. Basically, the SV is adjusted dependent on the amount of returning blood volume during the diastole. The more blood returns from the veins into each ventricle, the more the CMs are stretched causing their stronger contraction. For more details, the reader is referred to Marieb and Keller [2].

1.2 Cardiovascular diseases (CVDs)

All disorders affecting the heart and blood vessels are summarized as so-called cardiovascular diseases (CVDs) [9]. According to the International Classification of Diseases, 10th Revision, (ICD-10) [10], CVDs include rheumatic fever/rheumatic heart disease (I00-I09), hypertensive diseases (I10-I15), ischemic coronary heart diseases (I20-I25), pulmonary heart disease and diseases of pulmonary circulation (I26– I28); other forms of heart disease (I30–I52); cerebrovascular disease (stroke) (I60–I69); atherosclerosis (I70); other diseases of arteries, arterioles, and capillaries (I71–I79); diseases of veins, lymphatics, and lymph nodes not classified elsewhere (I80–I89); and other and unspecified disorders of the circulatory system (I95–I99); and when data available congenital cardiovascular defects (Q20–Q28).

CVDs are the most common cause of mortality and morbidity worldwide, producing an immense health and economic burden every year [11]. Improvements of hygienic standards leading to a decline of infectious diseases accompanied with growing wealth of an ageing population that is privileged to have more food available than needed are the main reasons for a steady increase of CVD cases, especially during the last century. The relative surplus of food together with decreasing physical activity [12] resulted in a significant increase of various risk factors for CVDs such as high blood pressure and high cholesterol levels. As consequence the incidence of CVDs and consequential deaths grew steadily [11, 13]. In 2015, CVDs accounted with 17.9 million cases for more than 30 % of all deaths globally.

The same prevalence was detected in the United States of America with more than 800,000 people that died from CVDs [11]. In Europe, even 45 % of all deaths (3.9 million) could be attributed CVDs [13]. The prevalence of cases with at least one form of CVDs was in 2015 with 422.7 million worldwide even higher. On the basis of the data collected by the National Health and Nutrition Examination Survey (NHANES), 11.5 % of all US-Americans (27.6 million) suffered from at least one form of CVDs in 2015 [11]. More than the double of CVD cases (85 million) were registered in Europe with 11.3 million new cases alone in 2015. Already in 2015, CVDs entailed considerable costs of €210 billion a year for the European economies [13]. In 2013 to 2014, it was estimated that CVDs costed the US economy $329.7 billion. Caused by peoples' lifestyle leading to increased risk factors for CVDs, estimation indicate that CVDs remain the leading global cause of death also in the future and are expected to account for more than 23.6 million deaths worldwide in 2030. More than 130 million people alone in the USA are projected to suffer from at least of one form of CVDs by 2035 with total costs exceeding $1.1 trillion [11].

1.3 Myocardial infarction (MI)

Coronary heart diseases (CHDs) are the leading cause of deaths that are attributable to CVDs. Acute myocardial infarction is the most common form of CHDs being responsible for more than 800,000 cases in the USA per year. Consequently, every 40 seconds an American will suffer a MI [11].

1.3.1 Causes of MI

In most cases, MI is caused by thrombus formation in one or more coronary arteries inhibiting the blood flow through the coronary circulation system [14-16]. According to the Universal Classification of MI, this spontaneous type of MI is categorized as type I MI [17]. The pathologic coagulation cascade itself is initiated either by rupture or endothelial erosion of a fragile arteriosclerotic plaque [14, 15]. Both plaque disruption and endothelial erosion are especially induced by the high inflammatory activity of macrophages surrounding the lipid core of the arteriosclerotic

plaque [14]. Most of the macrophages are characterised by their foamy appearance that can be attributed to the pathological accumulation of cholesterol esters (CEs) as cytoplasmic lipid droplets, for which reason these macrophages are also referred as foam cells [18]. The production of inflammatory cytokines by macrophages [14, 18] entails apoptotic cell death of smooth muscle and endothelial cells [14]. Smooth muscle cells produce the essential extracellular components of the arteriosclerotic plaque required to maintain the structural integrity of the fibrous cap that encages the lipid core with its procoagulant ingredients. Endothelial cells lining the lumen of blood vessels are involved in many functions but regarding blood clotting these intact cells especially provide a non-thrombogenic surface [14]. Accompanied with the release of ECM degrading enzymes by activated macrophages the structural integrity of the arteriosclerotic plaque is weakened leading to plaque disruption or the subendothelial connective tissue is uncovered as result of endothelial denudation [14]. In both cases, highly thrombogenic substances are exposed to the blood initiating the coagulation cascade due to activation of platelets and clotting factors, which finally result in mural thrombus formation or platelet embolization downstream [15]. The consequential occlusion of blood vessels restricts the blood flow and hence the oxygen and nutrient supply of the affected heart regions. Even twenty to thirty minutes [19] of severe oxygen and nutrient shortage are sufficient to provoke necrotic cell death of CMs, which impairs the pumping function of the heart [8, 15-17]. Other rare cases causing an imbalance between required and actually provided nutrition and oxygen supply are for instance coronary endothelial dysfunction and coronary artery spasm, coronary embolism, anaemia, arrhythmias, hypertension or hypotension [17].

1.3.2 Procedures to restore blood flow

The primary goal for initial treatment of MI is the restoration of blood flow through the occluded blood vessel with the aim to confine necrotic cell death und thus expansion of the infarct [16]. Percutaneous coronary intervention (PCI) has been established as the standard treatment for myocardial infarction [15, 16, 20] but should be performed within 60 to 90 minutes upon arrival at the hospital. In case of longer transfer times to a hospital with PCI facility fibrinolytic therapy is employed to avoid prolonged ischemia by dissolving the thrombus [16]. The dissolving mechanism of

thrombolytic agents is based on the conversion of endogenous plasminogen to plasmin. Plasmin subsequently induces lysis of fibrin and thus dissolution of the blood clot [15]. Even though, thrombolytic agents can be administered immediately after arrival of medical professionals, primary PCI with balloon angioplasty or stenting is preferred compared to fibrinolytic therapy. Primary PCI ensures more reliable and complete reperfusion with approximately 90 % reperfusion rate compared to only 80 % reperfusion rate in case of fibrinolysis. Additionally, fibrinolytic therapy is accompanied with more contraindications such as increased risk of haemorrhagic stroke [15, 16]. Despite the benefit of blood flow restoration contributing to reduce infarct size, reperfusion induced abrupt reoxygenation causes the generation of reactive oxygen species (ROS) promoting tissue damage by further augmenting the immune response following MI [21].

1.3.3 Multiphase reparative responses after MI

Induced by the cell death of parenchymal cells and CMs due to MI, a sequence of inflammation, reparation (proliferation) and finally maturation is initiated with the purpose to prevent further damage and rupture of the ventricular wall affected by the MI [21, 22]. The inflammatory phase is initiated by so-called danger associated molecular patterns (DAMPs). DAMPs are released by necrotic, stressed or injured cells [21] but are also generated as consequence of ECM fragmentation [22]. ECM degradation is for instance triggered by matrix metalloproteinases (MMPs) that are secreted by surviving cardiac fibroblasts with the aim of allowing cell migration into the injured area. These DAMPs activate the innate immune system by interacting with cognate pattern recognition receptors (PRRs) on surviving cardiac cells and infiltrating leukocytes [21]. Leukocyte infiltration is already enabled during ischemia by increased vessel permeability as consequence of hypoxia impairing the integrity of endothelial cells. PRRs trigger further cellular signalling pathways downstream, which finally entail the release of a cascade of inflammatory cytokines, chemokines and cell adhesion molecules [21]. Provoked by the secretion of proinflammatory chemo-attractants, leukocytes are recruited to the injured tissue area to phagocytise dead cells and damaged ECM on the one hand. Infiltrating leukocytes furthermore augment repopulation of the infarcted area with proliferating immune cells, and later also with myofibroblasts, due to amplified generation of DAMPs and

secretion of ECM degrading enzymes (mainly proteases and oxidases) facilitating their attraction and migration, respectively [21]. In order to ensure sufficient nutrient and oxygen supply for the infiltrating cells, an increased expression of the vascular endothelial growth factor (VEGF) is triggered after MI beginning in the viable border zone that extends subsequently into the core infarct zone [21, 22].

Resolution of the inflammatory response is elicited by several cells and molecular signals suppressing proinflammatory signals [21, 22]. Apoptotic neutrophils have been implicated in suppression of inflammation by release of anti-inflammatory mediators stopping recruitment of new neutrophils, promoting neutrophil apoptosis and finally their effective efferocytosis by macrophages [21]. The phagocytotic uptake of apoptotic neutrophils changes macrophages to a tissue-repair encouraging M2 phenotype [21]. M2 macrophages produce anti-inflammatory and profibrotic cytokines such as interleukin (IL)-10 and transforming growth factor (TGF)-β that further restrain inflammation and stimulate the repair of the injured tissue, respectively. Increased concentration of TGF- β accompanied with changes of the damaged ECM following MI lead interstitial cardiac fibroblasts that survive the ischemia as well as infiltrating fibroblasts from surrounding viable tissue areas to differentiate into myofibroblasts, which become the most present cell type [21]. Myofibroblasts are phenotypically modulated fibroblasts with features of both fibroblasts and smooth muscle cells characterised by their expression of contractile proteins such as α-smooth muscle actin and non-muscle myosin [22]. But the most pronounced feature of myofibroblasts regarding cardiac repair is their ability to produce large amounts of matrix proteins. With the aim of stabilising the damaged ventricular wall and consequently preventing its rupture, myofibroblasts secrete immense amounts of structural matrix proteins such as collagen and fibronectin. Initially, mainly the elastic type III collagen is deposited [21, 22]. Moreover, matricellular proteins such as Thrombospondin and tenascin C are also secreted augmenting further myofibroblast migration [22].

Following the formation of a collagen-based matrix, most of the myofibroblasts are indicated to undergo apoptosis as consequence of decreasing levels of fibrogenic growth factors and matricellular proteins promoting typically the survival and activation of myofibroblasts. The disintegration of the before established microvasculature may further account for a substantial loss of myofibroblasts [22]. The

remaining myofibroblasts convert type III collagen to type I collagen, which is additionally enzymatically cross-linked by so-called lysyl oxidase (LOX). This processing of type III collagen increases the tensile strength of the collagen fibres and may lead to contraction of the newly synthesized collagenous scar tissue [22]. The final replacement of the injured myocardium affected by the MI with collagenous scar tissue instead of myocardial tissue with new CMs is caused by the limited capability of adult CMs to re-enter the cell cycle and proliferate [21, 22].

1.4 Heart Failure (HF)

1.4.1 Pathological progression of MI to HF

The remodelling of contractile myocardial tissue into non-contractile collagenous scar-tissue after MI entails the deterioration of ventricular pumping function but also biochemical, biomechanical and structural changes that may further initiate a cascade of pathological events continuously impairing cardiac function, respectively [23, 24]. The lost ability of the remodelled tissue to contract synchronously with each heartbeat reduces the amount of blood that can be pumped by the heart for each heart cycle. The reduced CO leads to a decreased mean arterial pressure (MAP) that in turn causes decreased tissue perfusion. Induced by this disturbance, a myriad of compensatory mechanism is activated in order to maintain a MAP that is appropriate to meet the metabolic requirements [23]. One option for the heart to compensate the reduced CO is the Frank-Starling mechanism. As the CO decreases, more blood accumulates in the LV resulting in an increased LV end diastolic volume (LVEDV). Triggered by the increased LVEDV, the myofibers are more stretched with the potential to generate a higher contractile force to restore CO [23, 24]. But the Frank-Starling mechanism is insufficient to maintain the necessary blood flow for longer time periods. In contrast, neurohormonal activation via the sympathetic nervous system (SNS) in response to a decreased MAP is capable to compensate the necrotic death of CMs for a longer period by enhancing cardiac contractility and increasing the resistance of the peripheral vasculature for instance. Another neurohormonal mechanism to compensate the decreased CO and MAP is the Renin-Angiotensin-Aldosterone system (RAAS), that can also directly be modulated by the SNS [24]. The RAAS induces an antidiuretic effect by

increasing the total blood volume with the goal to exploit the Frank-Starling mechanism in order to restore CO. The promoted vasoconstriction by Angiotensin II moreover increases the MAP and thus improve perfusion of vital organs. Despite the acute benefit by these adaptive neurohormonal based responses, sustained stimulation of the SNS and RAAS provoke further remodelling of the heart that progressively augment the dysfunction of the heart [23, 24]. SNS hyperactivation impairs cardiac contractility by affecting the synthesis of proteins that are related to the excitation-contraction coupling mechanism for instance [24]. The positive impact of the SNS and RAAS inducing increased peripheral resistance (vasoconstriction) on the MAP and elevated water retention by the RAAS is accompanied by an increased venous return to the heart for instance. Elevated levels of LVEDV increase the LV end-diastolic pressure (LVEDP) which again raises the ventricular wall tension. Consequentially, a hypertrophic growth of CMs is induced in attempt to reduce the increased ventricular wall tension due to the higher cardiac workload by the addition of serial arranged sarcomeres finally leading to a thinning of the LV wall [24]. The decreased thickness of the LV wall in turn further increases the stress in the myocardium developing a vicious cycle. The increased wall stress in the LV chamber triggering dilated cardiac hypertrophy can be further traced back to the deposition of collagenous scar-tissue that alters the compliance of the ventricle [22, 24].

The fibrotic response after MI is essential to maintain mechanical integrity in order to prevent rupture of ventricle regions affected by the MI [21, 22, 24]. However, increased stiffness of synthesized collagenous scar tissue even provokes remodelling of the non-infarcted ventricular wall by reactive interstitial fibrosis. Increased mechanical stress in the remote myocardium is indicated to provoke activation of pro-fibrotic TGF-β promoting the activation and differentiation of fibroblasts into myofibroblasts in the remote myocardium. The activation of fibroblasts in regions not acutely affected by MI is additionally intensified by already activated myofibroblasts in the infarct region secreting permanently pro-fibrotic factors that diffuse to remotely located non-infarcted regions. The consequential collagen deposition in interstitial compartments by activated myofibroblasts drives a reactive remodelling also in non-infarcted regions that progressively compromise diastolic and systolic heart function [22]. The inflammatory response leading to tissue fibrosis is also

stimulated by chronic activation of Angiotensin II provoking the synthesis of additional ROS [24]. Impaired resolution of the inflammatory response with persistent fibrosis may be also caused by larger infracts [21].

The replacement of damaged myocardial tissue with fibrous scar tissue as well as interstitial fibrosis additionally impair the transmission of the electrical impulse generated by the SA node. The collagenous scar can be considered as insulated area causing arrhythmias. The fabricated non-conducting collagen fibres in interstitial fibrosis further promote conduction disturbances by slowing or blocking the electrical depolarisation wave or even inducing focal ectopic activity [22]. Further information regarding activated mechanisms after MI which trigger progression to HF are more detailed in reviews by Kemp and Conte [23], Gabriel-Costa [24] as well as Sutton and Sharpe [25].

Chronically activated compensatory mechanisms continuously amplify the functional dysfunction of the heart which stimulate further geometrical and structural alterations of the ventricular wall. Remodelling again initiate the already discussed compensatory mechanism and further exacerbate hemodynamic disorders. The final consequence is heart failure (HF) [23, 24]. Figure 1.4 schematically shows the geometrical changes caused by the abnormal loading conditions and thereby stimulated compensatory mechanisms after myocardial infarction. The increased cardiac workload induces both ventricle dilatation with a more spherical appearance of the ventricle and concentric hypertrophic growth of the ventricle leading to systolic and diastolic dysfunction, respectively [26]. The loss of a critical amount of functional myocardial tissue resulting finally in HF is not only induced by MI but also by a multitude of other diseases affecting the heart. Apart from ischemic heart diseases, hypertension and diabetes are the most common causes for HF. Cardiomyopathies, valvular diseases, infections, myocarditis, prolonged arrythmias or cardiotoxic drugs are further but less common causes that may finally lead to HF [23].

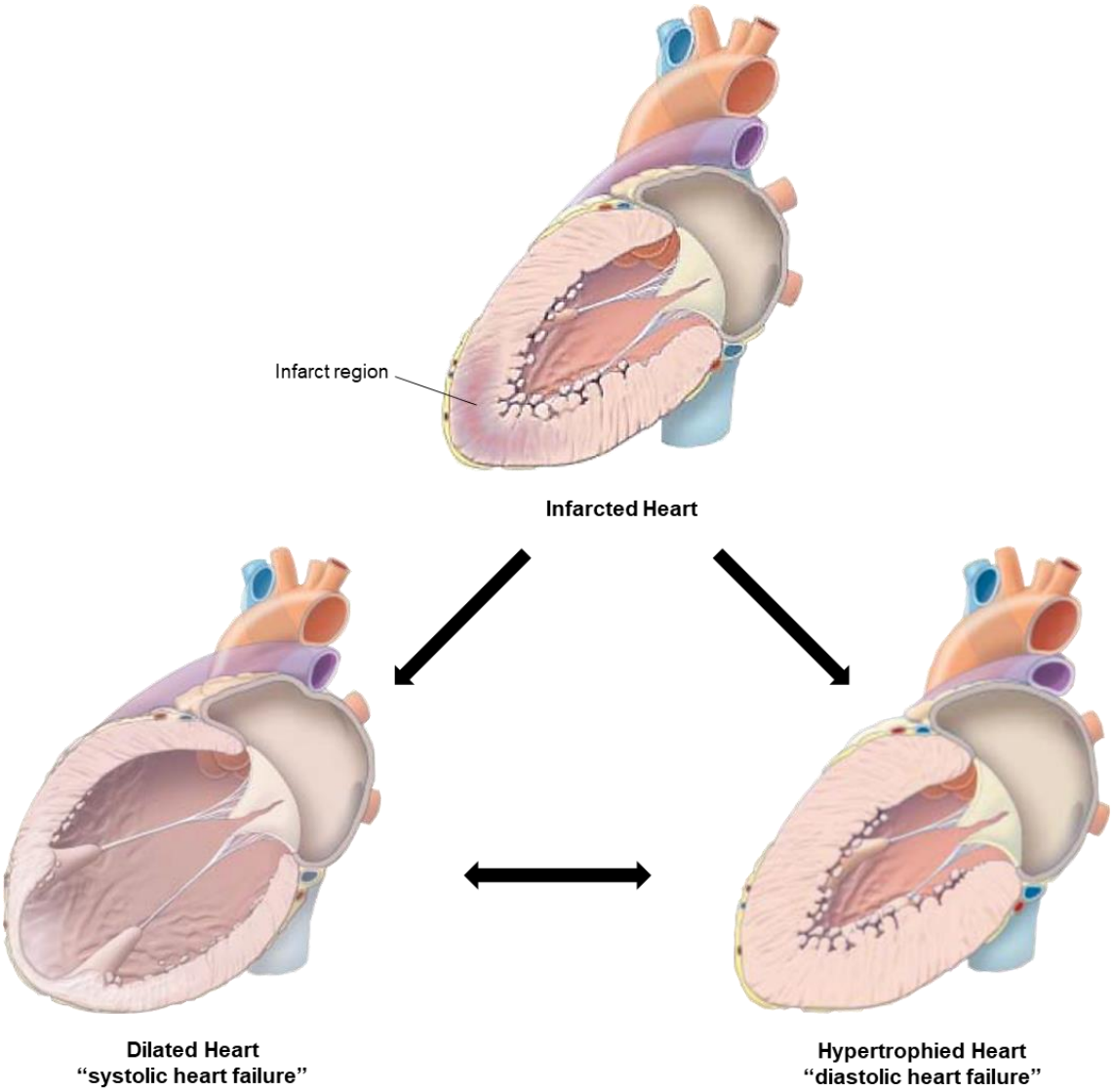

Figure 1.4: Sagittal section of the LV and LA showing schematically the geometrical changes in the LV induced by altered loading conditions after MI. Reproduced with permission from Jessup and Brozena [26], Copyright Massachusetts Medical Society.

1.4.2 Definition and symptoms of HF

Heart failure (HF) is commonly defined as a clinical syndrome, which is caused by any structural or functional disorders leading to impaired contractile performance or ventricular filling of the heart [27, 28]. The heart is incapable to provide enough blood flow to all body tissue in order maintain metabolic homeostasis or lack of efficient venous return from the systemic and pulmonary circuit. Caused by these malfunctions, patients affected by HF suffer from a plenty of symptoms that can be attributed to either of the malfunctions [23]. Elevated levels LVEDP as result of LV

dysfunction increases the pressure in the LA and thus lead to increased capillary pressure. Consequential pulmonary congestion causes symptoms such as dyspnoea, cough and wheezing. Failure of the RV shows a similar series of events but related to the systemic circuit. Increased amount of blood in the RV generates higher pressures in the RA and the connected vasculature system leading to increased pressure in lower extremities, liver and gastrointestinal tract. Accordingly, patients suffer from peripheral edema, hepatomegaly and abdominal dropsy (ascites). Symptoms such as fatigue or nausea can be traced back to the underperforming pumping function of the heart [23, 27-29].

1.4.3 Classification of HF

Physical disability during exercise execution and symptomatic status of HF are summarized by the classification of the New York Heart Association (NYHA) in four distinct groups as shown in Table 1.1 [30]. Each class outlines the severity of the functional limitations at normal conditions and under physical load.

Table 1.1: Classification of HF according to NYHA [30].

Class	Definition
I	No limitation of physical activity. Ordinary physical activity does not cause symptoms of HF.
II	Slight limitation of physical activity. Comfortable at rest, but ordinary physical activity results in symptoms of HF.
III	Marked limitation of physical activity. Comfortable at rest, but less than ordinary activity causes symptoms of HF.
IV	Unable to carry on any physical activity without symptoms of HF, or symptoms of HF at rest.

The categorisation of HF in four stages developed by the American College of Cardiology Foundation (ACCF) and the American Heart Association (AHA) provides complementary information regarding presence and severity of HF with emphasis on development and progression of the disease (see Table 1.2) [27]. This classification system sufficiently considers the progressive character of the disease and focuses that HF is closely associated with both structural abnormalities and risk factors.

Table 1.2: Stages of HF according to ACCF/AHA [27].

Stage	Definition
A	At high risk for HF but without structural disorders or symptoms of HF.
B	Structural heart disease but without signs or symptoms of HF.
C	Structural heart disease with prior or current symptoms of HF.
D	Refractory HF requiring specialised interventions.

Table 1.3 shows the correlation between both classification systems according to Yancy *et al.* [27]. Hence, Stage A of the ACCF/AHA classification refers to a pre-stage of HF, Stage B to NYHA Class I, Stage C compromise all NYHA Classes and Stage D corresponds to NYHA Class IV.

Table 1.3: Comparative correlation between ACCF/AHA stages and NYHA classes according to [27].

ACCF/AHA stages of HF	NYHA functional classes of HF
Stage A	None
Stage B	Class I
Stage C	Class I – IV
Stage D	Class IV

1.4.4 Epidemiology

Referring to the latest report of the AHA [31], more than 6 million US citizens older than 20 years were affected by HF between 2013 and 2016, which relates to an estimated increase of 500,000 compared to the evaluated period between 2009 and 2012. Caused by an increasingly aging population, improved survival rates of other CVDs such as MI and HF itself as well as changing lifestyle promoting hypertension or obesity as exemplary risk factors for HF the prevalence of HF is projected to exceed 8 million cases by 2030. Consequentially, the total costs for HF will also further rise from $30.7 billion in 2010 to approximately $70 billion by 2030 which conforms to an economic burden of more than $200 for every US adult. With also increasing prevalence of HF worldwide, at least 26 million already suffered from HF in 2017 [32].

1.5 Research objectives of this thesis

Biomaterial-based strategies have been pursued with great efforts aiming to suppress the pathological cascade after MI towards end-stage HF. However, comparable simple administration approaches of these therapeutics have mostly limited their final performance, motivating the need of advanced delivery strategies.

This PhD thesis aims to address current limitations for the targeted local delivery of biomaterials to the epicardial heart surface. The scope was to develop novel approaches that enable a minimal-invasive administration of both patch- and hydrogel-based biomaterials to the epicardium. The sustained contact of the delivered biomaterials with the heart surface should be additionally facilitated without employing any surgical aids.

More precisely, the specific aims of this PhD thesis were:

1) Development of a carrier device which is capable to deliver hydrogel-based biomaterials loadable with exogeneous cells and bioactive agents, respectively, to the epicardium
    - Concept development with applicability assessment
    - Exemplary assessment of device compatibility *in vitro* with an *in situ* crosslinking hyaluronic acid-based hydrogel, both without and loaded with exogenous adipose derived stem cells (ADSCs)
    - Exemplary assessment of pre-clinical feasibility *in vivo*
    - Exemplary assessment of pre-clinical efficacy *in vivo*
2) Development of a concept device that allows delivery of patch-based materials to the epicardium and is additionally capable to provide mechanical circulatory support
    - Concept development
    - Identification of suitable materials for concept implementation
    - Exemplary assessment of device compatibility *in vitro* with an already preformed hyaluronic acid-based patch
    - Exemplary assessment of pre-clinical feasibility *in vivo*

1.6 Outline

After having given an overview regarding heart anatomy and physiology, cardiovascular diseases with emphasis on maladaptive pathological processes initiated after myocardial infarction that may lead to ischemic heart failure, an introducing outline of treatment options after MI motivating the research of the presented work, the remaining thesis is arranged as follows:

- Chapter 2 will first highlight the predicament of currently approved therapeutic options for patients with impaired cardiac function after a myocardial infarct according to the guidelines given by the ACCF/AHA, being incapable of restoring cardiac function. Afterwards, regenerative strategies aiming to encourage cardiac regeneration will be discussed revealing the need of novel application strategies as motivation for my work presented in this PhD thesis.
- Chapter 3 will focus on the development of a novel bioresorbable carrier device for the targeted local delivery of an in situ-curing, fast-gelling hydrogel-based biomaterial to the epicardial heart surface via a single-stage minimal-invasive, closed chest procedure.
- Chapter 4 presents a novel device serving as cargo for the site-specific administration of a patch-based biomaterial to the epicardial heart surface in a minimal-invasive approach on the one hand, but having also the potential to provide acute assistance to the infarcted ventricle wall by epicardial augmentation on the other hand.
- Chapter 5 will draw conclusions from the work presented in this PhD thesis and will give an outlook on future work.

2 A review on literature: Therapeutic evolution from symptom alleviation towards cardiac regeneration

2.1 Preface

This chapter will review the progression of therapeutic approaches for patients with impaired cardiac function from attenuation of maladaptive compensatory mechanisms towards strategies encouraging cardiac regeneration. Limitations of recently emerged biological approaches will be discussed emphasizing the need to develop novel cargo devices providing the opportunity to better exploit the therapeutic potential of these regenerative strategies.

2.2 Predicament of current clinical treatment strategies

Once deterioration of cardiac function after MI has progressed to a point where HF is diagnosed, patients are commonly confronted with a poor prognosis and disabling symptoms. Medical treatment of patients with HF is therefore mainly focused at reducing mortality and improving morbidity [33]. The treatment of patients at any stage of HF is guided by the categorisation of HF according to the ACCF/AHA directing the therapy in accordance with the disease progression. The outline shown in Figure 2.1 represents the most important therapies applied dependent on the stage of HF with the respective goals of therapy. For more information the reader is referred to Yancy *et al.* [27].

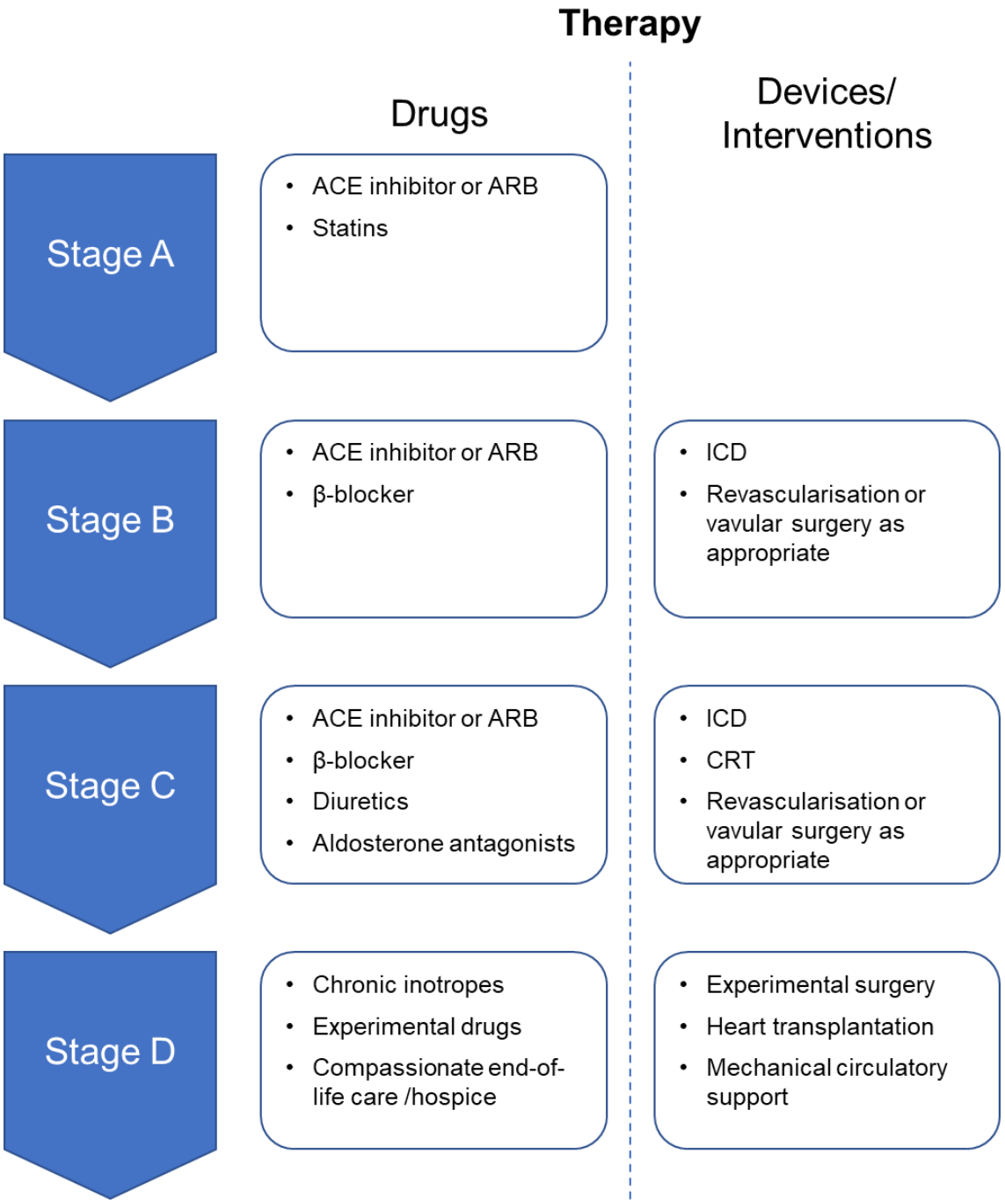

Figure 2.1: Recommended therapies according to the ACCF/AHA categorisation of HF. The abbreviation ACE indicates Angiotensin-converting enzyme, ARB Angiotensin II receptor blocker, CRT cardiac resynchronisation therapy and ICD implantable cardioverter defibrillator. Reprinted from Yancy *et al.* [27] with permission from Elsevier.

First of all, HF promoting risk factors such as obesity, diabetes mellitus, excessive tobacco and alcohol use should be reduced or even ideally completely avoided accompanied with regular physical exercises if possible at all stages [23, 27]. In most cases, patients receive pharmaceuticals targeting permanently activated compensatory mechanisms that are associated with impaired cardiac function as consequence of MI (see section 1.4.1) [23]. Usually administered drugs inhibiting the Angiotensin-converting enzyme (ACE) such as captopril, enalapril, ramipril, lisinopril and trandolapril aim to block the generation of the effector molecule Angiotensin II in order to prevent a steadily increasing cardiac workload and to relieve cardiac fibrosis. Despite the benefit of this mandatorily administered type of drugs, ACE inhibitors represent also a renal burden, promoting additional deterioration of the medical status. Further adverse side effects are cough, nausea or fatigue. Angiotensin receptor blockers such as valsartan, losartan and candesartan; β-blocking agents such as carvedilol, bisoprolol and sustained-released metoprolol; or aldosterone antagonists such as spironolactone intend to protect the heart and vasculature from maladaptive consequences of SNS overstimulation [23, 33, 34]. Symptomatic therapeutics such as positive inotropic agents (digoxin for instance) and diuretics such as furosemide are another important part of HF therapy intending to improve contractility and to reduce fluid retention, respectively [23, 33]. However, this pharmacological management only has the potential to ameliorate the symptoms and to delay progression of the disease but not to truly restore cardiac function for a long-term period.

Instead, disease progression occurs with development of persistent severe symptoms of HF. Advanced treatment strategies are required to improve survival of the patients. The gold-standard therapy for patients with end-stage HF (stage D) remaining symptomatic despite optimal medical therapy is cardiac transplantation [27, 35], since no other standard clinical procedure is capable of restoring the lost myocardial tissue [35]. Based on continuous advancements in immunosuppressive therapy since the first successful transplantation in 1967 by Christiaan Barnard, the long-term survival rate of transplant recipients 5 years after transplantation could be raised up to almost 72 % [27] with a median survival time of 9.5 years [31]. Caused by the ongoing shortage between available donor organs suitable to perform a heart transplantation and needed amounts of new hearts only an inadequate

portion of patients could benefit from this treatment approach. From 1987 to December 2012, 40253 patients with end-stage HF were waiting for a new heart in US but only 26943 received a donor organ [31]. The heart transplantation is additionally a highly invasive procedure accompanied by the risk of transplant rejection. Hence, it is obligatory for recipients to take immunosuppressive drugs lifelong, which in turn lead to renal stress and an elevated risk of cancer [35].

Stimulated by the supply-demand shortage of available donor organs, Ventricular Assist Devices (VADs) have emerged a feasible therapeutic option for patients with end-stage HF [23, 27, 33, 36]. VADs provide mechanical circulatory support with the aim to relieve the heart from increased workload. The original purpose of VADs was to bridge patients with deteriorating clinical status who are eligible for heart transplantation but are not stable enough stay alive any longer without mechanical circulatory support until the donor heart becomes available (bridge to transplantation therapy). The first device indicated as bridge to transplant was approved by the Food and Drug Administration (FDA) in 1994. Other use cases of VADs are “bridge to decision” or “bridge to candidacy”, “bridge to recovery” or “destination therapy” for patients with temporary or permanent contraindication to cardiac transplantation [36-38]. VADs are commonly differentiated according to their technical features such as flow characteristic (pulsatile versus continuous), pump mechanism (volume displacement, axial, centrifugal) and bearing of the blood flow generating impeller (contact bearing versus levitating) but also related to the final implant location of the mechanical pump (extracorporeal versus intracorporeal) and dependent on the ventricle(s) that are supported (left ventricular, right ventricular or biventricular) [27, 37]. The following Table 2.1 gives an overview of the respective VAD generations classified according their technical features.

Table 2.1: Overview of the respective VAD generations according their technical characteristics with schematic illustration of respective devices finally implanted and cross sections of the corresponding pumps. Exemplary figures of 1st and 2nd generation VADs were reproduced with permission from Slaughter *et al.* [39], Copyright Massachusetts Medical Society. Exemplary figures of a 3rd generation VAD, reprinted with permission from Aaronson *et al.* [40].

	Exemplary VAD	Pump cross section	Technical features
1st generation	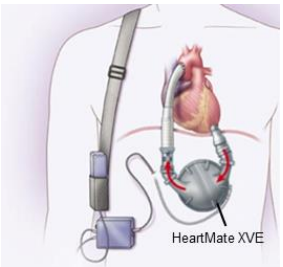	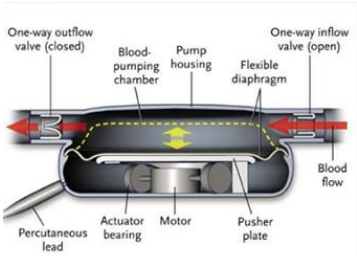	• Membrane pump generating a pulsatile flow via volume displacement • Contact bearing of the membrane
2nd generation	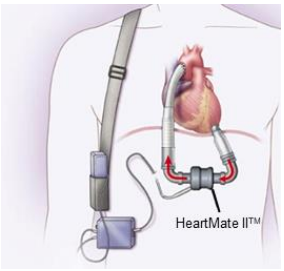	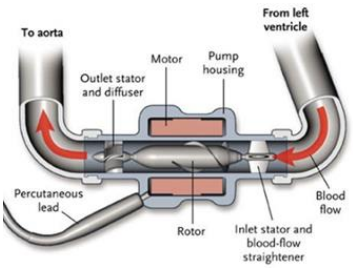	• Axial pumps generating a continuous flow • Impeller is suspended by contact bearings
3rd generation	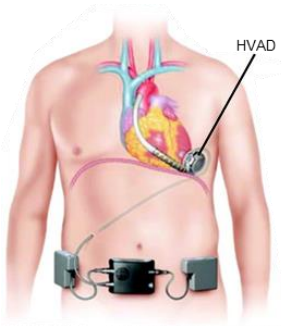	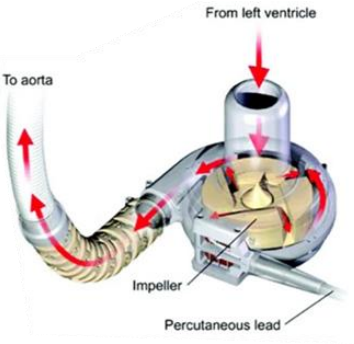	• Centrifugal or axial pumps generating a continuous flow • Levitation of the impeller without contact to the housing

Left Ventricular Assist Devices (LVADs) of the "first generation" such as the HeartMate XVE (St. Jude Medical Inc., St. Paul, MN USA) [41] or the EXCOR® (Berlin Heart Inc., Berlin, Germany) [42] are membrane pumps generating a pulsatile flow by volume displacement induced by a diaphragm. "Second generation" devices as for instance HeartMate II (St. Jude Medical Inc., St. Paul, MN USA) [43] and Jarvik2000® (Jarvik Heart Inc., New York, NY USA) [44] pump the blood continuously by axial operating impellers. One of the main complications associated with VADs of the second generation was mechanical wear caused by contact bearings of the respective impeller [37]. With the aim to improve long-term durability and

additionally reduce mechanical load to the blood components, VADs of the third generation as for instance the HVAD (HeartWare Inc., Framingham, Massachusetts USA) [45], INCOR® (Berlin Heart Inc., Berlin, Germany) [46] or HeartMate III (St. Jude Medical Inc., St. Paul, MN USA) [47] employ a levitation system where the moving impeller is suspended without any mechanical bearings [37]. Despite constant progress in device technology, some major limitations including an invasive implantation technique as well as risk of infections, bleeding, haemolysis and thrombosis remain unchanged [36].

Total Artificial Hearts (TAHs) such as AbioCor®IRH (Abiomed Inc., Danvers, MA USA) [48], SynCardia's temporary TAH (SynCardia Systems Inc., Tucson, Ariz) [49] or the ReinHeart TAH (ReinHeart TAH GmbH, Aachen, Germany) [50, 51] are another approach targeting the circulatory support of the failing heart. However, TAHs are faced with similar issues as VADs caused by the direct blood contact. Direct Cardiac Compression (DCC) devices on the contrary handle this challenge by compressing the failing heart from its epicardial surface. The consequential avoidance of direct blood contact by DCC devices constitutes the main advantage compared to VADs or TAHs devices eliminating all risks that have been associated with direct blood contact of these intravascular devices. The first DCC device was proposed by Anstadt and colleagues 1965 [52], which has been proven to effectively assist the pumping action of the heart in case of reverse cardiac arrest. However, the missing synchronisation with the heartbeat has raised concerns to injure the myocardium and provoke arrhythmias. Recently evolved DCC devices (see Figure 2.2) developed by Roche and colleagues [53], CorInnova (CorInnova Inc., Houston, TX USA) [54] or AdjuCor's individualised Biventricular Epicardial Augmentation Technology (BEAT) (AdjuCor GmbH, Munich, Germany) [55] have shown promising results in large animal models but are still under development and not yet approved for clinical use. For more comprehensive reviews of cardiac assist devices the reader is referred to Naveed *et al.* [56] and [57].

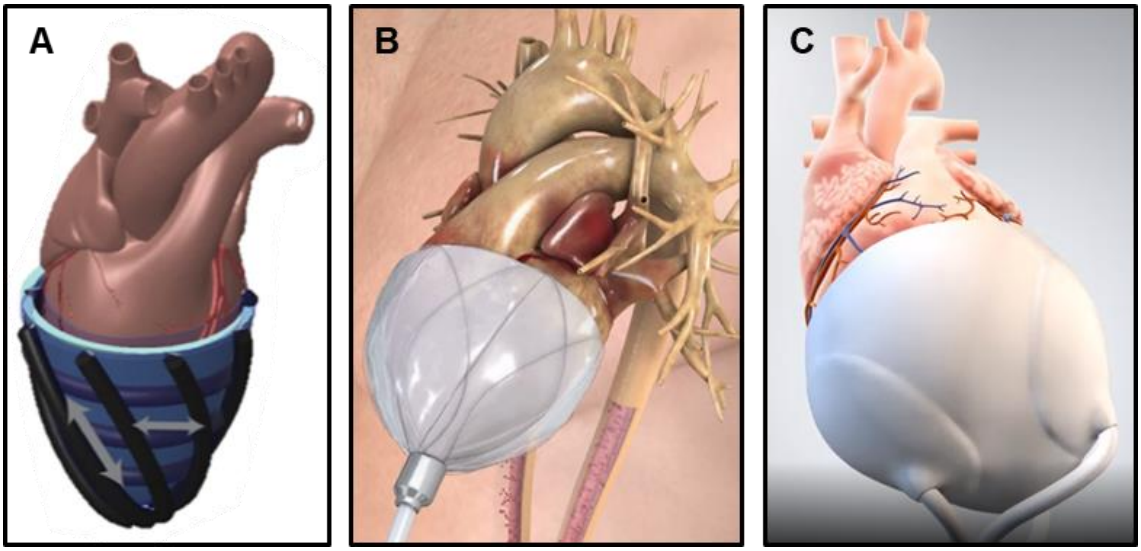

Figure 2.2: Schematic illustrations of recently developed DCC devices. (A) Biomimetic soft robotic sleeve from Roche *et al.* [53]. Reprinted with permission from AAAS. (B) CorInnova Heart Assist Device [54]. (C) AdjuCor Biventricular Epicardial Augmentation Technology [58].

All above-mentioned therapeutic options for patients with HF improve the survival rate, retard disease progression and alleviate symptoms associated with HF. However, all these currently approved therapeutic options are incapable of restoring cardiac function and are even partially accompanied with adverse side effects representing an additional medical burden for HF patients.

2.3 Strategies encouraging cardiac regeneration

2.3.1 Treatment targets

Numerous approaches have been emerged over the last decades with the aim to impede both the pathological cascade after MI towards ischemic HF and to animate an already remodelled heart to regenerate. Basically, the original goal of all these therapeutic interventions is the reduction of non-functional scar tissue in association with parallel generation of new functional cardiac tissue [59]. Several reviews [3, 6-8, 35, 59-66] provide a comprehensive overview regarding different strategies; employed materials, cell types and bioactive molecules that have been applied after MI. All therapeutic interventions target at least one of the following pathological aspects provoked by MI with the goal to suppress further disease progression accompanied with functional deterioration of the heart and to facilitate regeneration of the damaged tissue (see Figure 2.3): cardiomyocyte death, ischemia, inflammation, fibrosis, ECM degradation [64].

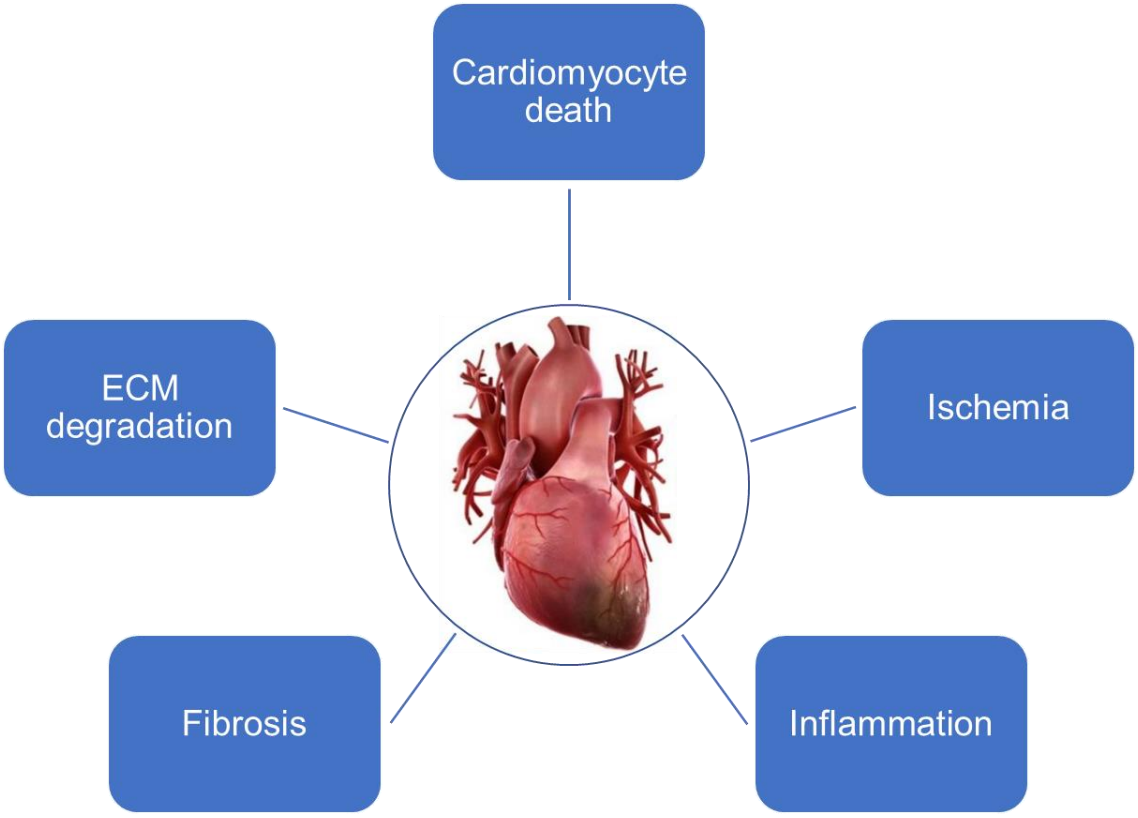

Figure 2.3: Pathological targets for therapeutic interventions after MI aiming to evoke regeneration of injured myocardial tissue according to Awada *et al.* [64]. Schematic illustration of an heart with MI from O'Neill *et al.* [66], reprinted with permission from John Wiley and Sons.

2.3.2 Biological support

Motivated by the massive loss of CMs as essential component to generate the vital pumping motion of the heart, restoration of cardiac function is inevitable associated with the recovery of CMs. Cell-based trials attempt to replace dead CMs by exogenously administered cells that are indicated to differentiate into new functional cardiac muscle cells [35, 59, 67]. Multiple cell types such as skeletal myoblasts, mesenchymal stem cells (bone marrow, adipose tissue or umbilical cord derived), embryonic stem cells, endothelial progenitor cells, cardiac stem cells or cardiopoietic stem cells as well as induced pluripotent stem cells [3, 8, 35, 59, 63] have been examined in various pre-clinical and clinical studies. Even though most studies have achieved a physiological benefit, true regeneration of contractile tissue to some degree could only be realized in a few cases [67]. Therapeutic efficacy of especially lineage-unselected bone marrow derived mononuclear cells was rather induced by the release of paracrine factors such as chemokines or growth factors. Secreted paracrine factors are indicated to potentially promote angiogenesis, protect residential surviving cells and encourage their proliferation or balance the immune response [63, 68]. Driven by high production costs of cell-based therapies associated with high translational hurdles, alternative approaches trying to avoid the use of cells such as gene- [63, 69-71] or protein-based [63, 64] therapeutic strategies have drawn increasing attention, which are also indicated to account for promoted stimulation of endogenous cardiac progenitor cells.

Adequate blood supply of the injured myocardial tissue is essential to provide at least sufficient amounts of oxygen and nutrition to the resident cardiac cells that survived the ischemic event or in case also to administered exogenous cells [64, 67]. However, the temporary established network of microvasculature as part of the natural immune response after MI disintegrates after initial formation of a collagen-based matrix at the infarct site impeding metabolic homeostasis [22]. Key mediators for angiogenesis such as VEGF and basic fibroblast GF (FGF-2) [64] could thus further augment regeneration by enhanced formation of new blood vessels.

The inflammatory response triggered after MI is necessary to clear dead cells, cellular debris and ECM fragments from the infarcted area to reduce tissue necrosis and further damage amongst others. But as result of elevated levels of proinflammatory cytokines (TNF-α, IL-1 and IL-6, e.g.) ECM degrading enzymes such as MMPs become more activated, which interfere the balance between ECM degradation and generation. Disturbance of ECM homeostasis is further amplified by the replacement with non-contractile scar tissue and further remodelling of the remote myocardium caused by interstitial fibrosis [22, 64, 67]. Therapeutics consequently trying to target the inflammatory reaction since rapid resolution of inflammation has been identified as crucial to promote regeneration [67]. Caused by the pleiotropic properties of some proinflammatory cytokines such as IL-1, the identification of suitable target sides remains challenging. Repression of critical effector molecules may even deteriorate the ECM imbalance and augment ventricle remodelling [22, 64].

2.3.3 Mechanical support

Even though collagen is characterised by its long half-life, the slow turnover compared to other proteins delays ECM replacement after MI induced degradation [64]. Consequential impaired mechanical integrity results in increased mechanical loads in the ventricular wall initiating a cascade of pathological reactions trying to compensate these elevated levels of mechanical stress, which finally end in thinning of the ventricular wall. Decreased wall thickness in turn exacerbate the mechanical load to the ventricle causing further geometrical changes as part of a vicious cycle (see section 1.4.1). Hence, several stabilisation techniques to mechanically support the weakened ventricle have received increasing attention over recent years as promising approaches to attenuate pathological mechanical changes occurring after MI. Mechanical support is principally provided by manipulating either the intraventricular pressure P, the LV chamber size and thus the curvature radius R of the ventricle or the thickness of the ventricular wall $t_{Ventricle}$ in order to decrease the respective tension in the myocardial wall T according to LaPlace's Law [35, 63], which is shown by the following equation (2.1).

$$T = \frac{P \cdot R}{t_{Ventricle}} \tag{2.1}$$

The benefit of passive mechanical support was first determined by Charpentier in the 1980s as positive side effect of cardiomyoplasty. Improvements regarding myocardial oxygen consumption, wall stress and adverse remodelling persisted even as the wrapped latissimus served just as passive muscle wrap [72]. Subsequently developed whole heart passive restraint devices such as the CorCap™ (Acorn Cardiovascular Inc., St Paul, Minn USA) [72-74] or HeartNet™ (Paracor Medical Inc., Sunnyvale, CA USA) [72, 74] (see Figure 2.4) have shown promising clinal data, but their overall performance regarding restoration of cardiac function remained limited [72]. The limited therapeutic capacity could potentially be attributed to the nonbiodegradable materials (polyethylene terephthalate (PET) and Nitinol mesh in case of the CorCap™ and HeartNet™, respectively) used devices being potentially incapable to adapt properly to the morphological changes of the ventricle that occur during reverse remodelling [75, 76]. The significance of a constantly suitable restraint level was shown by Lee *et al.* [77], who reported an impact of the restraint level on the degree of therapeutic benefit in terms of reverse remodelling verifying that an adaptive mechanical support is essential. An additional major disadvantage of whole heart passive restraint devices is the invasive surgical procedure that is required for implantation [60].

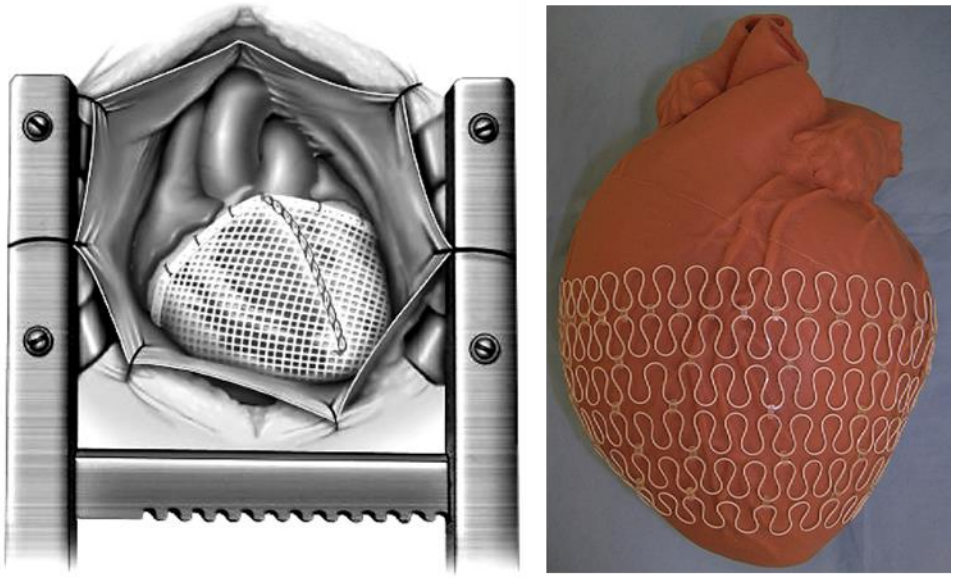

Figure 2.4: Whole heart passive restraint devices. Left: CorCap^{TM} (Acorn Cardiovascular Inc., St Paul, Minn USA). Right: HeartNet^{TM} (Paracor Medical Inc., Sunnyvale, CA USA). Reprinted from Kwon *et al.* [72] with permission from Elsevier.

Alternatively, epicardial patches could be applied to reinforce the ventricular wall by tissue bulking (see equation (2.1)) [63] with stiffer materials and more added fractional volume attenuate wall stress better [8]. Specific biomechanical properties provided by respective engineered microenvironment and architecture of such patches may have additionally the potential to support cellular differentiation and organisation of resident cardiac cells, promote angiogenesis and encourage the endogenous regenerative capacity of the myocardium [61, 78]. A number of studies have evaluated the effect of various patch compositions on the stabilisation of the myocardial wall and finally the prevention of geometrical and structural remodelling [78-83]. Evaluated patches were manufactured from both natural and synthetic materials or even a composition thereof by applying diverse production techniques ranging from thermally induced phase separation [79, 80] to two stream electrospinning processes [82] for instance. All applied epicardial patches improved cardiac performance (elevated levels of LVEF and LV fractional shortening), inhibited maladaptive geometrical and structural changes and promoted angiogenesis. Chi *et al.* [81] could even verify significantly elevated levels of secreted paracrine factors such as VEGF. However, all studied epicardial patches so far had to be delivered to the heart surface via surgical interventions and with exception of the adhesive patch recently developed by Lin *et al.* [83] sutured to the heart surface

addressing the motivation for development of novel minimal-invasive delivery approaches, which are part of my work presented in chapters 3 and 4.

Motivated by the main drawback of epicardial patches to require a surgical access for their administration to the heart surface, injectable biomaterials as alternative strategy have been pursued with growing efforts during the last years to propel the delivery of biomaterials towards a more minimal-invasive mode [6, 8, 63]. Hydrogels are polymeric materials characterised by the feature of being capable to turn from a liquid into a solid gel phase upon crosslinking by a specific physical or chemical stimulus [84, 85]. Hence, they can be applied in liquid form allowing them to be delivered minimal-invasively. Based on their ability to absorb huge amounts of water comparable to natural ECM [84], hydrogel based scaffolds have consequently received increasing attention to mechanically support the ventricular wall. Injectable hydrogels being studied in animal models to provide mechanical reinforcement to the ventricle comprise both natural and synthetic based materials including fibrin, collagen, gelatine, chitosan, hyaluronic acid, agarose, self-assembling peptides, alginate, Matrigel™, silk fibroin, polyethylene glycol, polyvinyl alcohols or acrylamide referring to various reviews [8, 63, 84-87]. Christman *et al.* [88] were the first, who successfully proved the ability of an injectable biomaterial alone to attenuate changes in fractional shortening, preserve infarct wall thickness and thus cardiac function. Moreover, Lee *et al.* [77] could already demonstrate therapeutic benefit of this concept by circumferentially injecting an acellular alginate based hydrogel called Algisyl-LVR™ (LoneStar Heart Inc., CA USA) in failing human hearts. They could provide evidence to increase EF and wall thickness as well as to decrease ventricular volumes myofiber stress. Most studied hydrogels were endocardially injected into the myocardium by employing respective catheter technologies providing a minimal access directly to the ischemic myocardium [3, 6, 63, 89, 90]. However, injecting *in situ* polymerizable biomaterials into the beating heart wall is a technically challenging intervention requiring calibrated equipment and expert operators for the procedure. The most serious risk of this procedure is potentially occurring material dissemination into the ventricle lumen, resulting in systemic embolization [89]. Hence, the gelation kinetics of the respective hydrogel needs to be adequately adapted so that life-threatening material leakage is excluded. A too short gelation time should be on the other hand also avoided since rapid gelation

may cause occlusion of the catheter needle [63]. The needle injection additionally may cause tissue injury and mechanical stress to the myocardium [3]. Other common problems of needle-based administration into dense tissues such as the myocardium are associated with backpressure and biomaterial reflux, needle track leakage, needle deflection or the challenge in case of multiple insertion points (see a review provided by O'Cearbhaill *et al.* [91] for more details). The novel epicardial carrier device developed within the framework of this thesis (see Chapter 3) thus aims to avoid these imposed constraints given by the administration approach on the design of the applied biomaterial.

2.3.4 Combination of biological and mechanical support: Adequate delivery as key component for therapeutic efficacy

Epicardial patches and injectable hydrogels have additionally received increasing attention regarding cell-based therapies as they may serve as provisional scaffold for exogenously administered cells [6, 60-63, 89, 92]. Cell differentiation and proliferation in living tissue is inevitable connected to a proper structural support which is naturally provided by the ECM. The collagenous scar tissue formed after MI however lacks from essential properties that are required to provide an adequate microenvironment for exogenously administered cells hindering their effective engraftment [35]. Scaffolds with appropriate architecture [93, 94] are indicated to enhance the cell survival in the harsh post-MI environment given by its larger surface area for instance which is capable to adsorb more proteins that in turn provide more binding sites for the cells and improve their survival. A significant number of preclinical studies as well as most of the clinical studies have moreover employed comparable simple methods such as saline-based cell solution which were either systemically administered or locally injected [63]. However, only a limited fraction of delivered cells can be retained even in case of intramyocardial injection when administered as simple suspension. Hou *et al.* [95] determined for instance merely 11 % cell retention just 1 h after direct injection into the heart muscle. A significant fraction of the delivered cells excited the heart into the pulmonary circulation. Superior results were however achieved by deploying biomaterials as preliminary

scaffold for the cells. Cell retention could be increased up to 60 % retention after 24 h [96].

Apart from choosing a suitable vector and adjusting a proper virus dose, the development of an adequate method for the vector delivery was considered as key component affecting cardiac gene therapy efficacy. Commonly applied strategies such as intravascular and pericardial injection have the advantages of simplicity and safety. However, only a fraction of the administered vectors take effect on the region of interest. Intramyocardial injection bypasses the impermeable endothelial barrier but is impaired by general obstacles associated with needle-based injection approaches such as leakage during delivery [70, 97-99].

Elaborated delivery strategies are also needed in terms of protein-based therapeutics to enable their directed and controlled application to the heart muscle. Depending on the local protein concentration and its gradient, the effects exerted by the delivered proteins may vary from inadequate to beneficial. The ability to control their concentration and spatiotemporal gradients upon delivery is vital to successfully exploit their complete therapeutic potential [64]. Analogously to cell-based strategies, patches and hydrogels turned out as promising carrier for proteins itself but also for more sophisticated constructs such as protein-encapsulating micro- and nanoparticles to enable better control of their release [3, 64]. Still, the delivery of patches and hydrogels in an always uniform, minimal-invasive way to the heart independently of the biomaterial and therapeutics to be applied is limited to date. The devices developed within the framework of this thesis are promising alternatives with the potential to overcome the issues associated with previous devices.

3 A bioresorbable carrier device for hydrogel-based biomaterials

3.1 Preface

The AMCARE (**A**dvanced **M**aterials for **Ca**rdiac **Re**generation) project funded by European Union's 'Seventh Framework' program for research, technological development and demonstration under Grant Agreement n° NMP3-SME-2013-604531 aimed to address current limitations of previous regenerative strategies thus achieving a truly restorative therapeutic approach for the injured myocardial tissue after MI. Coordinated development of respective biomaterials providing a provisional ECM for exogenous cells and accommodation for protective bioactive substances in combination with advanced delivery strategies adjusted to the needs of the respective biomaterials should push cardiac regeneration approaches to a next level feasible to better exploit the therapeutic potential of exogenous cells and bioactive substances, respectively. As part of AdjuCor's responsibility within the framework of this project, my work focused on the development of a novel bioresorbable carrier device which is capable to facilitate targeted local delivery of an *in situ*-curing, fast-gelling hyaluronic acid- (HA-) based hydrogel to the epicardial heart surface in coordination with the other project partners. Both preliminary *in vitro* trials to assess device compatibility with the respective biomaterials and pre-clinical *in vivo* studies to evaluate feasibility and efficacy of the overall concept were part of my work in close collaboration with the other project members. Some results associated with this novel and patented **S**urface **P**rone **E**pic**A**rdial **D**elivery **S**ystem (SPREADS) [100, 101] were partially published in Materials Science & Engineering C [76] recently. My contribution to both the published manuscript and the patents is outlined in the previous Chapter "Contributions".

3.2 Introduction

Based on the potential to manipulate the pathological cascade after MI, regenerative approaches and especially cell-based technologies have emerged as promising strategy preventing maladaptive remodelling processes of the ventricular wall [3, 8, 35, 59, 63] (see also section 2.3.2). It is assumed, that exogenous stem or progenitor cells with cardiogenic potential may account for both a protective effect of the viable myocardium after MI through release of paracrine factors [66, 102] but also for a restorative effect by promoting remuscularisation through generation of new functional CMs [66, 67]. After overcoming initial issues associated with lineage-unspecific cell mixtures, retention and survival challenges associated with initial simple delivery approaches of liquid cell suspensions [35, 95, 96] have been resolved by employing especially hydrogel-based biomaterials. Hydrogels can be tuned to serve as adequate ECM surrogate with improved growing and attachment conditions [66, 84].

Owed to the unique feature of hydrogels to transit from a liquid into a solid gel phase upon a specific stimulus, catheter-based transendocardial delivery strategies have been pursued with growing efforts to enable minimal-invasive administration of hydrogel-based biomaterials to the myocardial wall [63, 90, 91, 103, 104]. Even though continuous progression in catheter technology moved this delivery approach closer to clinical translation, individual viscosities of each hydrogel accompanied with different resistances of applied cells towards executed shear stress during injection still hinder the applicability of a single catheter type for a wide range of different materials and cells. Apart from constructional features such as the length of the catheter and the needle diameter, mechanical properties of the injected hydrogels highly influence the volume of the retained hydrogel [103, 104]. Intramyocardial injection approaches additionally require multiple injections to facilitate an equal distribution of the respective hydrogel to the distinct zones of the infarct area [91, 104]. Multiple injections however pose an increased risk of tissue trauma, which is especially pronounced in case of a dynamic organ such as the heart. Particularly in case of large infarcts, intramyocardial injection are not the preferred approach for an optimal therapy [76, 91].

As the epicardium has been identified as region with vast regenerative potential [105], direct application of biomaterial-based stem cell therapy to the epicardial surface may represent reasonable target that is capable to offer a large and homogenous coverage of the area topically to the infarcted ventricle wall instead with the potential to overcome previously discussed approach-related issues [56, 76]. Various types of natural and synthetic based hydrogel-based biomaterials have been studied to mechanically reinforce the injured ventricular heart wall (see section 2.3.3) or as ECM surrogate for cell-based regenerative strategies [87, 94]. However, the majority of currently studied hydrogels is characterized by low viscosities [90, 106] and intrinsic poor adhesion properties [107] in their liquid phase, especially to soft tissue surfaces in a wet environment such as the epicardial heart surface. Hence, a controlled and targeted administration of an *in situ* curing hydrogel-based biomaterial in its pre-curing state to a selected area on the dynamic heart surface without undefined dispersion of the hydrogel represents a remarkable challenge. But physical-chemical properties required to facilitate a minimal-invasive application and stable attachment of the hydrogels to the epicardial heart surface differ notably from preferred properties to provide an adequate environment for exogenous cells. Natural materials are the preferred choice especially for cell-based approaches compared to synthetic materials due to their superior cell and tissue compatibility which trigger less cytotoxic effects accompanied with a reduced risk of an immune response *in vivo* [76]. But insufficient mechanical properties of most natural materials such as low mechanical stiffness negate their potential to be directly applied to the epicardial heart surface. Their inadequate stability towards frictional stress provoked by the relative movement of the pericardium may cause partial displacement or even disintegration of the applied biomaterial [76, 87]. Natural biomaterials are additionally restricted to provide an adequate mechanical support to the fragile ventricular wall due to their intrinsic low mechanical stiffness [76, 108]. Synthetic materials on the other hand are privileged in terms of their capability to easier adjust the required mechanical and chemical properties but can induce cytotoxic reactions in case [76, 87]. A synergistic approach is consequently needed considering respective material requirements that enable a successful cell translation in a minimal-invasive fashion to the epicardial heart surface post-MI.

The novel carrier device developed as part of my work within the framework of the AMCARE project targets previously discussed application-related issues with the potential to better exploit the complete therapeutic potential of the applied cells. It is hypothesized that such an epicardial carrier device could capture both mechanical support to the fragile heart wall and provide in parallel an adequate environment promoting survival of the applied stem cells *in situ*, their migration and release of paracrine factors into the epicardial tissue. Based on the specifications given by the respective partners within the AMCARE project, my work focused on the creation of a novel patch which is feasible to encapsulate an *in situ* curing, fast-gelling hyaluronic acid-based hydrogel provided by Contipro (Czech Republic) that can be alone or loaded with human cardiopoietic ADSCs (c-ADSCs) provided by Celyad (Belgium) administered in a minimal-invasive way to the epicardial heart surface. Apart from its primary function as cargo device for biomaterials loadable with therapeutic agents it is furthermore assumed, that this patch may also serve as passive restraint thus imbibing a synergistic role in heart regeneration: temporary stabilization and biological support (see Figure 3.1). The concept development of SPREADS focused on its feasibility to administer Contipro's hydrogel to a well-defined area without fluid leakage and to facilitate sustained contact of the delivered hydrogel to the epicardial heart surface without employing any surgical aids. After adjusting the mechanical and viscoelastic properties of Contipro's hydrogel to the needs of the Celyad's cells by other project partners, the viability of the cells encapsulated in SPREADS was investigated in collaboration with Contipro and the Royal College of Surgeons in Ireland (RCSI). SPREADS' ability to be minimally-invasively implantable was verified in an acute porcine *in vivo* study. The therapeutic efficacy was finally assessed in a chronic porcine study by applying with the aid of SPREADS Contipro's hydrogel with or without Celyad's c-ADSCs 14 days post-MI to the epicardial heart surface topically to the infarct and comparing it to gold standard pharmacological therapy. The overall objective was to show that SPREADS can accomplish the delivery of exogenous cells immersed in a hydrogel-based biomaterial to the epicardial heart surface minimally-invasively and encourage cardiac regeneration post-MI [76].

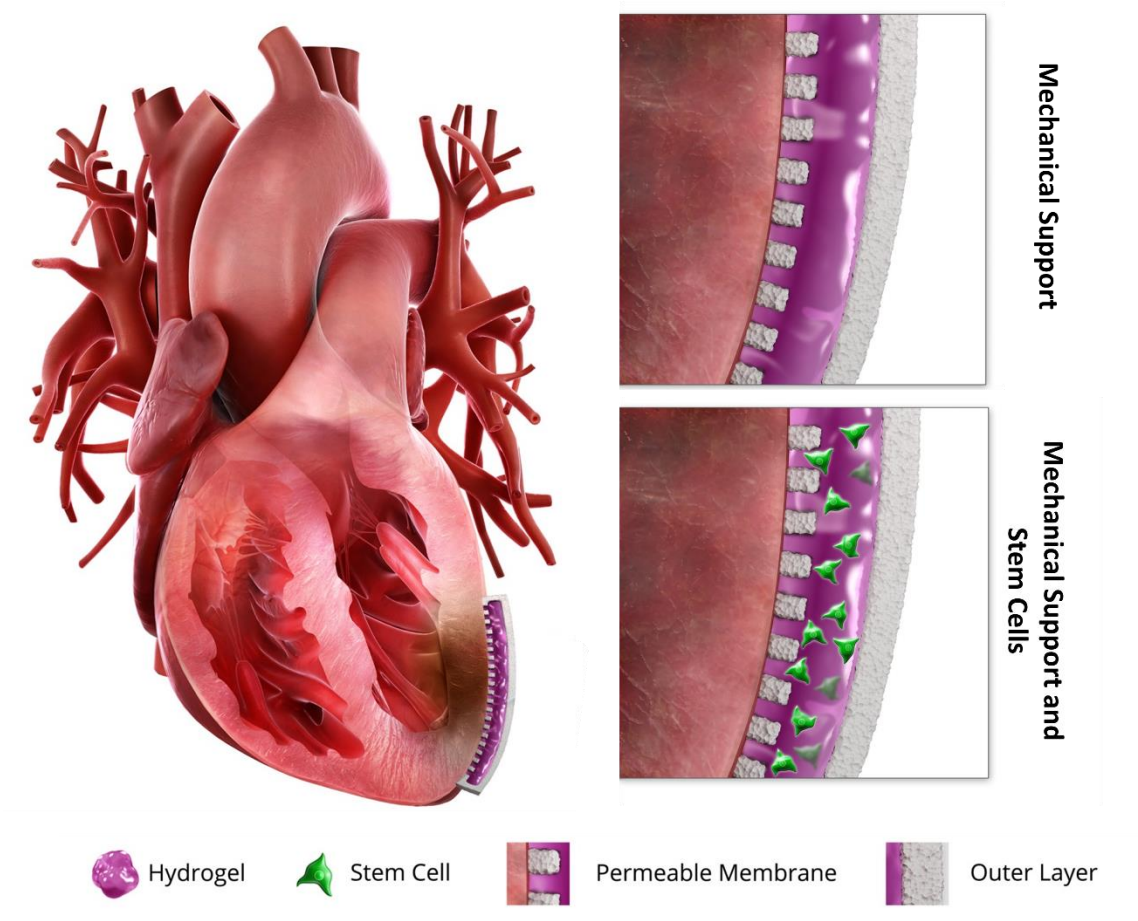

Figure 3.1: Schematic cross section of SPREADS placed on the epicardial heart surface topically to the infarcted heart wall. The illustration shows SPREADS with an encapsulated fast-gelling hyaluronic acid-based hydrogel alone or loaded with c-ADSCs indicating its synergistic potential to provide both mechanical and biological support to the injured myocardium post-MI. Reprinted from Dolan *et al.* [76] with permission from Elsevier.

3.3 Materials and methods

3.3.1 Concept development

Design generation 1

Controlled and targeted application of an *in situ* curing hydrogel such as the HA-PH-RGD hydrogel provided by Contipro in its pre-curing liquid phase to a well-defined area on the dynamic heart surface requires the ability to provide a defined space into which the hydrogel can be injected to prevent undefined dispersion of the injected hydrogel. To avoid backpressure associated issues as detected in case of needle-based intramyocardial injection [91], the initial concept development of SPREADS targeted to create a clearly defined reservoir with specified volumetric capacity. For implementation of this essential requirement a bulge like structure was considered in the outer layer of SPREADS enabling the specification of a defined room for the hydrogel administration. A truly separated lumen avoiding leakage of the initially fluid hydrogel until curing should be created by joining the outer layer with a second inner layer along its circumferential flat edge as shown in Figure 3.2. An additional challenge was to obtain a suitable adhesive strategy to ensure sustained contact of the injected hydrogel with the intended injured tissue area. The second layer was intended to facilitate sufficient adhesion of SPREADS to the wet epicardial heart surface exclusively through its capillary forces. Both layers were intended to be porous, a prerequisite for an adequate integration in the surrounding tissue [8, 109] and to facilitate sufficient interaction of the delivered hydrogel with the weakened myocardium. However, undefined leakage when injecting fluid hydrogels in its pre-curing state should be avoided by adaption of the respective porosities. The outer layer additionally aimed to provide mechanical support to the fragile myocardial wall after MI and to offer protection of the hydrogel against frictional stress provoked by the relative movement of the pericardium [76].

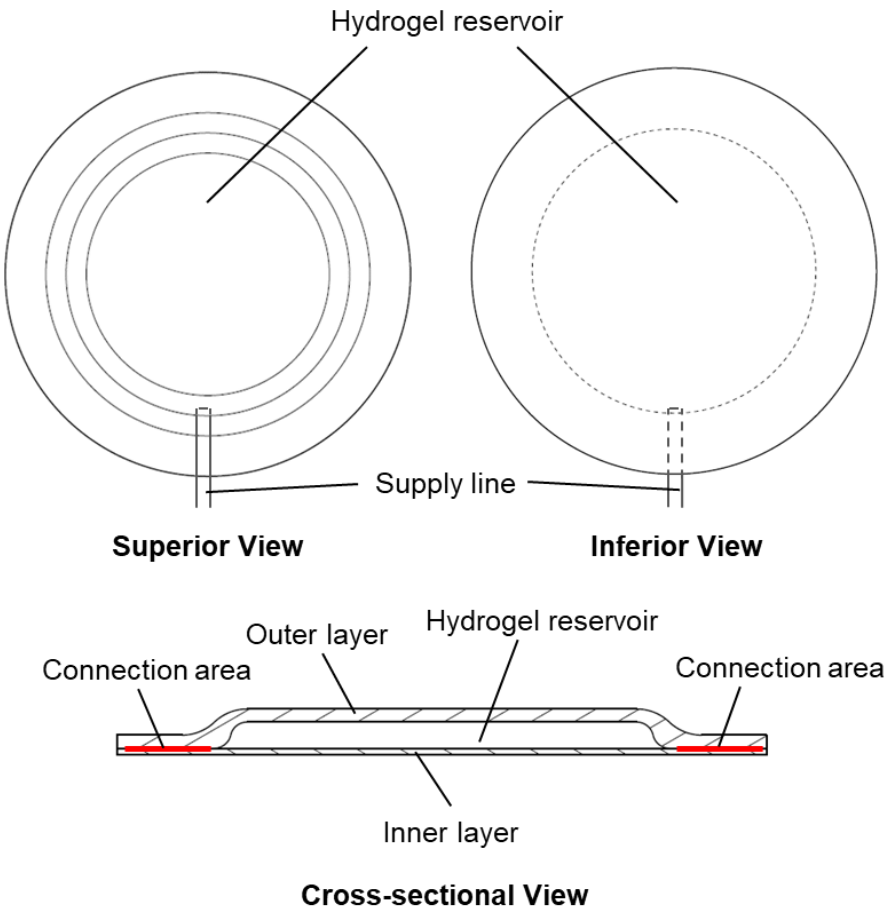

Figure 3.2: Superior, inferior and cross-sectional view of the first design concept for SPREADS consisting of an outer layer with bulge like structure in the centre that is intended to be connected along its flat edge with a second layer to generate a truly separated lumen into which a fluid hydrogel can be injected. The connection areas are indicated as red lines, respectively.

Design generation 2

The patented second design concept [100, 101] principally based on the first design generation but pursued another approach in terms of adhesion strategy. The respective design features of concept generation 2 are shown in Figure 3.3. The second design concept intended to facilitate stable attachment of SPREADS by additionally applying a biological adhesive to SPREADS. The bioadhesive was intended to be selectively released to ensure firm adhesion on the one hand but also to prevent spillage of the applied adhesive to the central space reserved for the therapeutic hydrogel [76, 100, 101].

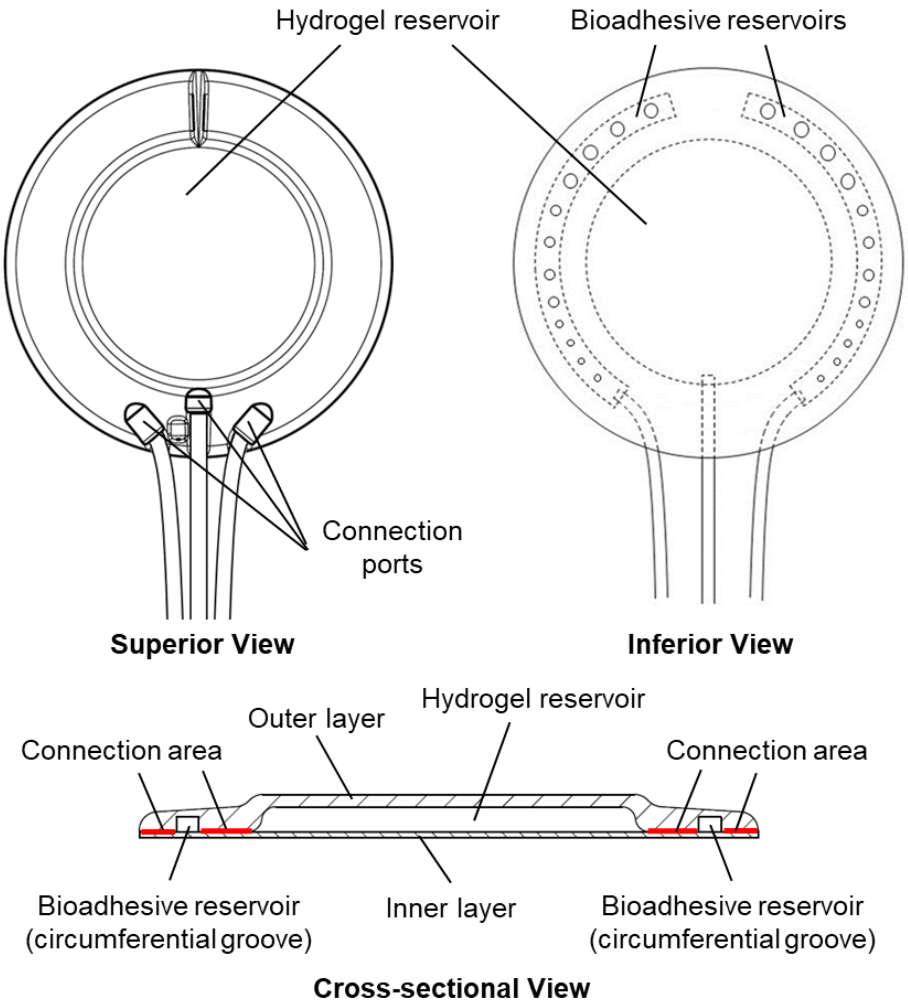

Figure 3.3: Superior, inferior and cross-sectional view of the second design concept for SPREADS consisting of an outer layer with a bulge like structure in the centre, two half-circumferential grooves along its edge and dome-like structures on its outer surface. The outer layer is intended to be joined with the inner layer along the respective cavity borders considered in the outer layer as indicated by the red lines, respectively. Reprinted from Dolan *et al.* [76] with permission from Elsevier.

Two half-circumferential grooves were incorporated in the outer layer along its edge in addition to the central bulge like structure. By interconnecting of the outer layer with the inner layer along the respective cavity borders considered in the outer layer of SPREADS, two additional separated lumina are intended to be generated besides the central hydrogel reservoir serving as independent bioadhesive reservoirs, respectively. The inner layer was additionally planned to be partially perforated in the region of each circumferential groove considered in the outer layer to ensure a defined release of the bioadhesive to the heart surface guaranteeing a safe fixation of SPREADS [76, 100, 101]. The second design generation considered moreover dome like structures on the outer surface of the outer SPREADS

layer which were aimed to serve as defined connection ports for the supply lines to the hydrogel and bioadhesive reservoirs. These ports intended to improve the linkage of the respective supply lines to the outer layer of SPREADS and to eliminate the potential risk to injure the second layer of SPREADS during the implantation procedure [76, 100, 101].

3.3.2 Production of SPREADS components

All SPREADS generations were principally made of two individually manufactured polymer layers [76]. The outer layer of each generation consists of a lysine diisocyanate (LDI) ethyl ester based poly(L-lactide-co-ε-caprolactone) (PLA-co-PCL) polyurethane (PU) foam [76, 110] and was kindly manufactured by INNOVENT e.V. according to their previously published protocol [110]. Briefly, the polyol component of the PU foam was made of a PLA-co-PCL-based, star-shaped oligoester that was generated by opening polymerization of L-lactide and ε-caprolactone with meso-erythritol as starter molecule. This PLA-co-PCL prepolymer was afterwards converted with LDI to generate the reactive PU-prepolymer with respective isocyanate-endcaps. Subsequently, the synthesized reactive PU-prepolymer was thoroughly mixed with dimethyl sulfoxide (DMSO), 1,4-diazabicyclo[2,2,2]octane (DABCO), LDI and water to initiate the foaming process [110]. This reactive mixture was finally cast into specific polytetrafluoroethylene (PTFE) moulds to generate the respective constructed outer layer considering all essential design features of the corresponding concept generation [76]. All PTFE moulds were milled from PTFE plates which were purchased form KTK (Germering, Germany). The respective technical drawings are attached in Appendix I, section 7.1.1.

The inner layer of each SPREADS generation was made of an electro-spun poly(ester urethane) (PEU), which was kindly manufactured by INNOVENT e.V. as previously reported by Gugerell *et al.* [111]. Briefly, an initial mixture of 1,8-octanediol and L-lactide was converted with the aid of catalytic stannous octoate followed by the addition of ε-caprolactone and further catalytic stannous octoate to generate the octanediol-bis(L-lactide-co-e-caprolactone) polyester-prepolymer. Like the outer layer, LDI was subsequently added to synthesize the respective isocyanate-terminated PLA-co-PCL prepolymer. Polyethylene glycol (PEG) 1000 was added in the last step to this isocyanate-terminated second prepolymer to generate PEU, which was finally employed to generate electro-spun PEU fleeces [111] for further assembly with the outer poly(ester urethane urea) (PEUU) foam [76].

3.3.3 Final assembly of SPREADS

For both design concepts of SPREADS, the PEUU foam and PEU fleece were thermally joined along the respective cavity borders considered in the PEUU foam, respectively [76] (see cross-sectional view of Figure 3.2 and Figure 3.3). In case of design generation 1, the connection was accomplished by manually pressing the PEU fleece with pre-heated forceps against the PEUU foam and keeping the forceps applied to the respective area on the PEU fleece for at least 3 seconds. A connection to the central cavity given by the shape of the outer PEUU foam was finally established by carefully pushing a supply line (0.86 x 1.75 mm, Medi-Line Inc., France) through the outer surface of the PEUU foam.

In case of SPREADS generation 2, both layers were thermally joined in specific areas by putting the PEUU foam with its heart averted surface in a separate positioning mould, placing the PEU fleece on top, pre-pressing the PEU against the PEUU foam with a PTFE stamp and finally pressing a pre-heated steel stamp on the PEUU fleece (see following schematically illustrated procedure in Figure 3.4). Both stamps have customized milling grooves to enable a connection of the PEUU foam and PEU fleece in well-defined regions.

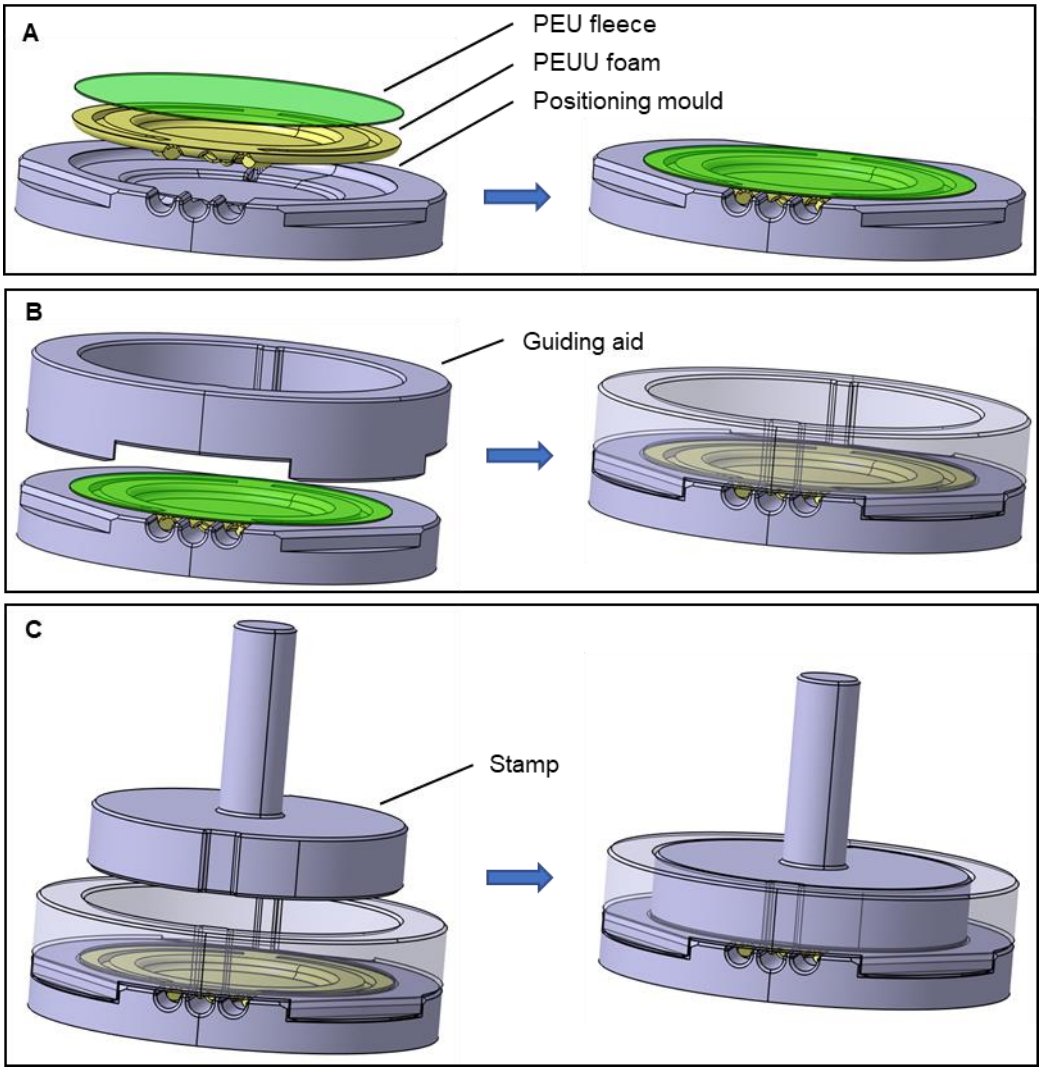

Figure 3.4: Schematic illustration of the procedure to thermally join the outer and inner layer of SPREADS' second design generation. (A) First, relative arrangement of both layers in a specific positioning mould. (B) Second, guiding aid placement for the respective stamp (PTFE- or steel-based) to (C) finally press a pre-heated steel-based stamp on the PEU fleece.

After thermal joining, the PEU fleece was additionally in the region of both circumferential grooves partially perforated with the aid of 0.4 mm and 0.8 mm cannulas. A plate with specific slot pattern serving as perforation aid ensured the exact positioning of the respective cannulas (see Figure 3.5).

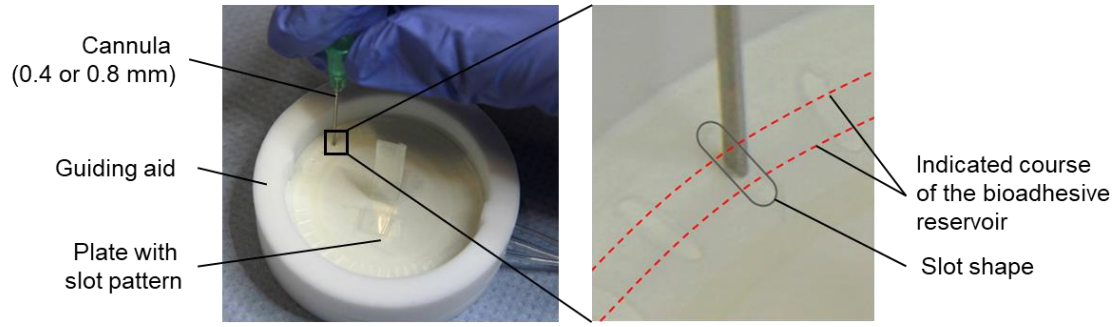

Figure 3.5: Procedure to perforate the PEU fleece along both circumferential bioadhesive reservoirs.

Supply lines (0.86 x 1.75 mm, MEDI-LINE SARL, Hundling, France) to the central and both circumferential grooves with a total length of 30 cm in each case were connected with the foreseen ports at the outer surface of the PEUU foam. The technical drawings of all aids employed for the final assembly of SPREADS in case of design version 2 are attached in Appendix I, section 7.1.2.

3.3.4 Assessment of SPREADS' degradability *in vitro*

The employed procedure to assess the long-term *in vitro* degradation of SPREADS has been already published by Dolan *et al.* [76]. Briefly, SPREADS' degradability was examined by incubating triplicate samples (10 – 50 mg) at accelerated oxidative conditions based on the experimental setup which has been already described by Weems *et al.* [112] and determining the mass loss. The samples were immersed in 1 mL of a phosphate buffered saline (PBS) based solution with 20 % (w/w) hydrogen peroxide (H_2O_2) (#9681.1, Carl Roth GmbH, Karlsruhe, Germany) and 0.03 M cobalt chloride ($CoCl_2$) (#769495-100G, Sigma-Aldrich, Steinheim, Germany) at 37 °C for up to 27 days. Incubation in this oxidative solution over 259 days corresponds to 1 year implantation *in vivo* based on a previously described correlation from Dempsey *et al.* [113]. Oxidative radicals present at the material-macrophage interface *in vivo* are simulated by oxygen and hydroxyl radicals that are generated from hydrogen peroxide through cobalt ions. The oxidative solution was changed every 3-4 days to maintain a relatively constant concentration of the radicals [76, 113]. The incubated samples (n = 3) were removed at 2, 7, 13, 17 and 27 days, dried under vacuum at ambient temperatures (Alpha 2-4-LOC1-M, Martin Christ Gefriertrocknungsanlagen GmbH, Osterorde am Harz, Germany) overnight

and weighed (Sartorius A200S Electronic, Sartorius AG, Göttingen, Germany). The weight loss W_t was determined according to following equation (3.1)

$$W_t = \frac{m_0 - m_t}{m_0} \cdot 100\% \tag{3.1}$$

with m_0 corresponding to the initial mass and m_t representing the weight of the dried sample at time t, respectively [76].

3.3.5 Preparation of the HA-PH-RGD hydrogel

Contipro's (Czech Republic) HA derivative HA-PH-RGD (60-90 kDa) modified with both hydroxyphenyl (PH) and RGD moieties was synthesised according to Contipro's protocol which has been already published by Dolan *et al.* [76]. For hydrogel preparation, Contipro's provided HA-PH-RGD powder was rehydrated in phosphate-buffered saline (PBS) (pH 7.4) overnight to form a 2 % w/v solution. The curing of the hydrogel was accomplished by horse radish peroxidase (HRP) and H_2O_2, which enzymatically crosslink the PH moieties. The HRP stock solution with a final concentration of 8 U/mL was prepared by dissolving HRP powder in 0.1% Bovine Serum Albumin (BSA) in PBS (pH 7.4). The final HRP stock solution was aliquoted and stored at -20 °C. 0.1 % (w/w) H_2O_2 solution was prepared fresh for every use. The 2% HA-PH-RGD solution was divided equally into two separate vials for hydrogel preparation, which are referred as hydrogel precursor solutions part A and part B. HRP stock solution was added to part A with the amount depending on the required cross-linking density of the final hydrogel, as shown in Table 1. Similarly, 0.1 % H_2O_2 solution as shown in Table 1 was added to part B. Parts A and B were mixed for 2 minutes to generate homogenous solution, respectively. Each precursor solution was drawn into a separate syringe (1 mL, Becton Dickinson Inc., Franklin Lakes, NJ USA) and mounted to the hydrogel mixer (ML2.0-16-LLM 1:1 mixer, Medmix Systems AG, Risch-Rotkreuz, Switzerland) containing a static mixer to ensure homogenous gelation. The static mixer was mounted to an adapter (MA 15-00M-L Adapter, Medmix Systems AG, Risch-Rotkreuz, Switzerland) enabling the connection via a Luer-Lock to the supply line which is attached to the hydrogel reservoir of SPREADS to inject 2 mL of the

hydrogel into SPREADS' foreseen gel cavity [76]. The following Figure 3.6 shows the assembled injection system with its respective components.

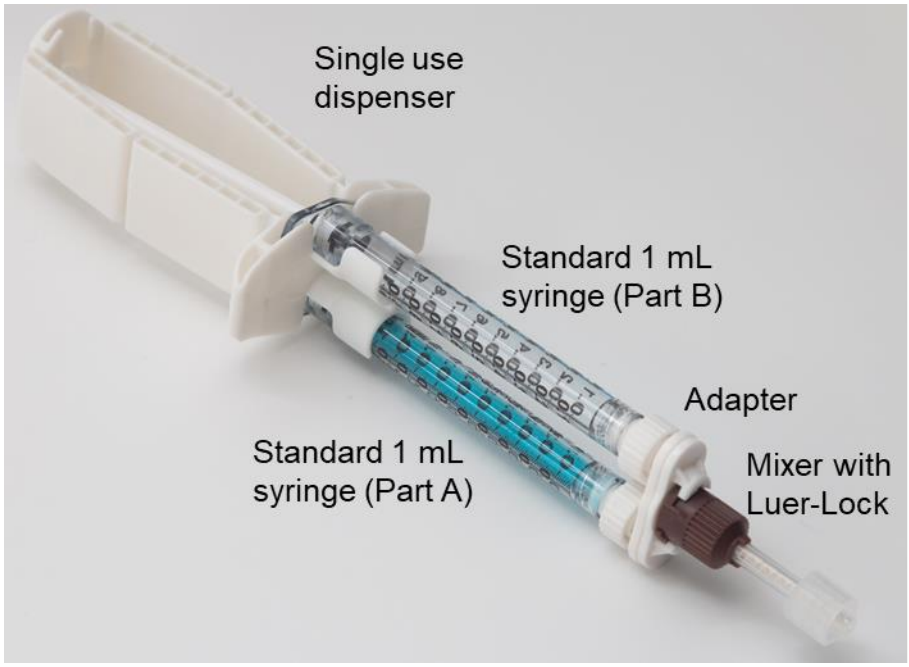

Figure 3.6: Injection system consisting of two standard syringes purchased from Becton Dickinson (USA), an Adapter, mixer with Luer-Lock and single use dispenser purchased from Medmix (Switzerland), respectively. Part A precursor solution was stained with methylene blue for better visual differentiation.

Since inclusion of high cell densities in Contipro's HA-PH-RGD hydrogel has been shown to impair the crosslinking reaction and thus the mechanical properties of the final hydrogel, higher concentrations of HRP and H_2O_2 were employed to ensure comparable mechanical properties of the final hydrogel to the hydrogel version without cells. The shown crosslinking concentration 1 and 2 in the following Table 3.1 were utilized in case of no cells and when 20 million c-ADSCs/mL were encapsulated, respectively [76].

Table 3.1: Employed concentration and activity of crosslinking agents depending on encapsulation 20 million c-ADSCs/mL or not. Adapted from Dolan *et al.* [76].

Crosslinking concentration	Crosslinking agents	
	H_2O_2 [µmol/mL]	HRP [U/mL]
1	1.00	0.24
2	1.66	0.36

3.3.6 Determination of gelation kinetics, viscoelastic and mechanical properties and swelling behaviour of HA-PH-RGD hydrogels

All analyses of acellular and cellular HA-PH-RGD hydrogels prepared by the employed injection system (see section 3.3.5) regarding gelation kinetics, viscoelastic and mechanical properties as well as swelling behaviour were kindly carried out by Contipro and have been already published [76].

Determination of HA-PH-RGD hydrogel gelation kinetics

Evaluation of hydrogel gelation kinetics was required to determine the respective injection speed needed to deliver the desired hydrogel amount to SPREADS foreseen hydrogel cavity before phase transition of the hydrogel has been completed. Gelation was evaluated on an AR-G2 Rheometer (TA Instruments) with a parallel plate (40 mm) geometry and 400 µm gap as already published [76]. Briefly, 525 µL of each precursor solution was added to the plate and homogenized by a pre-shear of 2000 s^{-1} for 1 second. Afterwards, an oscillation time sweep at a frequency of 1 Hz and displacement of 0.001 radian was conducted at 37 °C (n = 5) [76].

Viscoelastic and mechanical characterisation

Viscoelastic properties of the prepared gels were measured by an AR-G2 Rheometer (TA Instruments) by a strain sweep test with a displacement range of 10^{-3} to 2 radians and a constant frequency of 1 Hz (n = 5). The cured hydrogels were placed on a special plate with cross-hatched surfaces to avoid slippage of the prepared hydrogels [76].

Characterisation of the hydrogels' mechanical properties was performed on a Single Column Materials Testing System (INSTRON 3342) in compression mode with a total capacity of 500 N and a compression plate capacity of 100 N. Measurements were carried with a constant testing speed of 2 mm/min [76].

Cylindrical hydrogel samples with a diameter of 11.1 mm (predetermined by the diameter of the respective moulds) and a measured height of 4±0.5 mm were employed for the viscoelastic and mechanical characterisation. Finally, the compressive Young's modulus was calculated as slope of the stress-strain curve between 0 and 10 % strain (n = 3-7) [76].

Swelling ratio of hydrogels

Hydrogel samples prepared from 100 µL precursor solution, respectively, were immediately weighed after preparation, placed into 3 mL of PBS (pH 7.4) at 37 °C for up to 8 weeks and weighed. Swelling ratio Q was calculated as ratio of mass after m_t and before m_0 swelling (n = 5) according to following equation (3.2) [76, 104].

$$Q = \frac{m_t}{m_0} \cdot 100\% \tag{3.2}$$

3.3.7 Assessment of HA-PH-RGD hydrogel cytotoxicity and viability assessment of encapsulated c-ADSCs *in vitro*

In vitro cytotoxicity evaluation of Contipro's HA-PH-RGD hydrogels

To exclude principal potential cytotoxic effects of HA-PH-RGD hydrogels on the cell viability, an EN ISO 10993-5 certified and accredited cytotoxicity assay using a human keratinocyte cell line (HaCaT, DKFZ Heidelberg, myoplasma free) was kindly carried out by the Fraunhofer Institute for Interfacial Engineering and Biotechnology (IGB, Germany). For details regarding the protocol, the reader is referred to [76]. To evaluate the cytotoxic effects of HA-PH-RGD hydrogels on a cell type that is more relevant for the heart, an analogous cytotoxicity assay was carried out by the Fraunhofer IGB with human immortalised cardiac fibroblasts (iCFs, #T0446, abm Richmond, Canada). To achieve the same confluence as with HaCaT cells, 30,000 instead of 20,000 cells were seeded in case of iCFs into each well of a 96-well plate [76].

Effect of application procedure to SPREADS on viability of c-ADSCs

To assess the effect of delivering exogenous cells into SPREADS' hydrogel cavity, 2 mL of Contipro's HA-PH-RGD hydrogel with incorporated c-ADSCs at a final cell concentration of 20 million cells/mL was injected into SPREADS' hydrogel reservoir. c-ADSCs were kindly provided by Celyad (Belgium). Isolation, culture and differentiation of the c-ADSCs was accomplished by Celyad according to previously published protocols [76]. Hydrogel preparation was carried out as described in section 3.3.4 with c-ADSCs incorporated into part A precursor solution (HA-PH-RGD + HRP) at a cell concentration of 40 million cells/mL. Samples for cell viability tests were collected from six different regions throughout SPREADS' hydrogel cavity as shown in Figure 3.7 15 minutes after injection by a 5 mm biopsy punch [76].

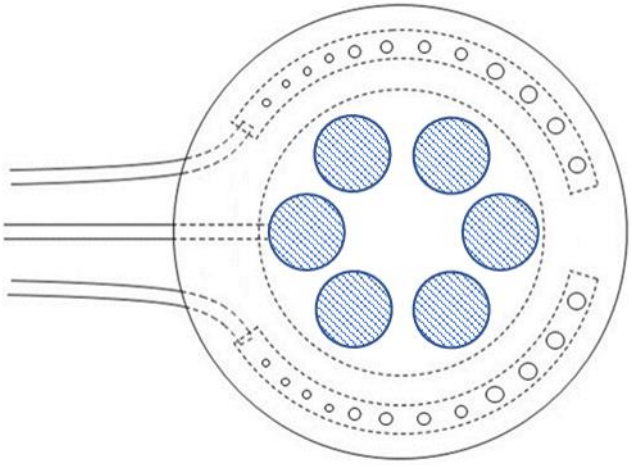

Figure 3.7: Sample scheme to evaluate cell viability after injection into SPREADS' foreseen hydrogel reservoir. The sample regions are shown as blue hatched area, respectively.

Each sample was subsequently transferred to a complete c-ADSC medium and incubated at 37 °C, 5% CO2 and 90 % humidity. The evaluation of cell viability was kindly carried out by Contipro after 24, 48 and 96 h hours by employing the LIVE/DEAD® Viability/Cytotoxicity Kit (BioScience Ltd., Dublin, Ireland) and incubation for 30 minutes in the dark. The incubated samples were analysed by fluorescent microscopy (Nikon Eclipse-Ti) with NIS-Elements AR software to obtain the images. Image analysis was conducted with the aid of CellProfiler software [76].

3.3.8 Suitability assessment of SPREADS' concepts

SPREADS' intrinsic adhesiveness to wet surfaces was evaluated by placing SPREADS design generation 1 with the PEU fleece surface overhead on a with deionized (DI) water pre-wetted poly(methyl methacrylate) (PMMA) plate. A 4%-albumin solution extracted from BioGlue® (CryoLife Inc., Kennesaw, Georgia USA) was afterwards injected into the foreseen hydrogel reservoir to determine the distribution of the liquid within this cavity during the injection procedure.

The assessment of all SPREADS concepts regarding capability to enable the application of an *in situ* curing hydrogel to a well-defined area on the epicardial heart surface and to ensure its sustained contact with the epicardium was carried out on *ex vivo* porcine hearts. All porcine hearts were freshly obtained from a local abattoir and were wetted with DI water to simulate the *in vivo* conditions given in the pericardial cavity before starting the experiments. Each SPREADS version was initially placed on the pre-wetted epicardium and gently pressed along its flat edge against the heart surface. SPREADS' initial attachment to the heart surface under influence of the gravitational force was tested by vertical alignment of the heart, respectively.

In case of SPREADS design generation 1, BioGlue® as substitute hydrogel was subsequently injected into SPREADS' foreseen gel cavity to examine, if inadvertent fluid leakage during the injection procedure could be principally avoided. Removability of the supply line without provoking dislocation of SPREADS was evaluated after curing of BioGlue®. Further evaluation of adhesion strength was conducted for SPREADS design generation 1 by manually grapping specific areas of the PEUU foam with forceps and pulling SPREADS in vertical direction relative to the heart surface. Resistance towards frictional stress evoked by the relative movement of the pericardium was simulated by manually exerting shear stress to the outer surface of SPREADS with cardiac adipose tissue as pericardium substitute.

SPREADS design generation 2 was employed to investigate its compatibility with Contipro's HA-based hydrogel in terms of ability to prevent unintended hydrogel leakage during the injection procedure and to facilitate sustained contact of the cured hydrogel with the epicardium. Contipro's 2 % HA-PH-RGD hydrogel (60-90 kDa) without cells at crosslinking concentration 1 was prepared according to the respective instructions given in section 3.3.4 and was either injected before or after

attachment of SPREADS to the heart surface. For better visualisation of the hydrogel homogeneity, methylene blue stock solution (1 mg/mL dissolved in DI water) was added to hydrogel precursor solution part A with a final concentration of 20 µL methylene blue per 1 mL of the injected HA-hydrogel. The attachment of SPREADS to the heart surface was accomplished by injecting approximately 1 ml BioGlue® within two to five seconds into each of both half-circumferential channels serving as bioadhesive reservoir while keeping forceps applied to the outer surface of SPREADS for at least 20 seconds after finalising the respective injection. Adhesion strength of the complete construct was tested by removing the respective supply lines and elevating the *ex vivo* heart just by pulling on an edge of SPREADS. Uniform distribution of BioGlue® and HA-hydrogel was finally evaluated by cutting SPREADS with the heart below in two halves.

3.3.9 *In vivo* pre-clinical feasibility assessment of SPREADS

The protocol employed to verify the anatomically appropriate delivery and stable attachment of SPREADS to the epicardial heart surface by a minimal-invasive approach *in vivo*, and to demonstrate site-specific application of Contipro's HA-based hydrogel to the surface of a beating heart has been already published by Dolan *et al.* [76]. The pre-clinical feasibility study was approved by the Italian Ministry of Health (protocol n°904/2015-PR) and was carried out in corporation with the AM-CARE project partner Explora Biotech Srl (Italy). All animals were housed in single cages following the Directive 2010/63/EU to ensure sufficient acclimatization before starting with the experiments. Four female Landrace pigs with an average weight of 40.5 ± 3.2 kg were enrolled in this study [76]. Only prototypes of SPREADS' second design generation were employed.

Preparation of the animals

Prior to surgery, 200 mg amiodarone (Sanofi, Italy) were administered 24 h in advance *per os* and further 50 mg were applied as single bolus injection immediately pre-OP. Additionally, all animals received before surgery an intramuscular injection of a premedication mixture consisting of 0.02 mg/kg atropine (ATI, Bologna, Italy), 0.5 mg/kg diazepam (Hospira, Naples, Italy) and 10 mg/kg ketamine (KetaVet 100, MSD, Rome, Italy). Anaesthesia was induced by intravenous injection of 0.5 mg/kg diazepam and 1.5 mg/kg ketamine. After intubation, anaesthesia was maintained with the aid of 2-3% isoflurane (IsoFlo, Esteve, Rome, Italy) by mask and a constant infusion rate of atracurium (1 mg/kg). Moreover, 150 mg amiodarone dissolved in 500 mL NaCl infusion were administered during the entire procedure accompanied with two additional single bolus injections immediately before first incision and first manipulation at the pericardium with the aim to prevent arrythmias. Before starting with the intervention, preparation of each animal followed a defined surgical instrumentation protocol with 10% Poviderm (Farmec, Italy) and Neoxinal Alcolico 0.5% + 70 % (Farmec, Italy) [76].

Implantation procedure

The minimal-invasive implantation of SPREADS was accomplished via a subxiphoidal access as shown in Figure 3.20 A. Straight forceps were employed for handling of SPREADS to achieve the implantation. The access to the pericardial space was generated by a horizontal apical incision of the pericardium with a length of approximately 3 cm. Once SPREADS was placed on the heart surface, BioGlue® (Cryolife Inc., USA) was subsequently injected into both adhesive reservoirs to achieve firm attachment of SPREADS to the epicardial surface while holding SPREADS with the straight forceps in position. Stable fixation of SPREADS was evaluated by both visual inspection checking that all supply lines move synchronously with the heart beat and by slightly pulling on both adhesive supply lines. Afterwards, 2.4 mL of cell-free HA-PG-RGD hydrogel at crosslinking concentration 1 (see Table 3.1) stained with methylene blue for better visualisation were administered to SPREADS' foreseen central cavity at an injection rate of 0.2 mL/s. All supply lines were finally removed once the applied hydrogel was completely

cured. After finishing the intervention, the pericardial incision was left alone because of its very small size required to access the pericardial space for implantation of SPREADS, the skin incision necessary of the sub-xiphoidal access was sutured and the animal was maintained under anaesthesia for 2 hours. Subsequently a full sternotomy was carried out for position and attachment evaluation of SPREADS. Assessment of adhesion quality and retention of the injected hydrogel was assessed after opening the pericardium. Finally, each animal was euthanized by injection of saturated KCl-solution into the left ventricle [76].

3.3.10 *In vivo* pre-clinical efficacy assessment of SPREADS

Details regarding the procedure to assess the pre-clinical efficacy of SPREADS have been already published by Dolan *et al.* [76]. The pre-clinical efficacy study was approved by the Italian Ministry of Health (protocol n°904/2015-PR) and was carried out in corporation with the AMCARE project partner Explora Biotech Srl (Italy). All animals were housed in single cages following the Directive 2010/63/EU to ensure sufficient acclimatization before starting with the experiments. Fifteen female Landrace pigs with an average weight of 39 ± 3.4 kg were used for this study and randomly divided into following treatment groups with five animals per group, respectively. Only prototypes of SPREADS' second design generation were employed.

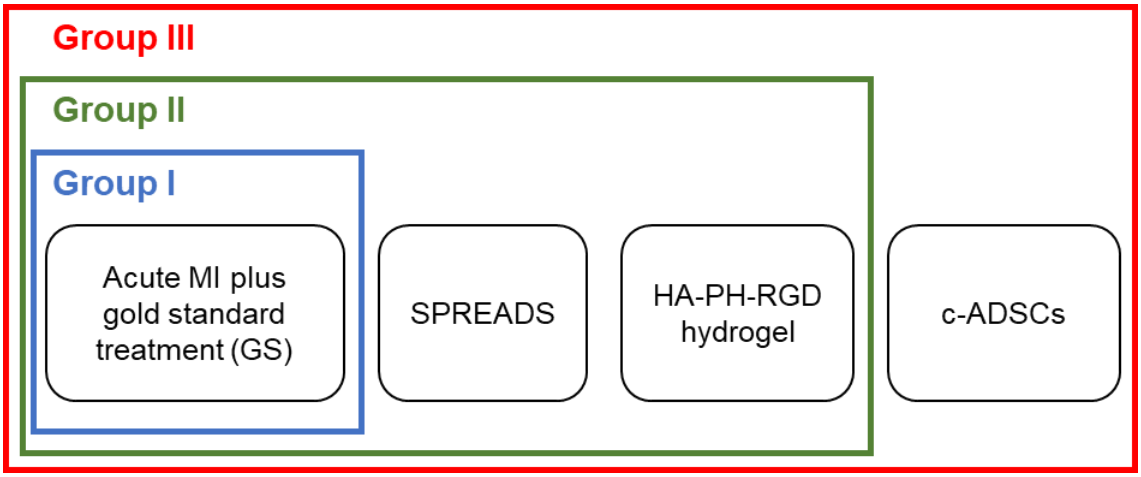

Figure 3.8: Schematic showing the different treatment groups of animals to assess pre-clinical efficacy of SPREADS *in vivo*.

As shown in Figure 3.8, all animals were treated with clinical gold standard (GS) therapy compromising administration of 25 mg Aldactone (Sanofi, Milano, Italy), 5 mg bisoprolol (Recordati, Milano, Italy), 20 mg Enalapril (MSD, Roma, Italy), 100 mg aspirin (Bayer, Milano, Italy) every day over the study beginning at day 14 (beginning of treatment) until euthanasia at day 42 by intravenous administration of 3 mL/10 kg Tanax (MSD, Roma, Italy). The body weight of each animal was continuously monitored over the whole study time. Treatment was started two weeks after inducing acute MI at D1 with a follow-up period of 28 days. Midterm examination of each animal was carried out at D7 and D28 by echocardiography and electrocardiography (ECG). Animals were euthanised at D42 for histological analysis. All animals received 10 mg/Kg ketamine (KetaVet 100, MSD, Rome, Italy), 0.5 mg/Kg diazepam (Hospira, Naples, Italy) and 0.02 mg/Kg atropine (ATI, Bologna, Italy) before surgery. Anaesthesia was induced by intravenous injection of 0.5 mg/kg diazepam and 1-5 mg/kg ketamine. After intubation, anaesthesia was maintained with the aid of 2-3% isoflurane (IsoFlo, Esteve, Rome, Italy) by mask [76].

Induction of acute MI

Induction of acute MI was accomplished by temporary occlusion of the left anterior descending (LAD) coronary artery for 90 minutes as previously described [114-116]. In brief, embolization of the artery distally to the second diagonal branch was accomplished by a 2.5 x 6 mm balloon catheter (Euphora, Medtronic, Minnesota, USA) under angiographic guidance (OEC 9800 Plus, GE HealthCare, Salt Lake City, Utah, USA). Reperfusion after balloon deflation was confirmed by angiography as shown in Figure 7.10 (Appendix I, section 7.1.4). In the post-anaesthesia recovery period and over the following 48 hours post-intervention, the animals were continuously monitored. 200 mg amiodarone (Sanofi, Italy) were administered daily starting one week before treatment (D7) *per os* with the aim to prevent arrythmias during implantation of SPREADS. Additionally, 24 h prior to treatment (D13) administration of 15 mg/kg cyclosporine (CyS A, Sandimmun Neoral, Novartis Camberley, UK) per day was started to suppress the immune system [76].

SPREADS implantation and administration of HA-PH-RGD hydrogels with and without c-ADSCs

14 days after induction of acute MI, each animal was anaesthetized as described before and intubated with a cuffed tracheal tube (7 mm; Medtronic, Italy). The pigs were ventilated mechanically controlled with oxygen (2-3 % inhaled isoflurane) at a respiratory rate of 12-20 per minute. Delivery of SPREADS to the epicardial heart surface and administration of HA-PH-RGD hydrogels with or without c-ADSCs to SPREADS' central hydrogel reservoir was accomplished similarly as specified before. SPREADS was loaded with HA-PH-RGD hydrogel +/- c-ADSCs before implantation of SPREADS to visually confirm uniform hydrogel distribution within SPREADS' foreseen central cavity. Pre-loaded SPREADS was after hydrogel curing implanted as described in section 3.3.9. Continuous monitoring of vital parameters was accomplished during the entire procedure [76].

Cardiac function assessment

Assessment of cardiac function was kindly carried out by Explora Biotech Srl (Italy). With the aim to evaluate therapeutic efficacy of each treatment group, cardiac function was examined by echocardiography and electrocardiography (ECG) as illustrated in Figure 7.11 and Figure 7.12 (Appendix I, section 7.1.4). Echocardiographic images were captured at D1 before acute MI induction, D7, D14, D28 and D42 post infarction under general anaesthesia and in right lateral recumbency. Left ventricular ejection fraction (LVEF) was determined from long parasternal axis images and calculated according to equation (1.2). Diameters of the LV and the end of the diastole and systole (LVEDd and LVESd) were however measured in M-mode short axis view. Analysis of all obtained echocardiographic 2D images was conducted with the aid of the MyLab30 Gold VET software (Esaote). Further assessment of LV systolic function was carried out by determining the fractional shortening (FS) as shown in the following equation:

$$FS = \frac{LVEDd\text{-}LVESd}{LVEDd} \cdot 100\% \tag{3.3}$$

ECGs were recorded at D1 before and 30 minutes after induction of acute MI to validate successful occlusion of the LAD artery and reperfusion, respectively. Analysis of infarct injury was blindly carried out by a cardiologist [76].

3.3.11 Histology and Immunohistochemistry

All histological and immunohistochemical assessments were kindly carried out by project collaborators at the National University of Ireland Galway. Details regarding the employed protocols have been already published by Dolan *et al.* [76]. Briefly, the heart of each pig was initially extracted after euthanasia and stored overnight at 4 °C in PBS solution. Afterwards, the heart was sectioned below the atria into equidistant parallel slices orthogonal to the longitudinal axis [117] to obtain basal (B), mid ventricular (M1-M3) and apical (A) slices with a thickness of approximately 1 cm. Tissue fixation was accomplished in 10 % buffered formalin solution. Afterwards, processed tissue samples were embedded in paraffin wax to generate 5 µm thick sections. Histological sections were subsequently mounted onto glass slides and stained by various histological and immunochemical methods as described in more detail below [76].

Infarct quality was assessed by Haematoxylin and Eosin as well as Masson's trichrome staining as already described previously [71, 118, 119]. For that purpose, histological sections were initially deparaffinized in xylene, rehydrated through graded ethanol washes (100-70 % v/v) to water before starting with the respective staining. The infarct scar extent was examined with the aid of picrosirius red by staining histological sections with 0.1 % fast green (pH 7, Fast Green FCF; Sigma Aldrich) and 0.1 % Sirius red in saturated picric acid (picrosirius red stain), both in the same solution at a 1:1 ratio for 1 hour as already described by Monaghan *et al.* [71]. Subsequently, the histological sections were rapidly dehydrated through graded ethanol washes (70-100 % v/v). Staining was automatically accomplished by employing a Leica ST5010 Autostainer XL (Leica Biosystems; Wetzlar, Germany). Mounting of the slides was performed using a the DPX mountant (Sigma Aldrich) and left in horizontal orientation for five hours to get dried [76].

Picrosirius red stained sections were afterwards analysed by polarized light microscopy with the aim to assess the maturation level of stained collagen fibres. An

Olympus BX4 polarised light microscope (Mason Technology Ltd. Dublin, Ireland) at 20x magnification was employed for that purpose with positioning one polarising lense on the light path before the sample and a second polariser (analyser) after the sample. Polarised light micrographs were taken once at maximum polarisation and orthogonally to the maximum polarisation by respective adjustment of the polarising lenses. The taken images were merged afterwards with the aid of the *MAX* function available by the ImageJ software (freely available from https://imagej.nih.gov/) facilitating the complete visualization of present collagen fibres [120]. After determining the total area which was covered by collagen (calculated in number of pixels employing ImageJ), areas of collagen that polarised in red, orange, yellow and green within each pixel were determined by excluding the dark background with the aid of colour thresholding and selecting unambiguous hue ranges. The portion of each type of polarised collagen on the total amount of collagen pixels was calculated according to the following equations (3.4) to (3.7), respectively:

$$\%\ Red\ fibres = \frac{Red\ pixels}{Total\ Collagen\ Pixels} \cdot 100\ \% \tag{3.4}$$

$$\%\ Orange\ fibres = \frac{Orange\ pixels}{Total\ Collagen\ Pixels} \cdot 100\ \% \tag{3.5}$$

$$\%\ Yellow\ fibres = \frac{Yellow\ pixels}{Total\ Collagen\ Pixels} \cdot 100\ \% \tag{3.6}$$

$$\%\ Green\ fibres = \frac{Green\ pixels}{Total\ Collagen\ Pixels} \cdot 100\ \% \tag{3.7}$$

Additionally, analysis of the fibre direction on the birefringent images was carried out with the aid of the *OrientationJ* plugin in ImageJ enabling fast Fourier transform analysis. The aim was to evaluate the orientation of collagen fibres by analysing the gradient structure tensor with emphasis on fibre direction and examining to which degree a dominant fibre orientation exists in the respective sample [121]. If a local image feature exhibits are certain orientation or not is ascertained by the coherency. Coherency equals 1 in case a local structure exhibits one dominant orientation or 0 in case the local structure is essentially isotropic in the local neighbourhood.

For immunofluorescence staining, 5 µm thick paraffin sections were dewaxed and rehydrated though graded ethanol washes (100-70 % v/v) to water before heart

mediated antigen retrieval was carried out in sodium citrate buffer with tween. As samples were blocked by peroxidase, incubation with a rabbit primary CD31 antibody (Ab28364, Abcam, Cambridge, United Kingdom) was carried out for 1 hour in a 1:150 dilution at room temperature. Visualisation of this primary antibody was accomplished by employing a goat anti rabbit secondary antibody as described by the manufacturer's instruction in the used Dako EnVision™ kit (Dako Denmark A/S, Glostrup, Denmark) resulting finally in the formation of brown 3,3'-diaminobenzidine (DAB). Subsequently, histological sections were counterstained by Haematoxylin, dehydrated through graded ethanol washes (70-100 % v/v), cleared in xylene before finally mounted. A virtual slide microscope (Olympus VS120) was employed to capture respective immunohistochemical images and processed by the Olympus software (OlyVIA Ver2.9). Quantification of CD31-positive blood vessels was randomly carried out on 10 fields per infarct zone, border zone and unaffected adjacent myocardium, respectively, in each section by two blinded experts [76].

Separate sections of the infarct zone (GS n = 4, GS + SPREADS + Gel n = 5, and GS + SPREADS + Gel + Cells n = 3), border zone (GS n = 4, GS + SPREADS + Gel n = 5, and GS + SPREADS + Gel + Cells n = 3), and adjacent myocardium (GS n = 4, GS + SPREADS + Gel n = 4, and GS + SPREADS + Gel + Cells n = 3) were evaluated for each treatment group with *n* referring to the amount of enrolled animals per treatment group, respectively [76].

3.3.12 Statistical analysis

Prior to examination of statistical significance, normal distribution of respective data was verified by employing the Shapiro-Wilk test. A Student's t-Test was applied in case of comparing two groups. A one-way ANOVA with Tukey's post-hoc test was applied to compare Young's moduli, amount of CD31-stained blood vessels, relative amount of birefringent fibres and fibre coherency. A two-way ANOVA with Tukey's post-hoc test was applied to determine differences between the treatment groups in terms of cardiac function (% LVEF, FS, LVEDd, LVESd). Significance was considered for $p < 0.05$, respectively. Unless otherwise stated, all data are depicted as mean ± standard deviation [76].

3.4 Results

3.4.1 *In* vitro material characterisation of SPREADS

The ultrastructure of the PEU fleece was analysed by scanning electron microscopy (SEM), which was kindly carried out by project collaborators at the National University of Ireland Galway. The SEM image of the PEU fleece with its corresponding pore size distribution is shown in the following Figure 3.9. The electron-spun PEU fleece is characterized by a high degree of interconnective porosity and surface-volume ratio, a prerequisite to facilitate the sufficient nutrient and oxygen supply to exogenous cells on the one hand as well as removal of metabolites such as carbon dioxide and other waste products from cells on the other hand [35]. Analysis of the SEM image revealed a homogenous pore distribution of the PEU fleece with an average pore size of 3.52 ± 1.44 µm [76].

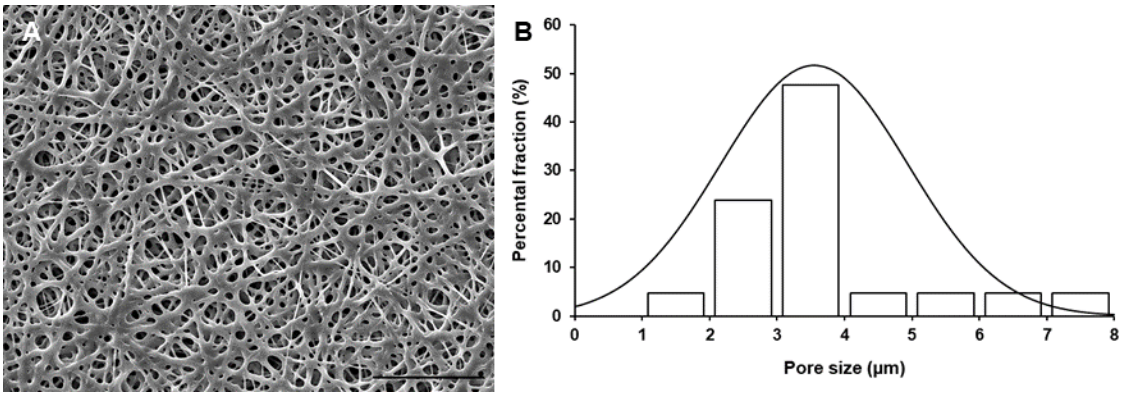

Figure 3.9: (A) SEM image of the PEU membrane (scale bar = 50 µm) (B) Pore size distribution with indicated normal distribution (µ = 3.52 µm, σ = 1.44 µm). Reprinted from Dolan *et al.* [76] with permission from Elsevier.

The following Figure 3.10 A shows the course of SPREADS' mass loss determined at accelerated oxidative conditions *in vitro*. An initial mass loss of 5.6 % was determined after 2 days incubation. The mass loss did not significantly increase for the next 11 days with a total mass loss of 6.5 % after 13 days. A faster degradation rate was subsequently determined with a constant rate of approximately 1.2 % mass loss per day for the following 14 days with a significant mass loss of 4.47 % between day 13 and day 17 ($p = 0.03$). SPREADS could after 27 days incubation at accelerated oxidative conditions no longer be identified as foam. Instead, only a viscous paste could be retained exhibiting no recognizable porosity as shown in

Figure 3.10 B. More than 22 % of the original weight was degraded at that time point (p = 0.006 compared to day 13, p = 0.002 compared to day 17) [76].

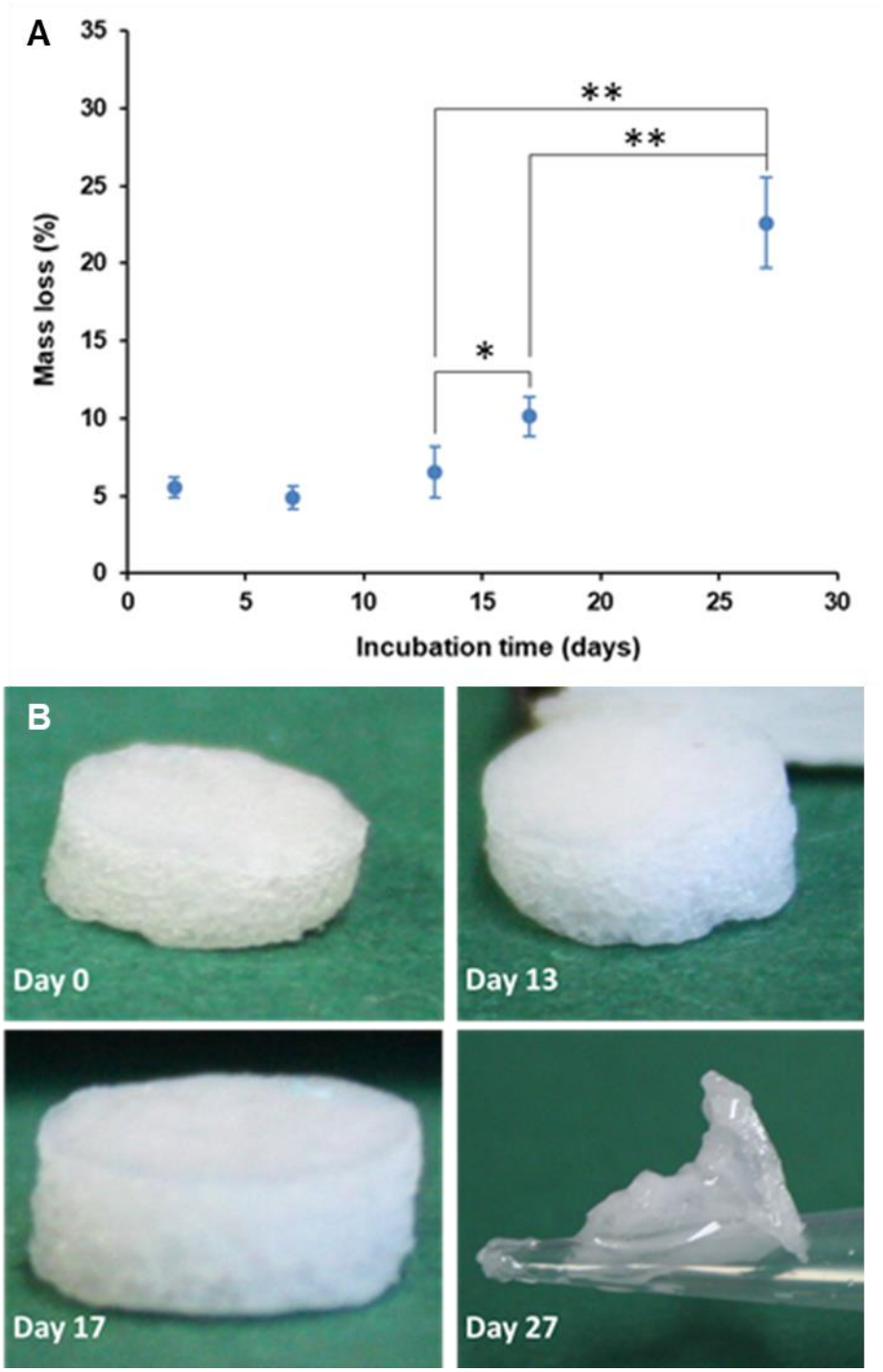

Figure 3.10: (A) Weight loss (n = 3) and (B) representative macroscopic images of SPREADS samples 0, 13, 17 and 27 days after *in vitro* incubation of triplicate samples with 10 – 50 mg in an oxidative solution consisting of 0.03 M $CoCl_2$/20 % H_2O_2 at accelerated oxidative conditions, respectively. Significance was evaluated by an unpaired t-Test with p<0.05 considered as significant compared to control. *p<0.05, **p<0.01. Reprinted from Dolan *et al.* [76] with permission from Elsevier.

3.4.2 *In vitro* characterization of HA-PH-RGD hydrogels

Gelation Kinetics of HA-PH-RGD hydrogels

The gelation of both acellular and cellular (c-ADSCs at a final concentration of 20 million cells/mL) 2% HA-PH-RGD hydrogels (60-90 kDa) at cross-linking concentration 1 and 2 (see Table 3.1 in section 3.3.5) occurs between 0-3 minutes with a gelation time of 19 and 20 seconds, respectively, as shown in Figure 3.11 A. The dependence of the viscosity on the shear rate for the acellular 2% HA-PH-RGD hydrogel (60-90 kDa) at crosslinking concentration 1 is attached in Appendix I, section 7.1.3 [76].

Impact of c-ADSCs on mechanical properties of HA-PH-RGD hydrogels

Dispersion of c-ADSCs at a final concentration of 20 million cells/mL has been shown to impede the crosslinking reaction of HA-PH-RGD hydrogels and thus affect the final mechanical properties of the hydrogel. Hence, higher concentrations of the crosslinking agents HRP and H_2O_2 were employed in case 20 million c-ADSCs/mL are intended to be included in HA-PH-RGD hydrogels in order to antagonize the physical interference provoked by the cells (see Table 3.1). As shown in Figure 3.11 B, both for cross-linking concentration 1 and 2 (see Table 3.1) a statistical significant reduction in Young's modulus was determined in hydrogels prepared without and with 20 million c-ADSCs/mL (9.7 versus 5.6 kPa and 12.6 versus 8.6 kPa in case of crosslinking concentration 1 and 2, respectively; $p < 0.01$). In contrast, no statistically significant differences could be observed between the Young's modulus of hydrogels prepared at crosslinking concentration 1 without cells and at cross-linking concentration 2 with 20 million c-ADSCs/mL. Crosslinking agents at concentration 2 were consequently used to generate hydrogels with comparable mechanical properties independent of cell inclusion or not [76]. Innocuousness of employed crosslinking agent concentrations was confirmed by a CellTiter-Glo assay (Promega, USA) and has been already previously published [104].

In vitro stability of HA-PH-RGD hydrogels

The following Figure 3.11 C and Figure 3.11 D show the course of the swelling coefficient and the Young's modulus after placing samples of cell-free 2 % HA-PH-RGD hydrogel (60-90 kDa) prepared at crosslinking concentration 1 for up to 8 weeks in PBS, respectively. As shown in the following Figures, the swelling coefficient increased by 78.9 % and the Young's Modulus decreased from 9.7 kPa by 34 % to 6.4 kPa [76].

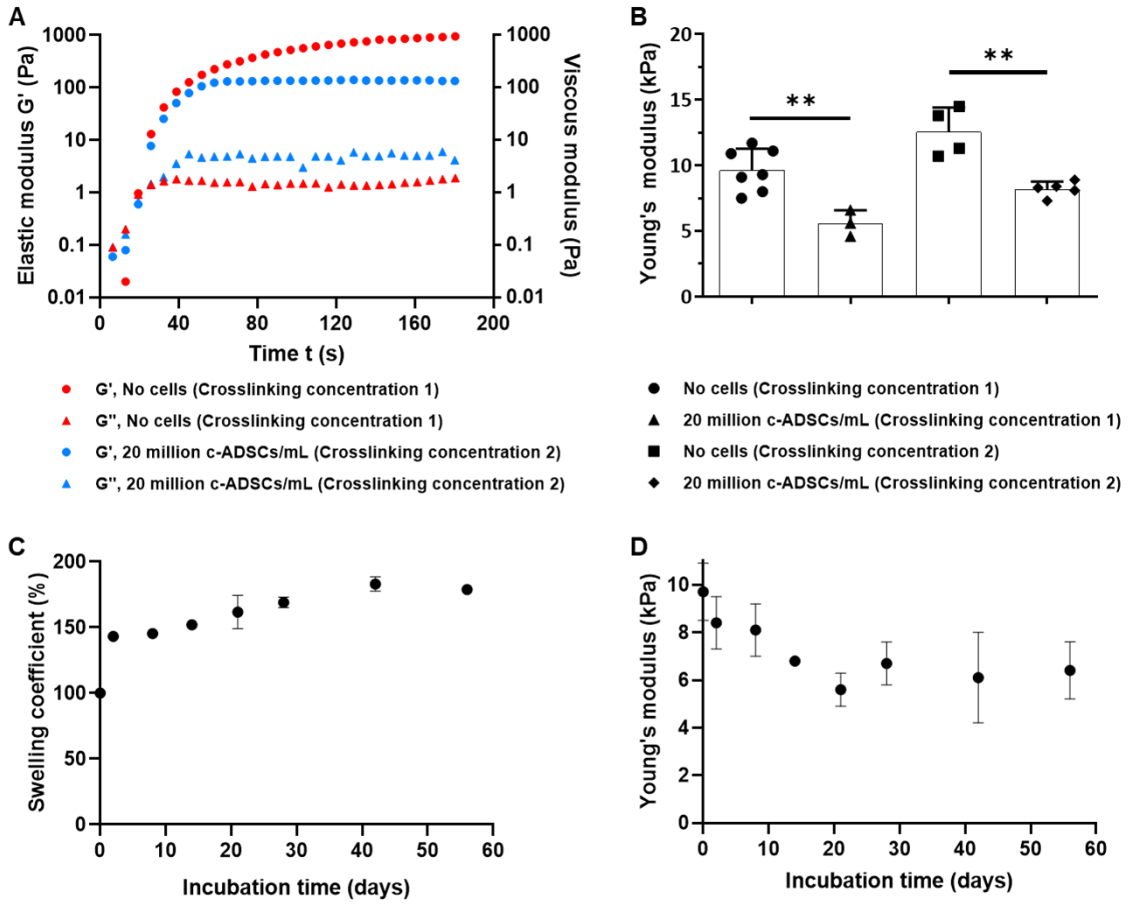

Figure 3.11: (A) Representative gelation curves of acellular and cellular (20 million c-ADSCs/mL) 2 % HA-PH-RGD hydrogels (60-90 kDa) at cross-linking concentration 1 and 2, respectively (n = 5). (B) Young's modulus of various types of 2 % HA-PH-RGD hydrogels (60-90 kDa) with and without 20 million c-ADSCs/mL at crosslinking concentration 1 and 2 (n = 3-7). One-way ANOVA with a Tukey's post-hoc test was performed (considered significant for p<0.05 compared to control, **p < 0.01). (C) Swelling coefficient and (D) Young's modulus of acellular 2 % HA-PH-RGD hydrogel (60-90 kDa) samples prepared at crosslinking concentration 1 after *in vitro* incubation in PBS (pH 7.4) for up to 8 weeks (n = 5). Reprinted from Dolan *et al.* [76] with permission from Elsevier.

3.4.3 Cell viability after encapsulation in SPREADS

Cytotoxicity of HA-PH-RGD hydrogels

No cytotoxic effect of 2 % HA-PH-RGD hydrogels (60-90 kDa) on both HaCaT cells and iCFs were observed as shown in Figure 3.12 A guaranteeing innocuousness of the employed HA-PH-RGD hydrogel [76].

Effect of application procedure to SPREADS on viability of c-ADSCs

The following Figure 3.12 B shows representative fluorescence microscopy images of living/dead c-ADSCs after delivering them at a final concentration of 20 million cells/mL to SPREADS' central cavity immersed within Contipro's 2 % HA-PH-RGD hydrogel (60-90 kDa). Resulting data of percental cell viability are illustrated in the corresponding graph showing the course dependent on incubation time [76].

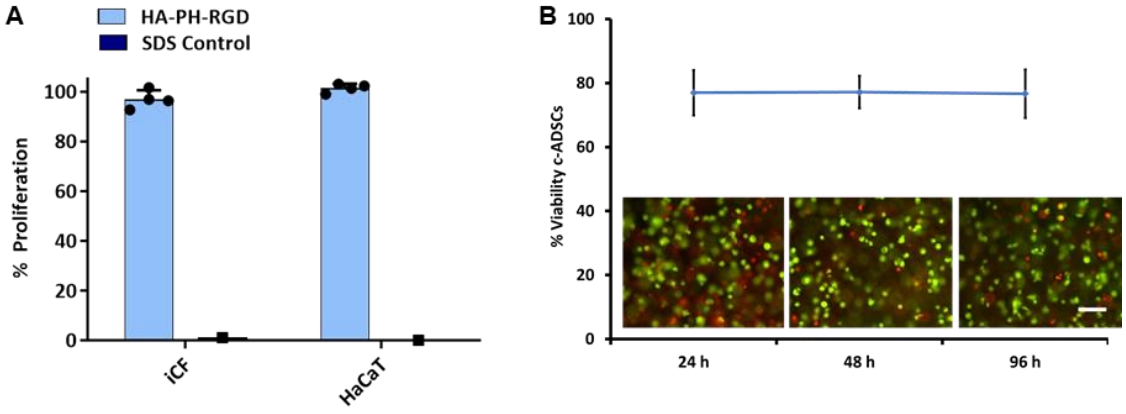

Figure 3.12: (A) Cytotoxicity assessment of Contipro's 2% HA-PH-RGD hydrogel (60-90 kDa) showing the proliferation of HaCaT and iCF cell lines (n = 4). (B) Viability of c-ADSCs (red cells are dead, green cells are viable) in Contipro's 2 % HA-PH-RGD hydrogel (60-90 kDa) at crosslinking concentration 2 after injecting them into SPREADS' central cavity (n = 6) with representative fluorescence microscopy images (scale bar = 100 µm) at corresponding incubation times. Reprinted from Dolan *et al.* [76] with permission from Elsevier.

As depicted in Figure 3.12 B percental c-ADSC viability after delivery to SPREADS remained above 70 %, which is generally considered as acceptable viability specification by the FDA [122] and did not significantly change with increasing incubation time. A percental c-ADSC viability of 77 %, 77.2 % and 76.7 % was determined 24, 48 and 96 hours incubation time, respectively. The incorporated c-ADSCs were homogenously distributed within each sample as shown in the corresponding fluorescence microscopy images [76].

3.4.4 Applicability evaluation of developed concepts for SPREADS

Design generation 1

The generated prototypes of SPREADS' first design generation could be adequately attached to the bottom of a PMMA plate which was pre-wetted with DI water. The porous PEU fleece provided adequate adhesive strength through capillary forces keeping the respective SPREADS version in position (see Figure 3.13).

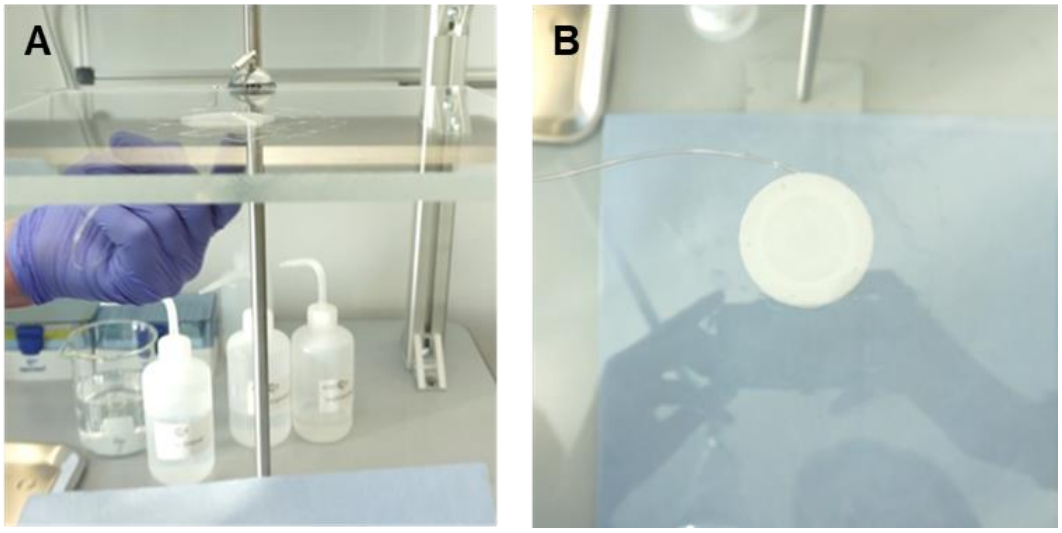

Figure 3.13: Assessment of SPREADS' intrinsic adhesiveness to wet surfaces by (A) placing a prototype of SPREADS' first design generation with the PEU fleece facing surface overhead on a with DI water pre-wetted PMMA plate. (B) SPREADS was kept in position just through capillary forces provided by the PEU fleece.

Subsequent injection of a 4% albumin solution extracted from BioGlue® as substitute for the liquid HA-PH-RGD hydrogel revealed a uniform distribution of the injected hydrogel dummy in SPREADS' foreseen hydrogel reservoir (see Figure 3.14) and did not impair the adhesion of SPREADS. Inadvertent leakage of the injected albumin solution was not observed.

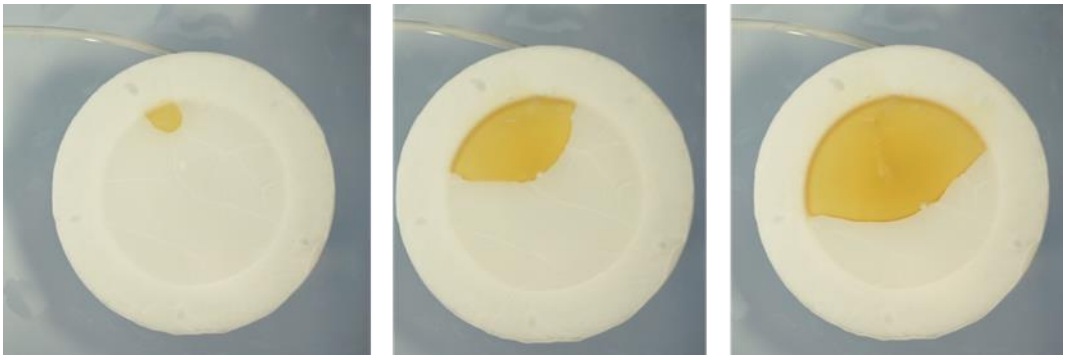

Figure 3.14: Image sequence showing the distribution of a 4 % albumin solution within the foreseen hydrogel reservoir of SPREADS' first design generation during injection.

SPREADS prototypes of the first design generation also demonstrated sufficient initial attachment to a non-planar surface of an *ex vivo* porcine heart and remained in position even under the impact of gravity as shown in Figure 3.15 A below but could be comparatively easily detached from the heart surface again by pulling on the PEUU foam in vertical direction relative to the heart surface. Analogously to the experiments on a planar PMMA plate, no fluid leakage was observed during the injection procedure of BioGlue®. The connected supply line to SPREADS' hydrogel cavity could be easily removed after curing of the injected bioadhesive BioGlue® without causing any dislocation of SPREADS. Adequate resistance of SPREADS against selective tensile load (see Figure 3.15 B) and frictional stress (see Figure 3.15 C) was demonstrated by manually pulling SPREADS with forceps in vertical direction relative to the heart surface and by manually exerting shear stress to the outer surface of SPREADS with cardiac adipose tissue as pericardium substitute, respectively. The injected BioGlue® was also uniformly distributed within its foreseen space as shown in Figure 3.15 D below.

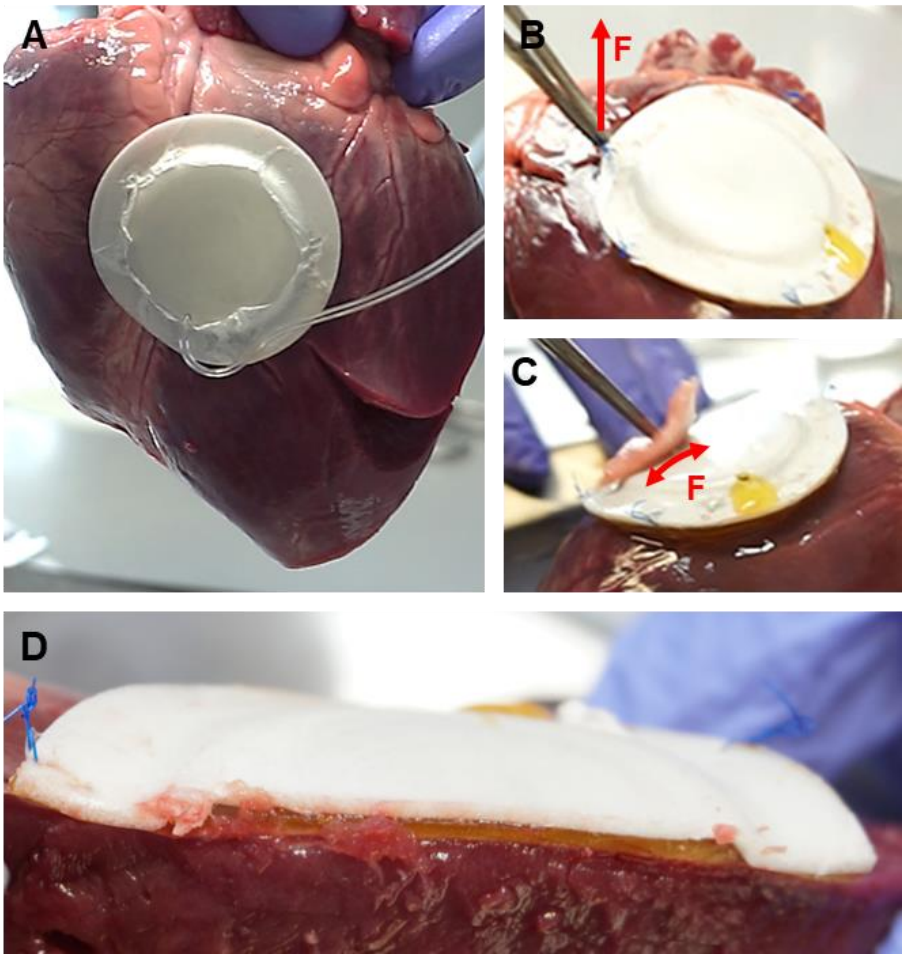

Figure 3.15: Suitability assessment of the first design generation for SPREADS on an *ex vivo* porcine heart. Reaction of SPREADS' first design generation in case of (A) vertical alignment of the heart before injection of BioGlue®, exertion of (B) tensile load and (C) frictional stress after curing of the injected BioGlue® as gel dummy. (D) Distribution of the injected BioGlue® within SPREADS foreseen central cavity.

Design generation 2

Even though SPREADS' first design generation achieved promising results in terms of initial attachment to a wet surface and successful encapsulation of a liquid hydrogel in its pre-curing state, the idea to facilitate stable attachment of SPREADS to the heart surface just through capillary forces provided by the PEU fleece was not possible. Based on the positive results regarding stable attachment of SPREADS generation 1 to the epicardial heart surface through injection of BioGlue®, the concept of SPREADS generation 2 pursued the approach to facilitate stable attachment of SPREADS by controlled release of BioGlue®.

Empty prototypes of SPREADS' second design generation demonstrated an analogous adhesion performance compared to the first design generation of SPREADS when placed on a pre-wetted surface of an *ex vivo* porcine heart and gently pressed along its circumferential edge against the heart surface. No visible leakage was observed during the successive BioGlue® deployment in both half-circumferential bioadhesive reservoirs as well as during injection of Contipro's 2 % HA-PH-RGD hydrogel (60-90 kDa) into SPREADS' central cavity (see Figure 3.16 A). All supply lines connected to SPREADS could be easily removed without causing any dislocation of SPREADS as shown in Figure 3.16 B-C.

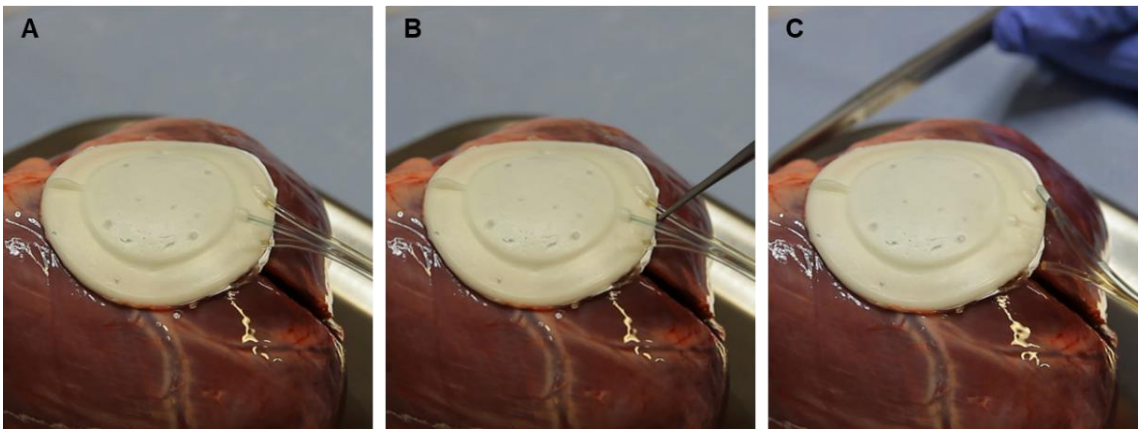

Figure 3.16: Image sequence showing the second design generation of SPREADS after (A) attaching SPREADS with the aid of BioGlue® to the heart surface of an *ex vivo* heart and injecting the acellular 2 % HA-PH-RGD hydrogel (60-90 kDa) which was stained with methylene blue. (B) Withdrawing of respective supply lines, which (C) did not cause any dislocation of SPREADS.

Even lifting of the complete *ex vivo* porcine heart by pulling with forceps on an outer edge of SPREADS' PEUU foam did not cause any detachment of SPREADS (see Figure 3.17) ensuring a stable attachment of SPREADS' second design generation to the heart surface and thus a sustained contact of the injected therapeutic hydrogel with the injured tissue area as intended.

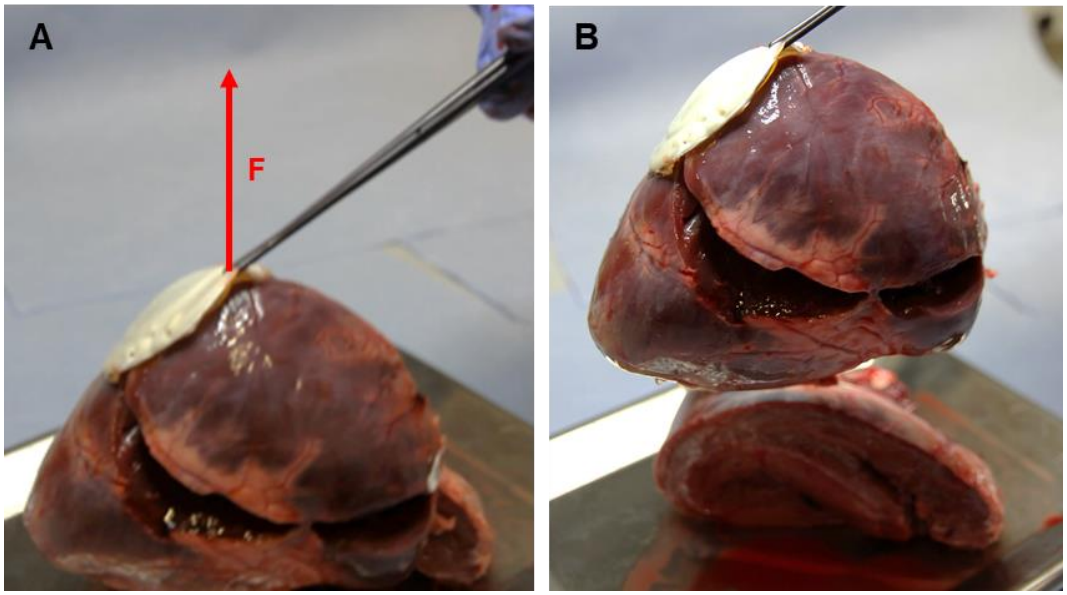

Figure 3.17: Adhesion strength assessment of SPREADS's second design generation after attachment with BioGlue®. Image sequence showing the elevation of the *ex vivo* heart just by pulling on an edge of SPREADS.

After cutting SPREADS with the heart below in two halves, uniform distribution of both BioGlue® and HA-PH-RGD hydrogel in its respective reservoirs could be determined (see Figure 3.18).

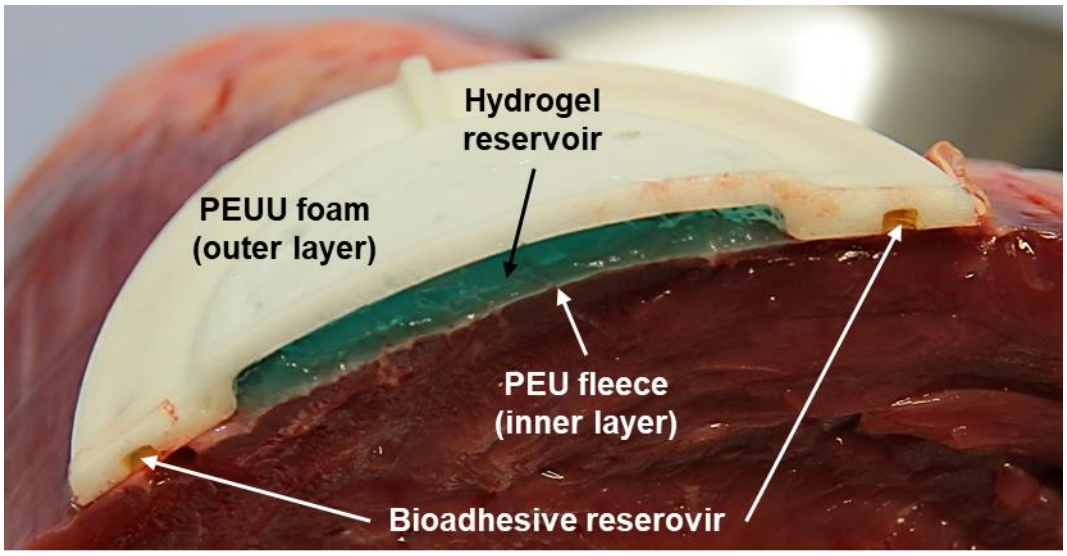

Figure 3.18: Macroscopic sectional view showing the second design generation of SPREADS loaded with a methylene blue stained 2 % HA-PH-RGD hydrogel (60-90 kDa) and stable attached to the epicardial surface with BioGlue®. Reprinted from Dolan *et al.* [76] with permission from Elsevier.

Alternatively, HA-PH-RGD hydrogel was injected into the central cavity of SPREADS second design generation before attaching it to the heart surface with BioGlue® to evaluate SPREADS' capability to facilitate also delivery of a pre-cured hydrogel. As shown in Figure 3.19, the HA-PH-RGD hydrogel was uniformly distributed. Unproblematic stable attachment of this pre-loaded carrier device could be also achieved by keeping forceps applied to the outer surface of SPREADS for at least 20 seconds after finalising the injection of BioGlue® into each of both half-circumferential bioadhesive reservoirs. Apparently, the developed second design generation of SPREADS appears to conform to the essential requirements of enabling the application of an *in situ* curing hydrogel to a well-defined area on the epicardial heart surface and to ensure its sustained contact with the epicardium.

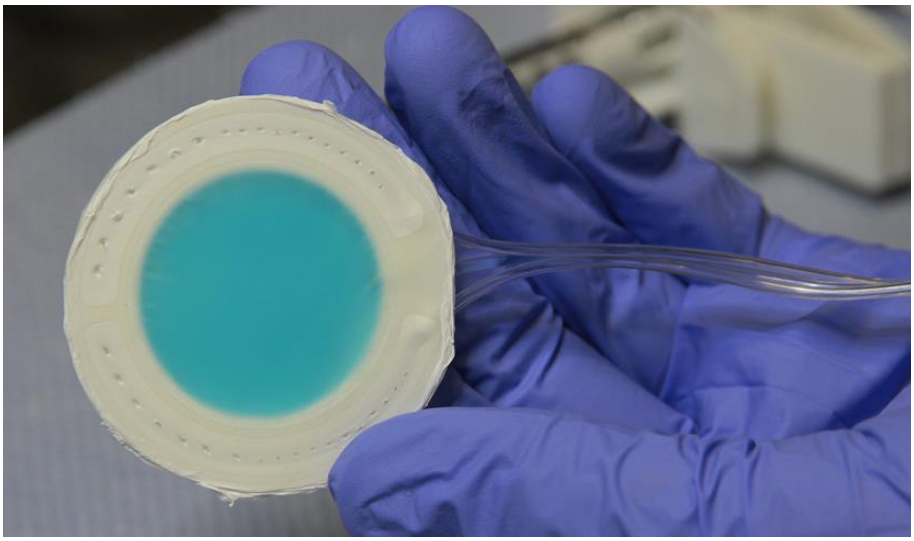

Figure 3.19: Inferior view of SPREADS' second design generation after injecting of methylene blue stained 2 % HA-PH-RGD hydrogel (60-90 kDa) into the foreseen hydrogel reservoir.

3.4.5 Pre-clinical feasibility of SPREADS *in vivo*

SPREADS could be successfully delivered to the epicardial heart surface via a subxiphoidal access as shown in Figure 3.20 A. The implantation procedure of SPREADS itself as well as the administration of the HA-PG-RGD hydrogel did not provoke any disturbances of vital signs and hemodynamic (see Figure 7.13 in Appendix I, section 7.1.4) as well as did not cause any cardiac arrhythmias. The minimal and maximal value of the heart rate (HR) and oxygen saturation (SpO_2) differed during the entire procedure in average by 17.5 BPM and 2.1 %, respectively.

The required folding procedure of SPREADS to get inserted into the pericardial cavity via a 3 cm apical incision of the pericardium was successfully tolerated by SPREADS. After loosening the forceps, SPREADS expanded inherently and retained its position but could be also shifted on the epicardial heart surface in case a reposition was necessary. None of the supply lines connected to the hydrogel and adhesive reservoir was inadvertently detached during the entire manipulation. Adequate attachment of SPREADS to the epicardium could be successfully achieved by injecting BioGlue® in its foreseen half-circumferential grooves as proven by the movement of the connected supply lines in synchrony with the heartbeat. The HA-PH-RGD hydrogel could be subsequently injected into SPREADS' central hydrogel reservoir without any interruptions. All supply lines could be finally removed out of the respective ports without inadvertently detaching SPREADS from the epicardial heart surface again. The complete intervention consisting of positioning, attachment to the epicardial heart surface and hydrogel delivery lasted maximal 30 minutes in average [76].

As the pericardial space was exposed by full sternotomy (see Figure 3.20 B) 2 hours after implantation, SPREADS was found in position with its shape adapted to the heart curvature fitting closely to the epicardial heart surface. No signs of hydrogel or BioGlue® leakage around SPREADS could be determined by inspecting the epicardium after opening the pericardium. Even after completely removing the pericardium, SPREADS remained attached to the epicardial heart surface in position and moved synchronically with each heartbeat. Detachment of SPREADS from the heart surface could be only accomplished by active pulling (see Figure 3.20 C). As shown in Figure 3.20 C, BioGlue® was uniformly distributed within its foreseen half-circumferential groove with BioGlue® residues spread over the area on the epicardial heart surface where the adhesive reservoir was originally positioned. No damage of the PEU fleece could be determined and the injected HA-PH-RGD hydrogel stained with methylene blue for better visualisation could be successfully retained by SPREADS, as illustrated in Figure 3.20 D [76].

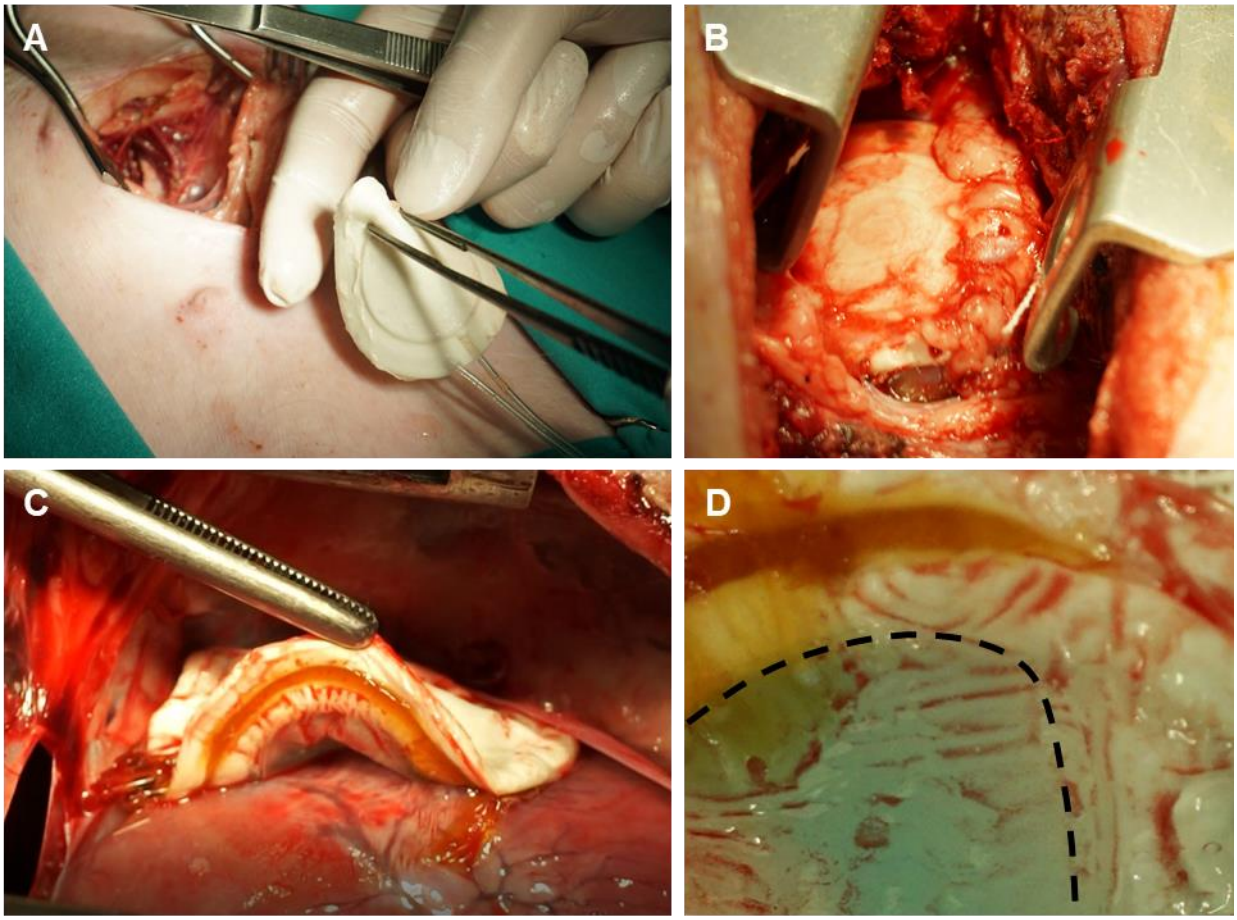

Figure 3.20: Representative images of acute *in vivo* trials (n = 4) to assess the pre-clinical feasibility of SPREADS. (A) Minimal-invasive implantation procedure of SPREADS via a sub-xiphoidal access. (B) Position and (C) attachment validation of SPREADS 2 hours after implantation. (D) Hydrogel retention validation as shown by the dashed line. Reprinted from Dolan *et al.* [76] with permission from Elsevier.

3.4.6 Pre-clinical efficacy of SPREADS *in vivo*

A significant improvement in %LVEF was determined 14 days ($p \leq 0.002$) and 28 days ($p = 0.028$) post-treatment (28 and 42 days after inducing acute MI) comparing treatment Group II (GS + SPREADS + Gel) with treatment Group I, respectively, as shown in Figure 3.21. Treatment Group III (GS + SPREADS + Gel + Cells) showed also a significant increase ($p \leq 0.002$) in %LVEF 14 days post-treatment (28 days post-MI) compared to the GS control but did not result in an further significant improvement of %LVEF compared to the GS + SPREADS + Gel group at this time point. No significant difference ($p = 0.150$) was determined when comparing the %LVEF of the GS + SPREADS + Gel Cells group with the GS group 28 days post treatment (42 days post-MI). No statistically significant differences

were ascertained neither in FS nor in LVEDd and LVESd between any of the treatment groups at any time point (see Figure 3.21). The time course of animal body weight during the entire procedure revealed no significant differences as well (see Figure 7.14 in Appendix I, section 7.1.4) [76].

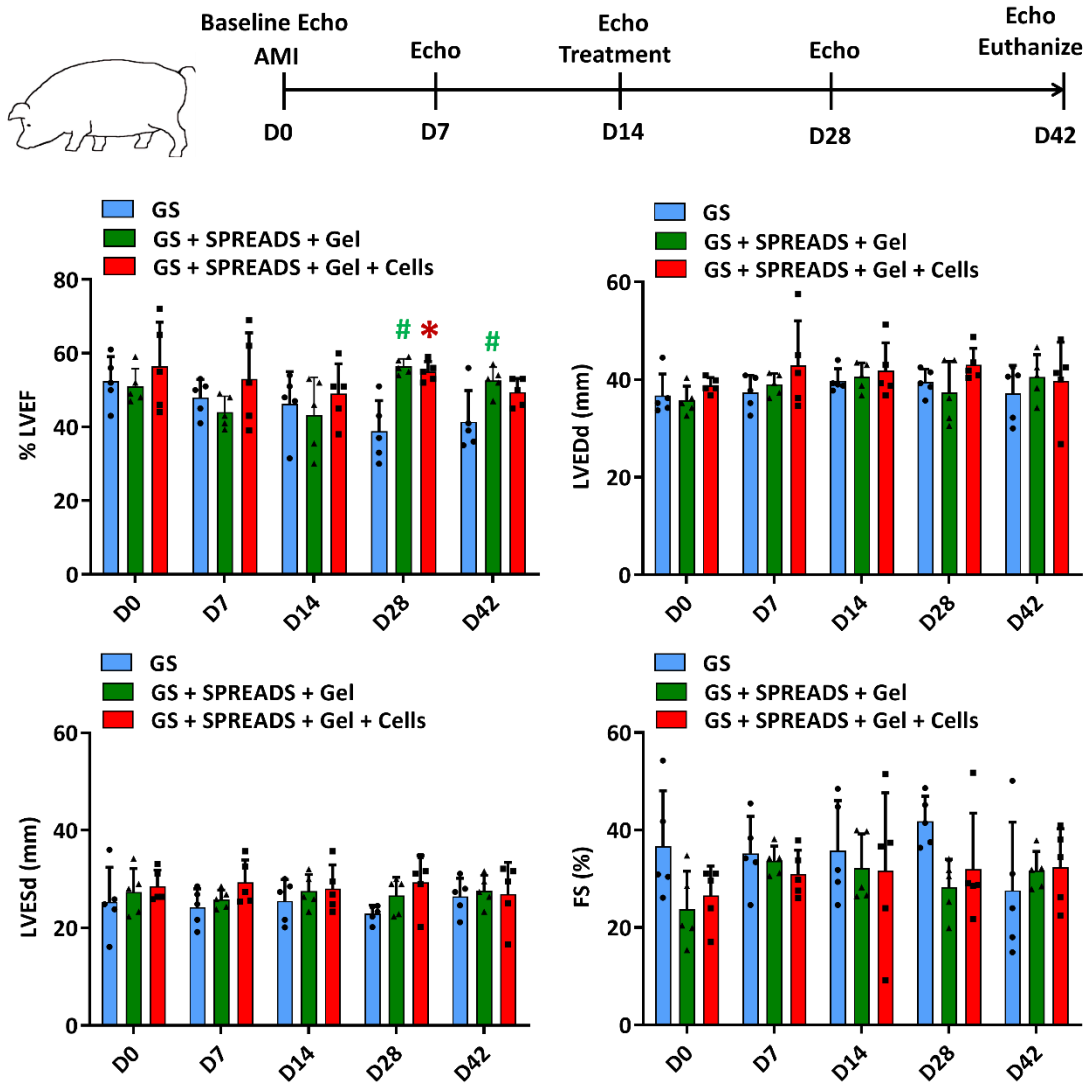

Figure 3.21: Time course of left ventricular ejection fraction (LVEF), left ventricular end diastolic diameter (LVEDd), left ventricular end systolic diameter (LVESd) and fraction shortening (FS) determined from echocardiographic images in long parasternal axis view (n = 5 animals/treatment group). Two-way ANOVA with Tukey's post-hoc test was performed considering significance in case of $p < 0.05$ compared to GS control. Reprinted from Dolan *et al.* [76] with permission from Elsevier.

Extracted hearts of each treatment group were processed according to the following sampling scheme shown in Figure 3.22 A with slicing the heart initially into equidistant parallel slices orthogonal to the longitudinal axis [117] generating parts B (Basal slice), M1-M3 (Mid Ventricular slices) and A (Apical slice). Figure 3.22 B

shows exemplary gross histological images of the M2 infarct region after staining with Picrosirius red (infarct and epicardium) and Fast Green (myocardium). To enhance birefringence of collagen fibres, picrosirius stained sections were microscopically examined under orthogonal polarized light (see Figure 3.22 C). As shown in Figure 3.22 E, quantification of birefringent fibres employing colour threshold segmentation for mature fibres (red/orange) and immature fibres (green) did not show any statistically significant differences between any treatment groups irrespective of polarisation colour ($p > 0.05$). Representative images of fibre directionality obtained from coherency and fast Fourier transform analysis are shown in Figure 3.22 D. Each angle is assigned to a different colour enabling subsequent visual orientation analysis of the collagen fibre direction as illustrated by the corresponding colour coded angle wheel. No statistically significant differences were determined in the fraction of fibres between any treatment group for location M2 ($p > 0.05$) obtained by visual orientation analysis and quantification of the collagen fibre direction uniformity (coherency) according to the illustrated colour coded angle wheel (see Figure 3.22 F). Neither SPREADS loaded with acellular HA-PH-RGD hydrogel nor the extra addition of c-ADSCs induced significant alterations of infarct scar composition and collagen fibre orientation when compared to treatment Group I (GS) [76].

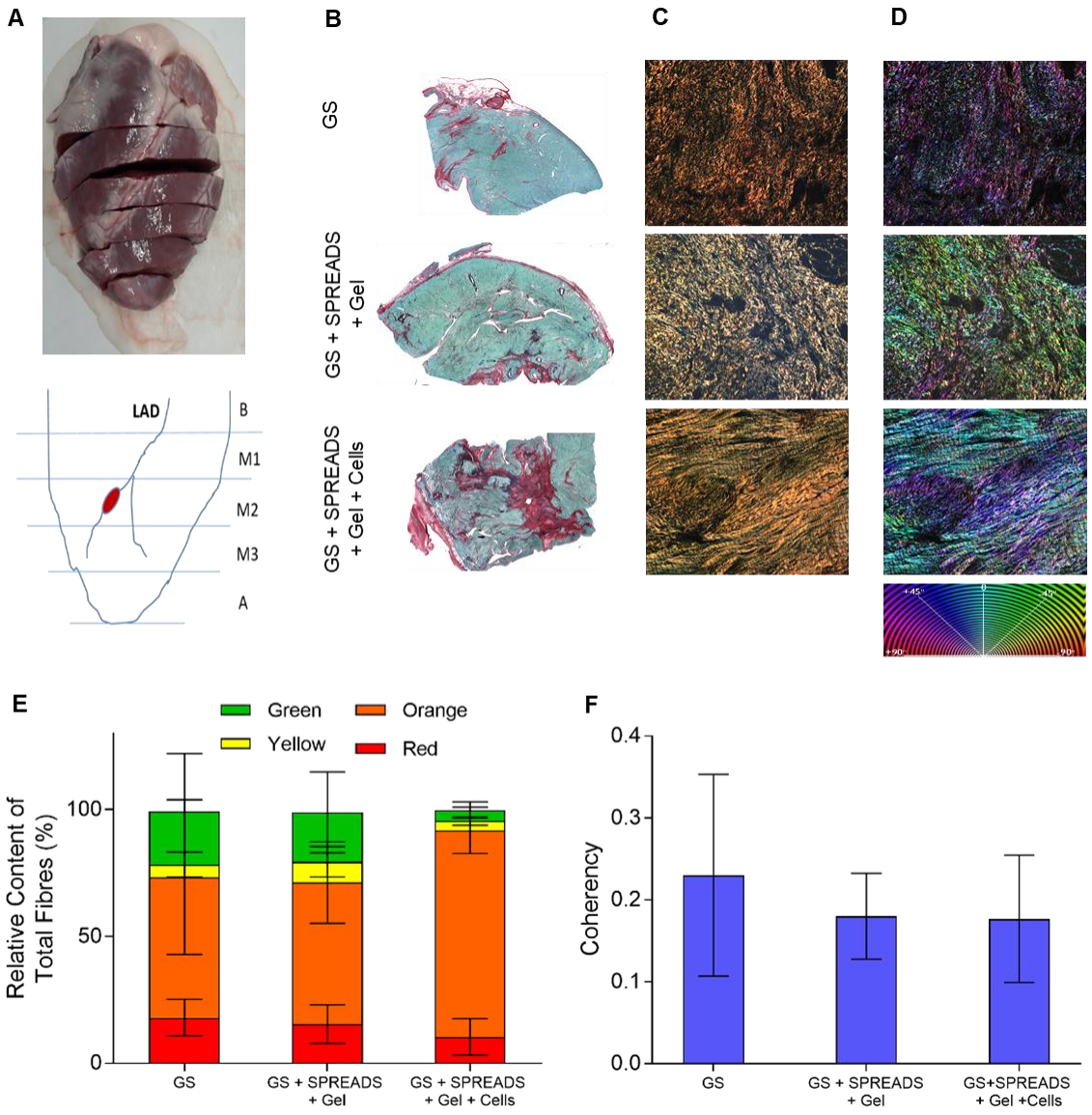

Figure 3.22: (A) Processing scheme of extracted hearts orthogonal to its longitudinal axis to receive the basal slice B, mid ventricular slices M1-M3 and the apical slice A. (B) Representative gross histological images of the M2 infarct region after staining with Picrosirius red (infarct and epicardium) and Fast Green (myocardium). (C) Polarized light microscopy images of Picrosirius red stained sections under orthogonal polarized light to enhance birefringence of collagen fibres (scale bar = 200 µm). (D) Representative images obtained after coherency and fast Fourier transform analysis showing fibre directionality according to colour coded angle wheel below employed for subsequent visual orientation analysis of collagen fibre direction, respectively. (E) Evaluation of birefringent fibres employing colour threshold segmentation for mature fibres (red/orange) and immature fibres (green). (F) Evaluation of directional uniformity (coherency) of collagen fibres in the M2 infarct region. One-way ANOVA with Tukey's post-hoc test was carried out to evaluate significance between any of the treatment groups with $p < 0.05$ as threshold for significance. n = 3-5 animals/treatment group. Reprinted from Dolan *et al.* [76] with permission from Elsevier.

Three distinct regions could be determined by histochemical staining with Haematoxylin and Eosin (H&E) as depicted in Figure 3.23: the infarct zone (IZ) composed of hypocellular fibrotic tissue, the border zone (BZ) consisting of hypertrophic cardiomyocytes with pleomorphic cells and the unaffected adjacent myocardium (AM) characterized by long spindle cells with prominent striations. Masson's trichrome staining revealed distinctive blue/green regions synonymously for prominent scar tissue [76].

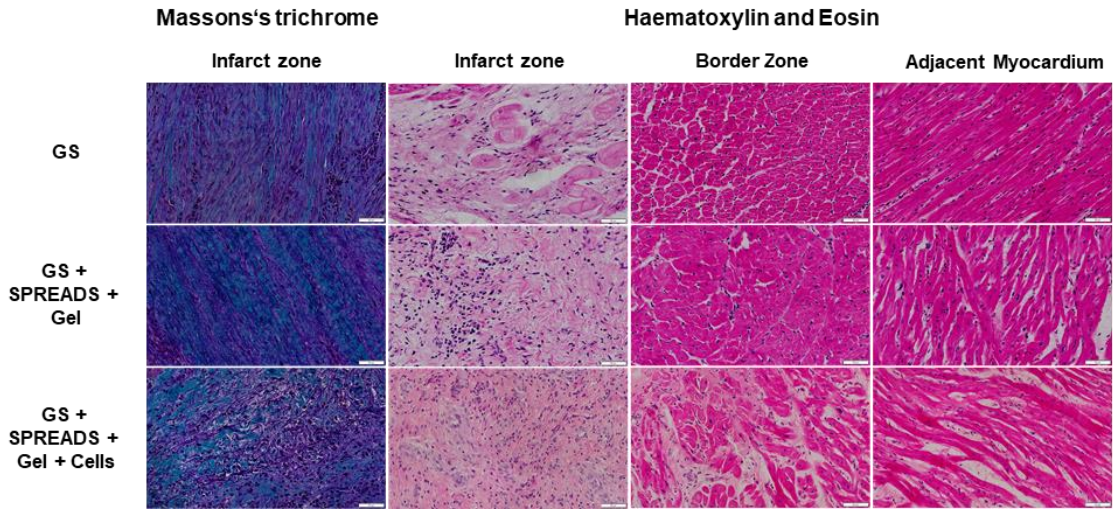

Figure 3.23: Masson's trichrome staining (collagen is blue and green, cytoplasm is pink, nuclei are black) showing the scar tissue in the infarct zone. Haematoxylin and Eosin staining (nuclei are blue, extracellular matrix and cytoplasm are pink) demonstrating the infarct zone characterised by hypocellular and fibrotic tissue, the border zone characterised hypertrophic cardiomyocytes with pleomorphic cells and nuclei and the unaffected adjacent myocardium characterised by spindle shaped cardiomyocytes with prominent striations. Representative histological images (scale bar = 50 µm). Reprinted from Dolan *et al.* [76] with permission from Elsevier.

Analysis of blood vessel formation in the M2 infarct region directly beneath SPREADS revealed CD31 positive blood vessels in the IZ, BZ and AM as illustrated by brown staining (DAB) in Figure 3.24 A. No statistically significant differences ($p > 0.05$) were found by comparing the number of CD31 positive blood vessel/field in the M2 infract region between any of the treatment groups in any of the regions (see Figure 3.24 B), indicating that neither SPREADS loaded with acellular HA-PH-RGD hydrogel nor the extra addition of c-ADSCs resulted in a significant impact on local vascularisation [76].

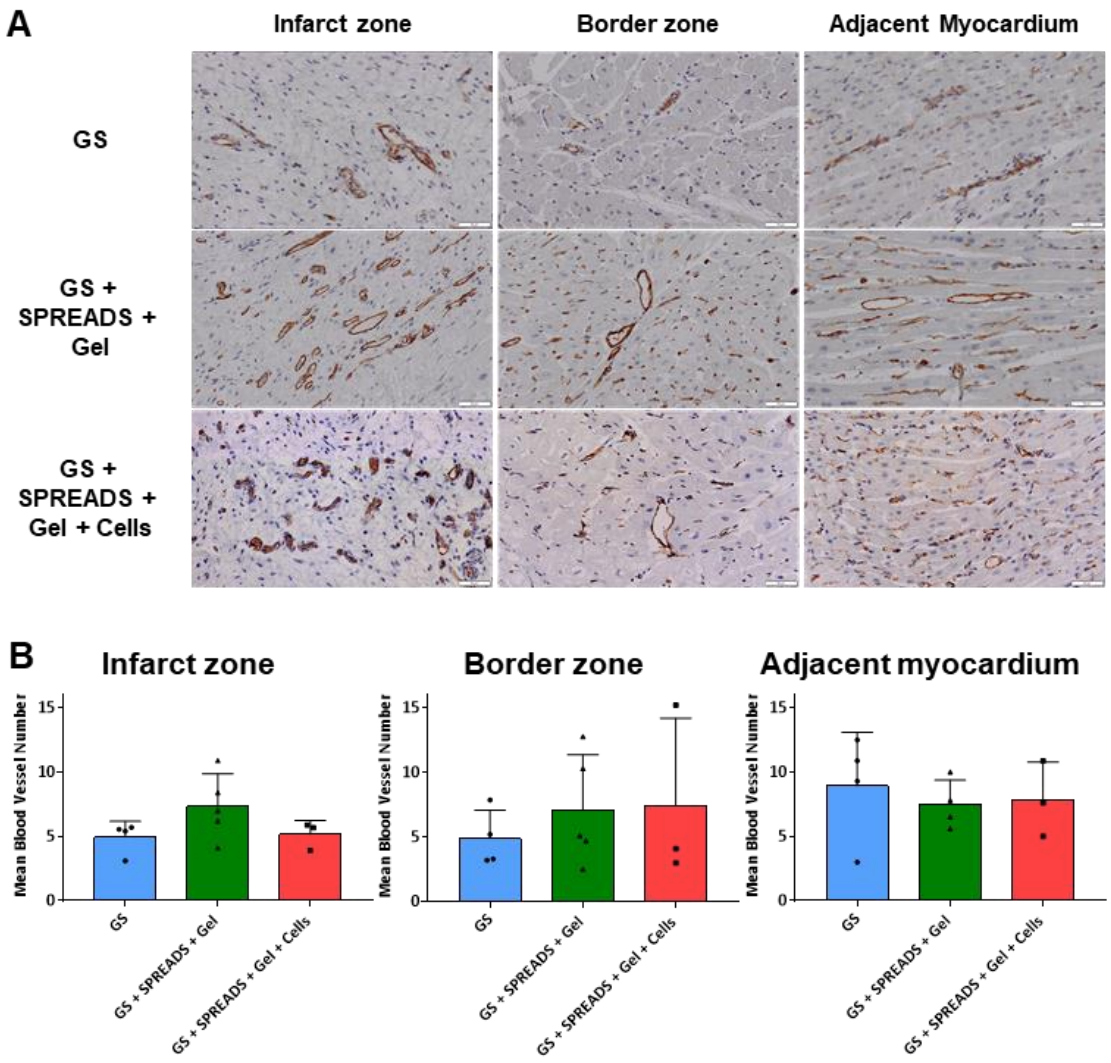

Figure 3.24: (A) Representative images of CD31 immunohistochemical staining showing CD31-positive (brown) capillaries in the infarct and border zone as well as in the unaffected adjacent myocardium. (B) Determination of blood vessel amount per field in each region. One-way ANOVA with Tukey's post-hoc test was carried out to evaluate significance between any of the treatment groups with $p < 0.05$ as threshold for significance. n = 3-5 animals/treatment group. Reprinted from Dolan *et al.* [76] with permission from Elsevier.

3.5 Discussion

The limited ability of the adult mammalian heart to restore damaged contractile myocardial tissue after a MI results in deterioration of the normal ventricular pumping function of the heart. A cascade of pathological mechanisms is consequently initiated stimulating remodelling processes which can progress finally to a state called congestive heart failure (CHF), where the heart is incapable to provide adequate blood supply to all tissue organs. Numerous approaches have emerged over

the last decades including both mechanical support of the weakened myocardium and regenerative strategies with emphasis on stem cell-based procedures aiming to prevent this pathological cascade but to encourage regeneration of functional cardiac tissue instead. However, comparable simple administration strategies have mostly limited their final performance, motivating the need of an advanced delivery approach to enhance therapeutic efficacy and potentially facilitate a more rapid translation into clinical routine. As part of my work within the framework of the AM-CARE project, a novel device SPREADS was developed being capable to serve both as cargo device for biomaterials loadable with therapeutic agents to the epicardial heart surface via a single-stage minimal-invasive, closed chest intervention, and to provide passive mechanical support to the weakened myocardium post-MI. Application of SPREADS' final design generation (second design concept) 14 days after inducing acute MI resulted in a significant improvement in percental LVEF compared to GS treatment alone [76].

The outer layer of SPREADS was manufactured from a PEUU based on its suitable mechanical properties (adequate stiffness, flexibility, structural integrity), processability (to meet all structural design features) and its expected host compatibility owing to the material's biocompatibility and biodegradability. Sufficient compliance of SPREADS' mechanical properties with the healthy myocardial tissue is crucial to successfully facilitate stress transfer from the weakened infarct and border zone while avoiding impairment of native cardiac contractility on the other hand [72, 76, 87, 123]. Previous passive restraint devices such as the CorCap^{TM} is characterized by a minimal stiffness of 3 MPa [76, 124] in its cross-fibre direction, which is much higher than that of the native myocardium at the end of the systole (500 kPa) [76, 87] impairing finally the diastolic function of the right ventricle [76, 124]. Within the framework of all *in vivo* trials, neither diastolic nor systolic functional impairment was determined after implantation of SPREADS by echocardiographic and ECG analyses suggesting that SPREADS' mechanical properties are in good agreement with those of the native myocardial tissue [76].

No residues of HA-PH-RGD hydrogel were detected four weeks after delivering SPREADS loaded with HA-PH-RGD hydrogel +/- c-ADSCs to the epicardial heart surface. Consequently, the PEU fleece porosity provided adequate interaction of the encapsulated hydrogel with the epicardial environment while avoiding

undesired leakage of the injected *in situ* curing hydrogel in its liquid state. SPREADS however appeared after four weeks *in vivo* partially degraded but with an almost preserved geometrical shape as shown in Figure 7.15 (see Appendix I, section 7.1.4) [76]. This observation agreed well with results obtained from SPREADS' degradability assessment *in vitro* at accelerated conditions but also with previously published data of a LDI-based PU incubated in PBS solution at 37 °C [110]. 17 and 27 days incubation of SPREADS *in vitro* (corresponding to 23.5 and 37.5 days implantation *in vivo* according to Dempsey *et al.* [113]) resulted in 11 % and 23 % loss of SPREADS' initial mass, respectively. A similar result was determined by Laube *et al.* [110] for a LDI-based PU scaffold composed of a poly(L-lactide-co-ε-caprolactone) with a mass loss of 17 % after 28 days incubation *in vitro*. The bioresorbable properties of SPREADS facilitates potential treatment of patients as a single-stage procedure, while degradability of the respective hydrogel delivered by SPREADS can be further adapted to match with the stabilisation needs of the patient [76].

Numerous types of hydrogels (acellular or cellular; physically or covalently cross-linked) have been developed over the past decades with the aim to treat patients with cardiovascular diseases [125-129]. As an alternative approach to whole heart passive restraint devices, acellular injectable hydrogels have received increasing attention based on their ability to be locally administered in a less invasive intervention [60, 76] and their more adjustable mechanical properties that may improve therapeutic efficacy [76]. The alginate-based hydrogel Algisyl-LVR™ (LoneStar Heart Inc., CA USA) for example is already at an advanced level in terms of clinical development with promising results [130], providing mechanical support of the weakened myocardium by ventricular wall thickening and geometry recovery similarly as the assumed therapeutic benefit provided by SPREADS [76]. Algisyl-LVR™, which is characterised by storage modulus of 3-5 kPa *in vivo*, was delivered by epicardial injections after exposing the heart via an anterior thoracotomy [77, 130]. Intramyocardial injections may however not always be the best therapy option especially in case of treating large infarcts, since multiple injections may imply an increased risk of tissue injury and mechanical stress to the myocardium [3, 76] apart from other hazards accompanied with needle-based administration into dense tissues such as the myocardium [91]. There is consequently a need in terms

of availability of minimal-invasive devices feasible to enable translation of these biomaterial therapies to clinic. The principal concept for SPREADS developed within the framework of this work has successfully shown its capacity to facilitate an atraumatic site-specific administration of a hydrogel to the epicardial heart surface representing a novel unique treatment option for patients after myocardial infarction. Undefined dispersion of the injected hydrogel from the defined space into which a fluid hydrogel in its pre-curing state can be injected was effectively prevented based on adequate porosities of both the PEUU foam and PEU fleece as demonstrated by initial *ex vivo* applicability as well as pre-clinical feasibility and efficacy trials. Applied HA-based hydrogels appeared uniformly distributed within the foreseen central cavities of both design generations conforming well to an essential requirement imposed to SPREADS, respectively. SPREADS could be delivered to the epicardial heart in a minimal-invasive way without causing any complications in vital signs due to its mechanical properties accompanied with its unique design features. Sustained contact of the delivered HA-based hydrogels with the epicardial heart surface could be effectively implemented by SPREADS' unique structure including two additional separate bioadhesive reservoirs (design generation 2) facilitating the controlled release of an *in situ* applied bioadhesive to securely and permanently attach SPREADS to the epicardial surface without employing any surgical aids. The PEU fleece employed as inner layer enables sufficient partial self-adhesion of SPREADS after its positioning on the epicardium through capillary forces adding stability in aid for bioadhesive deployment. Preclinical efficacy examination of SPREADS has successfully proven the preservation of SPREADS' intended position without any surgical sutures, as SPREADS was found in its original position 28 days after implantation. Both HA-PH-RGD hydrogels with and without c-ADSCs have been successfully delivered by SPREADS whose mechanical properties and degradation rate can be further modulated by adapting the concentrations of its cross-linking agents, respectively. This highlights SPREADS' capability to rapidly conquer translational obstacles accompanied with the delivery of hydrogels to the heart as SPREADS may serve as kind of platform device employable to potentially deliver a range of different hydrogel biomaterials [8, 63, 84-87] examined in previous studies. SPREADS moreover offers the potential to better exploit the therapeutic potential of regenerative substances such as cells, since development of the respective biomaterials serving as potential scaffold

can exclusively focus on meeting the requirements of the delivered cells or other bioactive substances (gene- and protein-based) [76].

Therapeutic efficacy of cell-based therapies applied in previous studies with the aim to encourage the weakened myocardium after MI to regenerate have been mostly restricted by retention and survival issues of the delivered cells [63, 66, 76, 96, 131]. Bartunek *et al.* [132] determined for instance within the framework of the C-CURE (Cardiopoietic stem Cell therapy in heart failURE) clinical trial a retention rate of only 2-25 % after delivering 600 million cells suspended in saline solution via 10-20 injections to the heart. The novel epicardial carrier device SPREADS was developed with the aim to address the retention issue at the target side. Even though % LVEF was significantly improved at day 28 by administration of SPREADS loaded with both acellular and cellular (40 million suspended c-ADSCs) HA-PH-RGD hydrogel compared to the GS treatment group I, no further significant improvement in % LVEF was achieved by administering additionally 40 million c-ADSCs/pig compared to treatment group II delivering only an acellular HA-PH-RGD hydrogel by SPREADS to the epicardial heart surface. The exact determination of the *de facto* reasons for the missing additional therapeutic effect by the applied stem cells was however not possible within the framework of the AMCARE project and remains unknown. Verified capacities of SPREADS such as efficient hydrogel encapsulation, stable attachment to the epicardial heart surface while not impairing viability of c-ADSCs as shown *in vitro* clearly demonstrated that SPREADS is capable to successfully serve as cargo device for living cells to the epicardial heart surface ensuring their adequate retention. Caused by the harsh inflammatory environment post-MI, the survival of the employed c-ADSCs could be impaired and thus limit the exploitation of their regenerative capacity [76]. Large animal models as employed in this work are additionally characterised to exhibit a comparatively greater persistence of the inflammatory phase. A not perfect timing of cell administration by SPREADS may consequential be a potential reason that may have impaired the survival of the delivered c-ADSCs. The window for therapeutic intervention is brief, since the reparative response induced after MI is a highly dynamic process [21]. A successful strategy to manage this issue is to deliver cells repeatedly as recently proven by Whyte *et al.* [133]. Further progression in hydrogel biomaterial development considering additional post survival agents for

instance may otherwise create a more suitable cell environment improving finally *in situ* stem cell survival and thus better exploit therapeutic efficacy even in case of a one-time procedure. Alternatively, more therapeutically potent cell sources [134] could be applied in future studies combined with a more detailed characterisation and tracking of the administered stem cells to better clarify potential reasons for the missing additional therapeutic benefit of stem cells compared to treatment with acellular biomaterials [76].

The observed improvement in %LVEF by administration of SPREADS loaded with both acellular and cellular (40 million suspended c-ADSCs) HA-PH-RGD hydrogel compared to the GS treatment group I could be ascribed of to multiple reasons [76]. First, both SPREADS and the encapsulated HA-PH-RGD hydrogel are suspected to target the reduced mechanical integrity of the infarcted myocardium, which is impaired as consequence of the induced inflammatory processes after MI disturbing ECM homeostasis [64]. They provide mechanical support to the ventricular wall by increasing the thickness of the ventricular wall and thus reducing the respective tension in the myocardial wall according to the LaPlace's Law as shown in equation (2.1). This mechanical support may attenuate the vulnerability to adverse remodelling and hence deterioration of cardiac function. The delivery of SPREADS may additionally impact the inflammatory response, which has been already determined as an crucial therapeutic avenue for cardiac regeneration [67]. The therapeutic targeting of the inflammatory and reparative responses after MI may prospectively even have the potential to prevent progression to post-MI heart failure [21, 135]. Normally, the temporary microvasculature that is established during the proliferative phase disintegrates after establishing a primary collagen-based matrix at the infarct site [22]. Consequently, it may appear more difficult for endogenous cardiac stem cells to potentially repopulate the infarcted area due to the limited oxygen and nutrition supply. According to a hypothesis proposed by Fujimoto *et al.* [79], local application of SPREADS at the beginning of the fibrotic response [136] may extend the proliferative phase in the infarct region that preserve apart from myofibroblasts also endothelial cells [137], thus potentially maintaining the microvascular network. Degradation of the encapsulated HA-PH-RGD hydrogel may additionally result in the release of fragments, which may potentially interact with cognate PRRs and therefore manipulate the immune reaction after

MI [21]. Modest fibrotic scar tissue was determined 42 days post-MI at explantation in all treatment groups with no statistically significant differences in scar composition between any of the treatment groups when analysing the resultant infarct fibrosis in each M2 region of the extracted heart, respectively. However, application of the respective therapy in this pre-clinical efficacy study was carried out 14 days after inducing acute MI [76] instead of directly after induction of MI as in many previous studies [138, 139]. Biomaterial administration via injection or epicardial placement within the hour of MI induction was usually caused by the fragility and healthcare considerations of rodent models that have been employed in these pre-clinical studies [76, 138, 139]. But other studies reported administration of experimental therapies rather during the chronic inflammatory stage before the peak stage of myocardial remodelling occurs [140, 141]. In clinical practice, treatment of patients with MI is also not immediately accomplished following MI, since patients are typically admitted to hospital hours to days following MI, require potentially stabilisation or need to wait until the intervention is organised. Hence, the treatment at day 14 as carried out in this study is much closer to the timeline in clinical practice. Histological analyses of M2 regions from the extracted heart revealed a cascade of events that are present during a chronic inflammatory/initial fibrotic phase. It is supposed, that some fibrosis (even though modest) occurred already before starting with the treatment in this pre-clinical study and still continued to compensate the loss of cardiomyocytes and stabilise the damaged ventricular wall to prevent its rupture. Nevertheless, impaired cardiac function at day 14 after inducing myocardial infarction (as determined by the %LVEF) could be restored to a degree by application of SPREADS at day 14 post-MI, independently whether loaded with HA-PH-RGD hydrogel alone or with additional c-ADSCs, by comparing %LVEF at day 28 and 42 post-MI with the functional output at day 14 post-MI. Improvement of cardiac function by treatment with SPREADS could be not distinctly attributed to an angiogenic effect, as quantification of CD31-positive blood vessels in the M2 region of the extracted hearts revealed no statistically significant differences when comparing treatment group II and III (SPREADS + Gel with/without cells) with the GS control treatment group I, respectively [76].

The application of SPREADS resulted in an enhanced %LVEF associated with the mechanical support and modulation of the multiphase reparative responses

initiated after MI. However, it must be emphasized that the wound healing reaction *per se* cannot be further considered in its 'classical sense', since the empty SPREADS device itself initiates already an altered cascade of wound healing. Consequently, a more long-term *in vivo* study is needed, also with the empty SPREADS device, to investigate the mechanisms of action in more detail but also to evaluate the potential of SPREADS to limit hypertrophy after MI. Indeed, the cardiac function could be not further improved by the delivery of c-ADSCs with SPREADS in this study yielding no standalone benefit of the employed cell source. But SPREADS offers the unique opportunity to serve as platform device being potentially capable to enable controlled and targeted delivery of arbitrary potent therapeutic cells or bioactive substances (gene- and protein-based) in an always uniform and minimal-invasive way to the epicardial heart surface. SPREADS may hence facilitate the identification of the most effective therapeutic approach for generation of new functional myocardial tissue after MI [76]. As the endogenous turnover of resident cardiomyocytes is only 0.3-1% annually [142], the biological support of the weakened myocardium by delivery of exogenous cells feasible to replace the massive loss of cardiomyocytes post-MI is supposed to be one of the therapeutic targets also in the future. Promising candidates to be delivered by SPREADS comprise patient derived cardiac progenitor cells, cardiomyocytes or cardiac progenitor cells obtained from patient specific induced pluripotent stem cells [143, 144] or even therapeutic extracellular vesicles [145]. Differentiation and hence the regenerative capacity of these cells can be moreover significantly influenced by mechanical stimuli [6]. A multimodal approach of combining SPREADS with a mechanical augmentation device [53, 55] that is capable to enable spatially adjustable epicardial augmentation represents an sophisticated approach to further improve cardiac regeneration. Combination with a mechanical augmentation may offer the opportunity to manipulate the delivered cells but also provide diastolic and systolic support of the weakened myocardial tissue following myocardial infarction [76].

4 A novel application approach for patch-based materials to the heart surface

4.1 Preface

Moreover to the concept presented in chapter 3, the AMCARE project aimed to pursue also the alternative strategy of employing a HA-based cardiac patch instead of a HA-based hydrogel as scaffold for Celyad's cADSCs. The HA-based cardiac patch should similarly serve as protective biophysical support to the stem cells delivered to the epicardial heart surface and should provide mechanical support to the weakened myocardium. This chapter describes my work as part of AdjuCor's responsibility within the framework of the AMCARE project regarding this alternative cardiac patch approach, which focused on the development of a respective device capable to apply a cardiac patch supplied by Contipro (Czech Republic) in a minimal-invasive way to the epicardial heart surface on the one hand. On the other hand, the device should also facilitate provision of controlled pressure to the patch or in case of more hemodynamically unstable patients even mechanical augmentation of the weakened myocardium post-MI.

4.2 Introduction

The application of exogenous stem cells represents a promising option to encourage the weakened myocardium post-MI to regenerate [94]. An adequate structural support is essential in this context to enable effective differentiation and proliferation of the delivered cells. Naturally, this functionality is provided by the ECM. But collagenous scar tissue formed after MI lacks from essential properties that are required to provide a sufficient microenvironment for exogenously administered cells impairing their effective engraftment [35]. Cardiac patches with adjustable architecture [93, 94] similar to the structural features as in natural myocardial ECM may hence represent a promising option to improve therapeutic efficacy of cell-based strategies applied to the weakened myocardium post-MI [35, 61]. Preformed scaffolds with defined textural features are also used to generate *in vitro* engineered tissue constructs that are finally delivered to the epicardial surface in form of a patch [56, 60] stimulated by the supply-demand shortage of available donor organs for heart transplantation. For more information regarding the range of employed materials for cardiac patches and the manufacturing methods thereof, the reader is referred to chapter 2. However, the delivery of patch-based biomaterials has been mostly accomplished in a surgically invasive manner during open chest procedures [63] with exception of the recently developed carrier device SPREADS [76] for instance, as described in the previous Chapter 3. Indeed, SPREADS can be administered to the epicardial heart surface minimally-invasively and remained firmly attached to the epicardium with the aid of an *in situ* applied bioadhesive into SPREADS' foreseen bioadhesive reservoirs. But SPREADS does not enable the application of additional mechanical cues to the delivered cells, which are known to impact cell differentiation and hence potentially also enhance the therapeutic efficacy of the delivered cells [6], especially in case of embryonic stem cells [146].

Normally, cardiomyocytes are part of a mechanically dynamic organ that are physiologically subjected to cyclic mechanical cues induced by the native rhythmic heart motion. Gwak *et al.* [146] have shown that application of cyclic strain to *in vitro* cultured embryonic stem cell-derived cardiomyocytes on an elastic scaffold promotes the expression of cardiac-specific genes such as those for cardiac α-myosin heavy chain, GATA-4 and Nkx2.5 compared to the unstrained control. Active

mechanical support may have even perhaps the potential to promote activation of endogenous cardiac stem cells and thus to enhance recovery of the weakened myocardium following myocardial infarction. In case of hemodynamically more unstable patients with a large infarct or at an advanced stage of HF with heavily affected contractility, the active mechanical support may moreover have the potential to augment the cardiac output by providing both diastolic and systolic support. Hence, mechanical augmentation may relieve the heart from the increased workload leading potentially to attenuation or even prevention of chronically activated compensatory mechanisms that amplify the dysfunction of the heart muscle. Unloading of the ventricle has been moreover proven to encourage resident cardiomyocytes to proliferate [147]. Previous results of this group [148] indicate that the inability of post-natal human cardiomyocytes to divide is connected to an increase in mitochondrial mass postnatally. An increased mitochondrial content causes elevated levels of ROS leading to oxidative DNA damage. Consequentially, DNA damage responses are activated that result finally in a permanent cell cycle arrest. This deleterious cascade is moreover intensified in case of increased mechanical load as existing post-MI which further impairs the capability of the heart to regenerate following myocardial infarction. Treatment with LVADs achieved a decrease of up to 60 % in mitochondrial content accompanied with a decrease of up to 45 % in cardiomyocyte size compared with pre-LVAD ventricles indicating that relief of the increased ventricular workload may even reverse cardiomyocyte hypertrophy [147]. Treatment of patients with a synergistic approach comprising regenerative agents while mechanically augmenting the heart may consequentially have the potential to better exploit the therapeutic potential of regenerative agents such as stem cells as maladaptive compensatory mechanisms initiated as result of the increased workload post-MI may be attenuated or even suppressed.

The elaborated concept for such a novel **Epi**cardial **P**atch **A**dministration **D**evice (EpiPAD) developed as part of my work within the framework of the AMCARE project aims to overcome limitations of previous approaches to facilitate in a multimodal approach the combinatorial biological and mechanical support of the weakened myocardium post-MI. The concept development of EpiPAD focused on its feasibility to enable the targeted local administration of Contipro's HA-based patch to the epicardial surface and to enable provision of spatially adjustable epicardial

pressure to facilitate sustained contact of the delivered patch to the epicardium, manipulate the delivered cells or to additionally support the cardiac output. Basic functionality of the manufactured EpiPAD prototype to be consecutively foldable and expandable without losing its initial geometrical shape as well as to accommodate a pre-formed HA-based patch was assessed *in vitro*. EpiPAD's feasibility to be minimally-invasively implantable and to deliver Contipro's HA-based patch to the epicardial heart surface was verified in an acute porcine *in vivo* trial. The overall objective was to generate a first prototype that may be potentially able to provide combinatorial mechanical and biological therapy to the weakened myocardium.

4.3 Materials and methods

4.3.1 Concept development

The patented concept of EpiPAD [149-152] aimed to address current limitations associated with the targeted local delivery of textile-like scaffolds such as the palmitoyl-hyaluronan (Pal-HA)-based mesh provided by Contipro to a well-defined area on the dynamic heart surface in a minimal-invasive approach and the challenge to ensure its sustained contact to the epicardium without employing any surgical aids or adhesives. As schematically illustrated in Figure 4.1, EpiPAD was constructed as an assembly consisting of the following three main components: a support frame, a patient-specific sleeve including an inflatable pad with a pocket on its inner surface and a separate patch carrier. The support frame is intended to ensure adequate expansion of EpiPAD in the pericardial cavity during minimal-invasive implantation of the folded device. Additionally, the support frame aims to enable convenient manipulation of EpiPAD to finally position the accommodated patch to the target region. The patch is intended to be thermally adhered to the polymeric foil of EpiPAD's detachable patch carrier aiding to facilitate easy and quick connection of a patch to EpiPAD at the day of treatment, especially in case of applying a cell-loaded patch. This carrier was considered to be insertable into a pocket that is part of a patient-specific sleeve, finally designed to facilitate correct alignment of a textile-like patch as provided by Contipro within the framework of the AMCARE project relative to the target area for treatment. To avoid displacement of the sleeve and hence the delivered patch as consequence of the native

heart motion, the concept development of EpiPAD considered the permanent connection of the sleeve to the support frame along its superior circle. Sustained and stable contact of the delivered textile patch with the infarcted area should be achieved by an inflatable pad that can be inflated and deflated in synchrony with the native heart motion by employing AdjuCor's already developed custom-made electropneumatic control unit [55]. Moreover, this inflatable pad offers the opportunity to mechanically manipulate delivered cells in case of a cellular cardiac patch or to actively augment the ventricular pumping function according to the idea of a therapeutically multimodal approach. The inflatable pad was intended to be embedded in the patient-specific sleeve with the purpose to ensure its correct positioning relative to the accommodated patch and to the akinetic area affected by the MI.

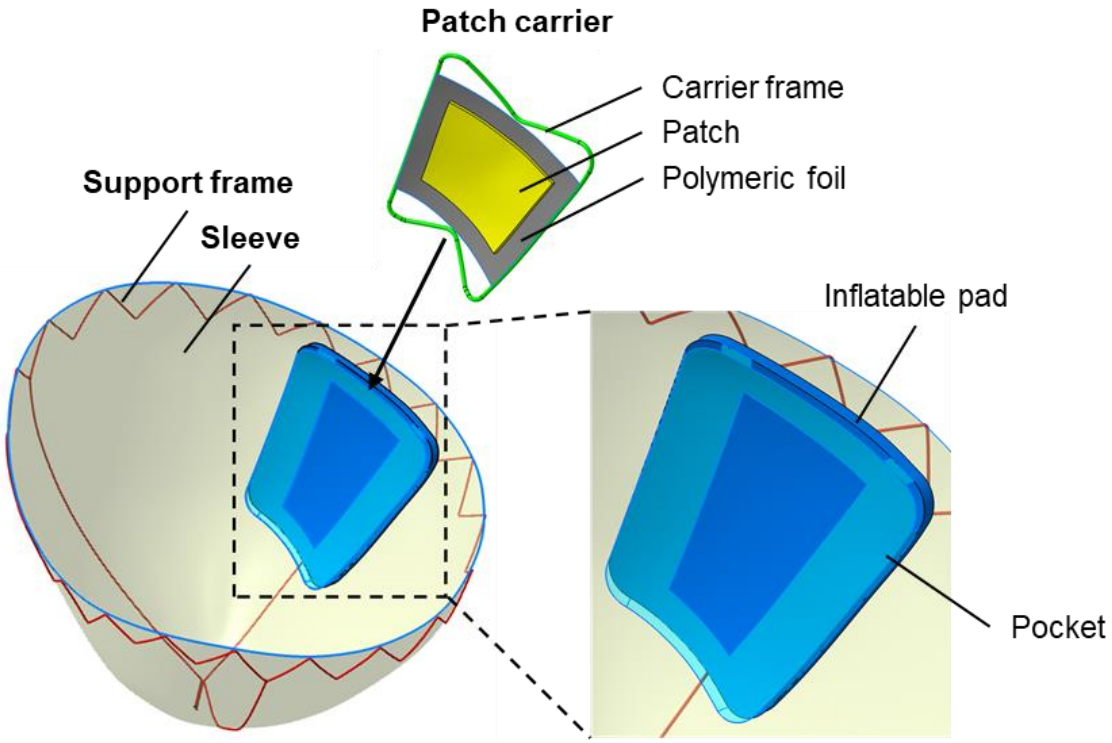

Figure 4.1: Schematic isometric illustration of the developed concept for EpiPAD consisting of a support frame, patient-specific sleeve including an inflatable pad with a pocket on its inner surface as shown in the magnification view on the right side, and a detachable patch carrier serving as aid to facilitate easy and quick connection of a patch to EpiPAD by inserting the pre-loaded patch carrier into the sleeve's foreseen pocket.

4.3.2 Component production and assembly of EpiPAD

The production of the support frame, sleeve and patch carrier for a first prototype of EpiPAD was based on a computed tomography (CT) scan of a Landrace pig employed in a previous study of AdjuCor [55] according to the already published protocol by Jagschies *et al.* [55]. Briefly, the CT scan was triggered to the time point of maximum diastolic filling to avoid device-related impairment of diastolic cardiac function. Based on the obtained CT images, the epicardial heart surface was segmented as shown exemplarily in Figure 4.2 A from the apex to the mitral valve plane by employing the software MIMICS (Materialise, Leuven, Belgium) to receive a virtual 3D geometry of the ventricle portion of the heart (see Figure 4.2 B). Offset patient-specific heart forms (sintered and milled) as illustrated in Figure 4.2 C and Figure 4.2 D were generated based on the segmented heart shape, which served as positive moulds to produce the support frame, sleeve and patch carrier, respectively.

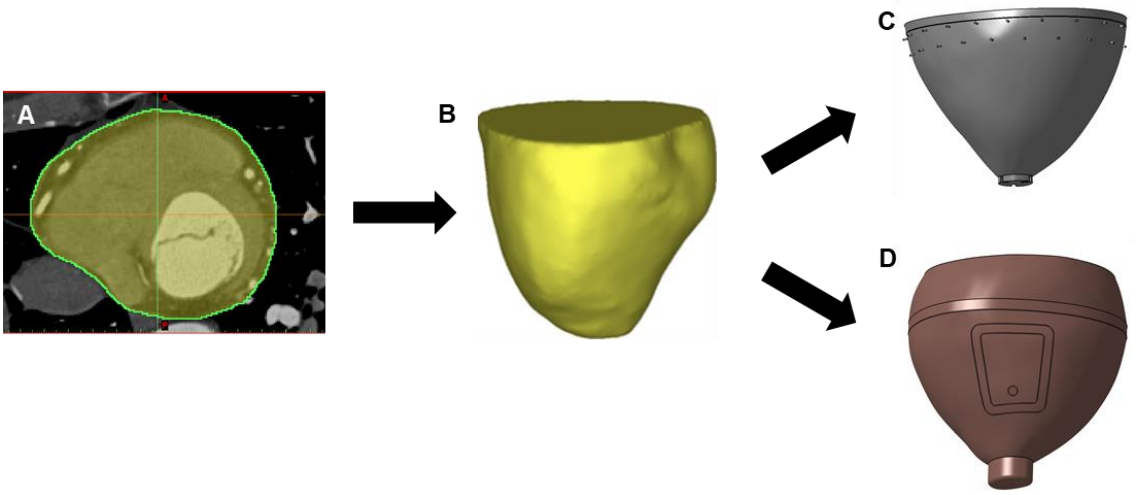

Figure 4.2: Schematic illustration of the procedure to obtain (C, D) offset patient-specific heart forms serving as positive moulds for the manufacturing processes of EpiPAD's components according to a previously published protocol by Jagschies *et al.* [55]. (A) Segmentation of CT images to (B) create a virtual 3D geometry of the ventricle portion of the heart with the aid of MIMICS. Based on the virtual 3D heart shape, offset (C) sintered and (D) milled patient-specific heart forms were generated. Adapted from Jagschies *et al.* [55].

The support frame was assembled from three separate segments that were manufactured from a 0.5 mm Nitinol wire, respectively. Each segment consists of a coiled structure along EpiPAD's upper boundary towards the mitral valve plane forming a part of the circumferential circle and two extension struts converging at

the apex. Forming of each segment was accomplished with the aid of an offset patient-specific sintered form, as schematically shown in Figure 4.3 A. Guiding of the Nitinol wire was accomplished by bolts and notches. To avoid squeezing of major blood vessels such as the inferior vena cava or pulmonary veins by the upper rim of EpiPAD, a recess for these major blood vessels was considered in the support frame by shifting the respective posterior part of the superior circle towards the cardiac apex (see Figure 4.3 B). All three segments were finally connected by joining proximate extension struts with 2 capsules as schematically shown in Figure 4.3 B.

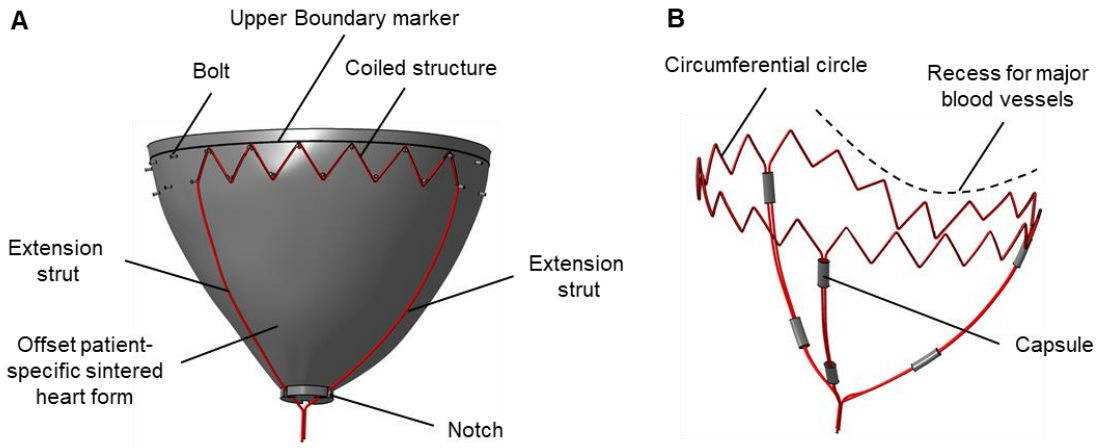

Figure 4.3: Schematic illustration of the procedure to manufacture EpiPAD's support frame. (A) Forming of a support frame segment consisting of a coiled structure towards the upper boundary of EpiPAD and two extension struts converging at the apex, respectively, on the surface of an offset patient-specific sintered form. Bolts and notches on the sintered heart form served for guiding of the Nitinol wire. (B) Assembled support frame consisting of three segments that are connected by joining proximate extension struts with two capsules, respectively.

The sleeve with its incorporated inflatable pad and pocket was made from a thermoplastic PU with the aid of thermoforming and solvent based gluing. A plane foil of a thermoplastic PU (Desmopan 385S, 0.4 mm thickness, Covestro AG, Leverkusen, Germany) was initially thermoformed over an offset patient-specific milled form to reproduce the segmented heart shape and to imprint the respective borders of the inflatable pad and pocket. Location and size of the inflatable pad and the pocket can be adapted depending on the extent of the infarcted region. The inflatable pad was generated by gluing a plane PU foil (Desmopan 385 S, 0.2 mm thickness) in the shape of the pad's unfolded border (cut out by laser) on the epicardium facing inner surface of the sleeve based on the respectively imprinted markers for the pad border and inner gluing edge (see Figure 4.4 A). A hole

with 3 mm in diameter was punched in the thermoformed sleeve according to the imprinted mark given by the milled form (see Figure 4.4 A) to provide air supply to the inflatable pad via a 3.35 x 5.1 mm PU-based supply line purchased from Medi-Line Inc. (France). Connection of the supply line to the inflatable pad was accomplished by a customized flange, that was centrally glued across the punched-out hole on the pericardium facing surface of the sleeve. The pocket on the inner surface of the inflatable pad was similarly generated as the inflatable pad itself. The shape of the inflatable pad's unfolded border with additional wings (intended to serve as gluing edges and as respective borders of the pocket) as shown in Figure 4.4 B was initially cut out of a plane PU foil (Desmopan 385 S, 0.2 mm thickness) for this purpose. This cut-out shape was additionally partially laser cut in the in the centre according to a quadrangular profile (see Figure 4.4 B) to create a window the can be removed by attached yarns after implantation to expose the accommodated patch. The wings of the cut-out shape were afterwards folded along the pad border to adhere them to the epicardium facing inner surface of the inflatable pad. Finally, the sleeve was cropped along its imprinted markers for the upper and lower cutting edge.

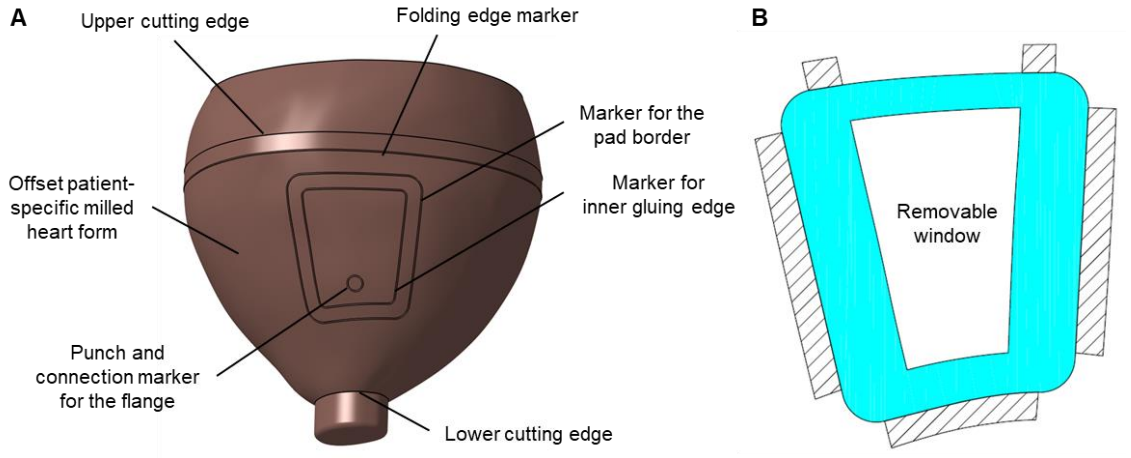

Figure 4.4: (A) Schematic illustration of the offset patient-specific milled heart form with its respective markers employed for production of the sleeve with its incorporated inflatable pad and pocket. (B) Schematic illustration of the pocket's unfolded epicardium facing front side depicted in turquoise and wings intended to serve both as gluing edges and respective borders of the pocket shown as hatched area, respectively. The removable window of the pocket's epicardium facing front side is shown as uncoloured area.

The patch carrier was assembled from a carrier frame and a PU foil (Desmopan 385S, 0.4 mm thickness). The carrier frame was manufactured from a plane

0.5 mm thick Nitinol sheet. The respective frame shape with a web thickness of 0.3 mm was cut out by laser and afterwards adapted to the 3D-curvature of the heart surface related to the corresponding position of the sleeve's pocket. For this purpose, the cut-out plane frame was accordingly aligned on the surface of the offset patient-specific sintered form, mounted and finally annealed. The PU foil was cut to the desired size to fit between the upper and lower rim of the carrier frame (see Figure 4.1). The cut-out PU foil was finally mounted to the lateral edges of the carrier frame with the aid of tetrahydrofuran, respectively.

Joining of the sleeve with the support frame was accomplished by aligning the support frame on the pericardium facing outer surface of the sleeve, folding the sleeve's upper rim along its imprinted folding edge marker (final upper edge towards the mitral valve plane) over the superior circle of the support frame and adhering it to the outer sleeve surface. The assembly was afterwards mounted to a customized sheath by embedding the extension struts in the sheath with an epoxy resin-based adhesive, which was finally filled with a silicon glue (SI-1511) purchased from Raumedic AG (Helmbrechts, Germany) as shown in Figure 4.5. The aim was to provide axial stabilisation of EpiPAD and to ensure adequate guiding of the pneumatic supply line to avoid potential tube kinking.

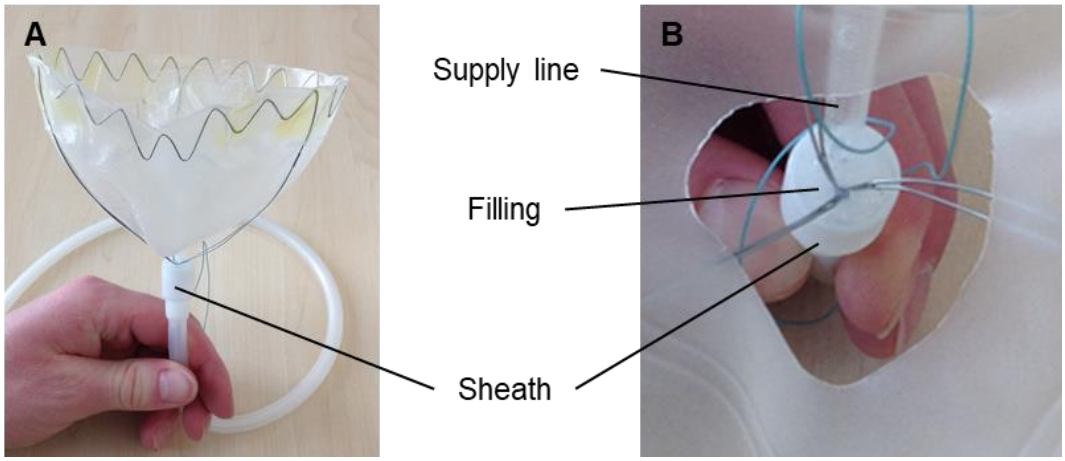

Figure 4.5: (A) Lateral and (B) top view of the EpiPAD after mounting the support frame to a customized sheath with the purpose to ensure axial stability of EpiPAD and avoid kinking of the pneumatic supply line for the inflatable pad.

4.3.3 Preparation of the Pal-HA patch

Pal-HA patch samples required for basic evaluation of EpiPAD's first prototype were kindly provided by Contipro and prepared according to their previously published protocol [153]. Briefly, the textile patch samples with dimensions of 25 x 25 mm were generated by warp-knitting of yarns that were simultaneously knitted on the front and back needle beds of the employed machine (DNB/EL-800-8 B double needle bed warp knitting machine, Comez) and joined by underlaps to avoid rolling up of the fabric edges. Yarns consisting of 3 monofilaments were prepared form Pal-HA-based fibres by a ring spinning machine (VUB a.s., Czech republic) combining S- and Z-twist with the aim to avoid later distortion of the patch. Pal-HA fibres were produced by Contipro's patented wet spinning process based on a Pal-HA derivative (320 kDa) that was dissolved in 50 % isopropanol at room temperature to generate a 6 % (w/w) Pal-HA solution for the wet spinning process. The lateral edges of the prepared patch samples were made from polypropylene with the purpose to facilitate connection of the prepared patch samples to the PU foil of EpiPAD's patch carrier via thermo-bonding, respectively. To attenuate fibre swelling of the warp-knitted fabrics, the generated fabrics were frozen at -18 °C for 5 hours after swelling in demineralized water for 20 minutes at room temperature and finally freeze-dried at -80 °C and 0.5 mbar for 16 hours [153].

4.3.4 Suitability assessment of EpiPAD's concept *in vitro*

Suitability assessment of EpiPAD's implemented concept regarding the connection of a patch to EpiPAD was carried out by evaluating the insertion process of a patch carrier into the sleeve's foreseen pocket in terms of operability and time needed for the coupling process. As pre-requisite to be minimally-invasively implantable, EpiPAD's capability to be consecutively foldable and expandable while preserving its geometrical shape was tested by successive crimping of EpiPAD, transfer of the folded EpiPAD into a tube with an inner diameter of 30 mm and release of the folded EpiPAD from the tube. Crimping of EpiPAD was accomplished by a simplified radial crimping device as shown in Figure 4.7 after cooling of EpiPAD in ice water.

4.3.5 *In vivo* feasibility assessment of EpiPAD

Anatomic appropriate delivery of EpiPAD to the epicardial heart surface by a minimal-invasive approach was examined in an acute porcine *in vivo* trial with the purpose to demonstrate EpiPAD's capability to facilitate targeted local administration of Contipro's HA-based patch to the surface of the beating heart.

Animal preparation

Animal preparation before starting with the intervention was carried according to the previously published protocol employed to assess SPREADS' pre-clinical feasibility [76].

Implantation procedure

Similarly as SPREADS, the minimal-invasive implantation of EpiPAD was accomplished via a sub-xiphoidal access as shown in Figure 4.9 A. The access to the pericardial space was generated by a horizontal apical incision of the pericardium with a length of approximately 3 cm. To avoid inadvertent expansion of EpiPAD outside of the pericardial space, a retractor was initially inserted into the pericardial space before beginning with the implantation of EpiPAD. Correct positioning of the retractor was validated by fluoroscopy (see Figure 4.9 B). Crimping of EpiPAD loaded with Contipro's Pal-HA patch to a diameter of 20 mm was accomplished as described in section 4.3.4. For easier implantation handling purpose, the crimped EpiPAD was transferred to a custom-made tube (20 x 25 mm) with angled abutting face (see Appendix II, Figure 7.16). For implantation of EpiPAD, this tube was positioned with its angled face into the retractor's channel providing the access of EpiPAD to the pericardial space (see Figure 4.9 C). The crimped EpiPAD was afterwards slowly pushed out of the custom-made tube into the pericardial space under fluoroscopic guidance. Heart rate, oxygen saturation, blood pressure (BP), and ECG was controlled during the entire implantation procedure. Expansion of EpiPAD and positioning of the accommodated patch carrier was subsequently evaluated by fluoroscopy (see Figure 4.9 D). Finally, the animal was euthanized by injection of saturated KCl-solution into the left ventricle.

4.4 Results

4.4.1 EpiPAD concept evaluation *in vitro*

EpiPAD's separate patch carrier could be easily inserted into EpiPAD's foreseen pocket by initially compressing the lower edge of the patch carrier frame in its circumferential direction (see first image in Figure 4.6) to fit through the pocket's opening (see second image in Figure 4.6), and subsequently align the patch carrier in the pocket with the aid of surgical forceps (see image 3 to 8 in Figure 4.6). The entire procedure as illustrated by the image sequence shown in Figure 4.6 took less than a minute. The carrier frame enabled a finally stable positioning of the carrier within the pocket.

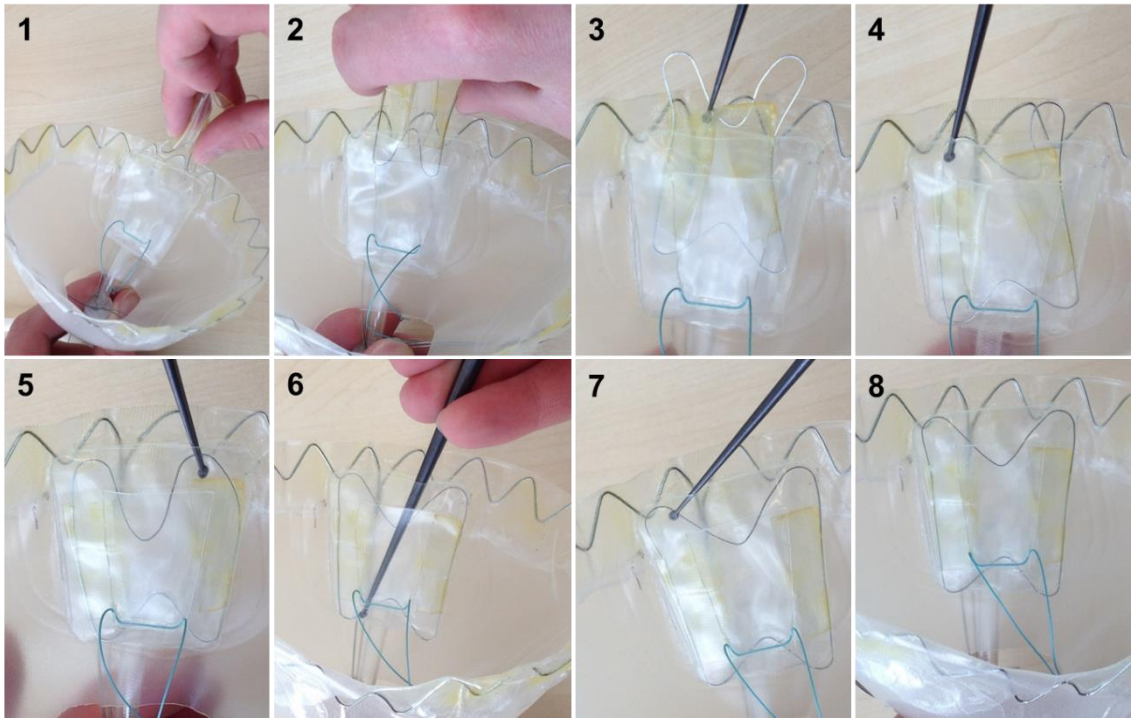

Figure 4.6: Image sequence showing progressive stages of the procedure to insert EpiPAD's patch carrier into the foreseen pocket of EpiPAD's sleeve.

As shown in Figure 4.7, in ice-water pre-cooled EpiPAD could be successfully crimped with the aid of a simplified radial crimping device and transferred to a tube with an inner diameter of 30 mm as shown in the first image of the sequence illustrated in Figure 4.8.

Figure 4.7: Crimping procedure of EpiPAD by employing a simplified radial crimping device.

Release of the crimped EpiPAD out of the tube could be easily accomplished by pushing out EpiPAD at its proximal end. During the release process, EpiPAD expanded by itself without the use of any additional aids as shown in Figure 4.8. No remaining deformations or damages of EpiPAD were determined after complete release out of the tube (see last image of the sequence shown in Figure 4.8). No displacement of the connected patch carrier as consequence of the consecutive crimping and expansion procedure was observed.

Figure 4.8: Image sequence showing progressive expansion stages of the crimped EpiPAD out of a tube with an inner diameter of 30 mm.

4.4.2 Exemplary assessment of EpiPAD's pre-clinical feasibility *in vivo*

EpiPAD crimped to a diameter of 20 mm could be successfully delivered to the epicardial heart surface via a sub-xiphoidal access as shown in Figure 4.9 A in a minimal-invasive approach with the aid of a custom-made tube (see Figure 4.9 C and Figure 7.16 in Appendix II for more details regarding the tube). Expansion of the crimped EpiPAD outside of the pericardial cavity was effectively prevented by a retractor that was inserted into the pericardial cavity before beginning with the implantation of EpiPAD. Verification of correct retractor positioning as well as appropriate expansion of the crimped EpiPAD into the pericardial space was succeeded by fluoroscopy (see Figure 4.9 B and D). The implantation procedure of the retractor and EpiPAD itself did not provoke any disturbances of vital signs and hemodynamic (see Table 7.1 in Appendix II) as well as did not cause any cardiac arrythmias. By slowly releasing EpiPAD out of the custom-made tube, EpiPAD expanded inherently around the ventricular portion of the beating heart (see Figure 4.9 D) accompanied with partial self-alignment in circumferential direction. In case a reposition would be necessary, EpiPAD could be conveniently manipulated by the sheath connected to the extension struts of EpiPAD's support frame. The entire manipulation was also successfully tolerated by the patch carrier, loaded with Contipro's Pal-HA patch before implantation, as no dislocation, no remaining deformations or damages of the patch carrier were determined after complete expansion of EpiPAD (see Figure 4.9 D). The entire implantation procedure comprising the preparation of the sub-xiphoidal access, insertion of the retractor and release of the crimped EpiPAD out of the custom-made tube was accomplished within 15 minutes.

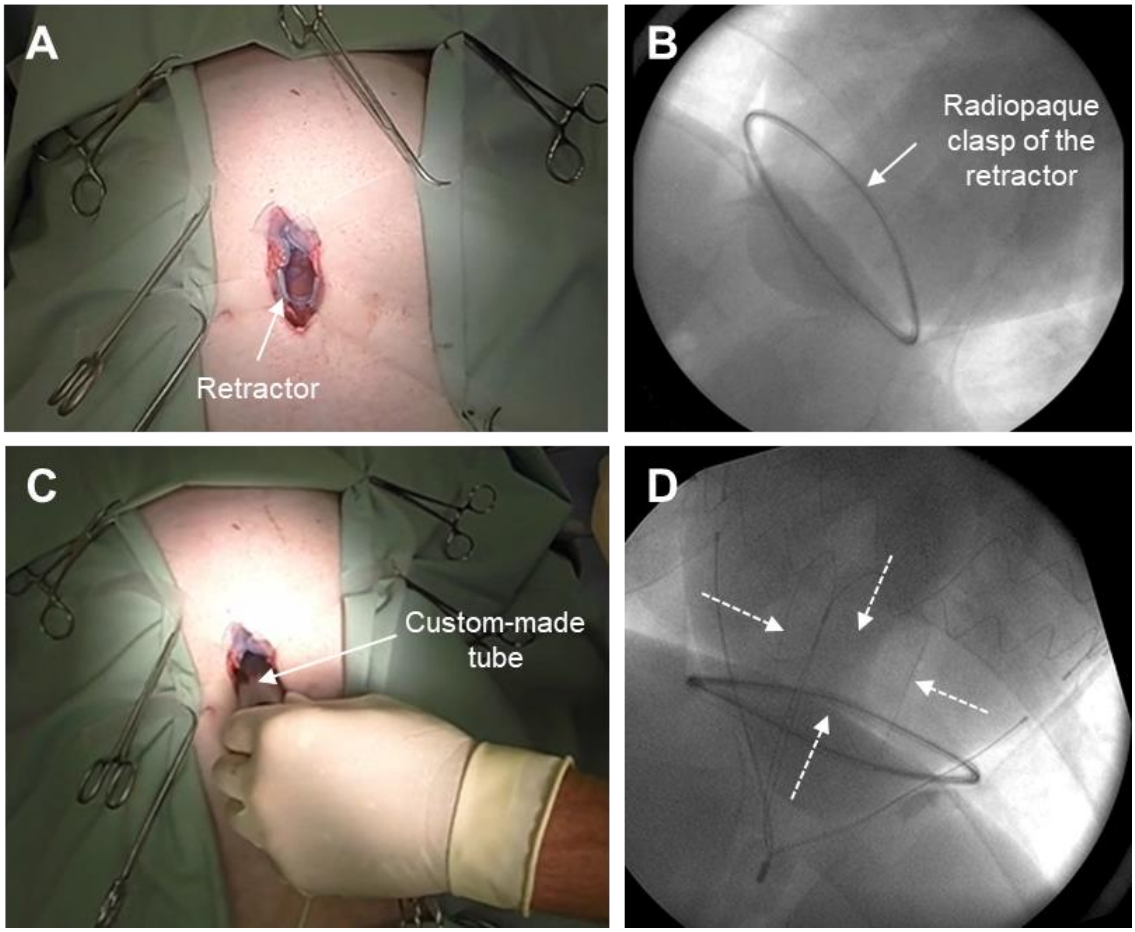

Figure 4.9: Images of the acute porcine *in vivo* trial (n = 1) to assess the pre-clinical feasibility of EpiPAD. (A) Prepared sub-xiphoidal access with a retractor inserted into the pericardial cavity to avoid inadvertent expansion of EpiPAD outside of the pericardial cavity. (B) Fluoroscopic position validation of the applied retractor. (C) Minimal-invasive implantation procedure of the crimped EpiPAD with the aid of a custom-made tube (20 x 25 mm). (D) Expansion and positioning validation of EpiPAD. The location of the connected patch carrier is indicated by the dashed arrows pointing on the radiopaque edges of the carrier's Nitinol frame.

4.5 Discussion

Motivated by the limited ability of the adult mammalian heart to restore damaged contractile myocardial tissue after MI, a multitude of acellular and cellular cardiac patches have been evolved in the course of the past decades (see Chapter 2). Developed cardiac patches aim to provide either solely passive mechanical support to the weakened myocardium or to facilitate additionally biological support by immobilized regenerative therapeutics such as stem cells with the purpose to encourage regeneration of the post-MI damaged cardiac tissue. However, comparable simple fixation strategies of most investigated cardiac patches by surgical sutures or manual application of a bioadhesive to the patch's back side limit their application to surgically invasive procedures [78-83] and thus hamper their potential translation into clinic, motivating the need of an advanced, minimal-invasive delivery approach for patch-based materials [63]. It has been successfully shown, that SPREADS is capable to overcome this application related limitation regarding clinical translation by being implantable in a minimal-invasive approach without employing any surgical aids for fixation on the epicardial surface. But SPREADS is not capable of providing spatially adjustable mechanical cues to immobilised cells, indicated to potentially enhance therapeutic efficacy by manipulating the cell fate [6, 146], or even hemodynamically support the weakened myocardium. Recently evolved DCC devices [53-55], which intend to provide both diastolic and systolic support to the heart, are on the other hand unable to deliver patch-based materials to a well-defined region on the epicardial heart surface. A device capable to manage both targeted local delivery of patch-based materials and active support of the heart function as in case of DCC devices has not been reported yet, prompting the development of a novel bifunctional device concept. As part of my work within the framework of the AMCARE project, the device EpiPAD was developed with the intention to play a dual role in heart regeneration post-MI. EpiPAD aims to facilitate delivery of patch-based biomaterials loadable with therapeutic agents to the epicardial heart surface via a single-stage minimal-invasive, closed chest intervention on the one hand. On the other hand, EpiPAD pursues the target to provide spatially adjustable epicardial pressure to either facilitate merely sustained contact of the delivered patch to the epicardium and manipulate the delivered cells or to additionally provide epicardial augmentation as AdjuCor's individualised Biventricular

Epicardial Augmentation Technology (BEAT) [55] aiming to relieve the heart from increased workload. Initial proof of concept assessment of EpiPAD's first prototype successfully demonstrated its capacity to serve as minimally-invasively implantable cargo device for textile-like scaffolds to the epicardial heart surface.

Therapeutic efficacy of cellular approaches is inevitably associated adequate viability of the delivered cells [154]. Hence, a convenient connection procedure of a cellular patch to EpiPAD at the day of intervention is essential to avoid stress-associated impairments of cell viability as in case of needle-based administration strategies [91]. For this purpose, EpiPAD was constructed as an assembly with a detachable patch carrier. Preliminary *in vitro* and *in vivo* concept evaluation of EpiPAD's first prototype suggest that the patented connection concept [149-152] may basically comply with all necessary requirements related to the targeted delivery of cellular patches to the epicardial surface. However, further proof-of-principle trials with cellular patches are needed to completely prove EpiPAD's compatibility with cellular therapeutics.

The modular design of EpiPAD with its detachable patch carrier may additionally positively affect the therapeutic efficacy of regenerative substances such as stem cells. Similarly as SPREADS [76], development of the respective biomaterials serving as potential scaffold can exclusively focus on meeting the requirements of the delivered cells or bioactive substances (gene- and protein-based). Moreover, EpiPAD owns the potential, to serve as platform device in a similar way as SPREADS to deliver arbitrary potent cardiac patches in an always uniform and minimal-invasive manner to the epicardial heart surface [76]. Since SPREADS is also manufactured from a thermoplastic polymer, SPREADS may also be connectable to EpiPAD. This may offer the unique chance to carry out comparable studies of hydrogels and patches manufactured from the same raw material that are intended to be employed as scaffolds for regenerative stem cell approaches, respectively. Based on EpiPAD's capacity to provide spatially adjustable pressure to the accommodated patch by the inflatable pad, the impact of mechanical cues on the cell differentiation and thus the therapeutic efficacy can be furthermore elucidated.

The elaborated concept for EpiPAD was based on AdjuCor's BEAT concept [55] for the following two main reasons:

1) Self-expandable implant that can be implanted via a minimal-invasive approach, a prerequisite to encourage more easy clinical translation of patch-based biomaterials.
2) Evidence of successfully providing mechanical augmentation of cardiac function parameters, a prerequisite for EpiPAD to provide as multimodal approach in case of hemodynamically unstable patients additionally diastolic and systolic support of the weakened myocardial tissue post-MI.

With the aim to crimp EpiPAD to a smaller diameter than the BEAT implant and thus to enable implantation via a smaller access, EpiPAD was constructed of a simplified support frame compared to the nitinol sheath employed for the BEAT implant. However, EpiPAD could be successfully implanted in a minimal-invasive approach via a sub-xiphoidal access within 15 minutes with the aid of a custom-made tube (20 x 25 mm), retaining its initial geometrical shape after complete expansion around the epicardial heart surface. The circumferential circle of EpiPAD's support frame running along EpiPAD's upper boundary towards the mitral valve plane provide consequently sufficient radial force to completely unfold EpiPAD without employing any additional aids. Tilting of EpiPAD was effectively avoided by extension struts connected to the superior circle and embedded into the sheath adding axial stability to EpiPAD. Partial self-alignment of EpiPAD in circumferential direction was achieved by EpiPAD's patient-specific sleeve similarly as Jagschies *et al.* [55] observed it in case of the BEAT implant. As demonstrated by the vital signs recorded during the implantation procedure of EpiPAD, neither the implantation of EpiPAD *per se* nor the finally expanded device provoke any disturbances of hemodynamic or provoke any cardiac arrythmias. Hence, this exemplary *in vivo* trial suggest that EpiPAD may satisfy the requirement to enable the delivery of textile-like patches in a minimal-invasive approach to a well-defined region on the epicardial heart surface. EpiPAD's intended ability for active mechanical augmentations could not be evaluated in the course of the pre-clinical *in vivo* trials approved within the framework of the AMCARE project. However, EpiPAD's elaborated concept has the great capability to potentially provide both biological and active mechanical support to the weakened myocardium as promising multimodal therapeutic option for patients post-MI and at an advanced stage of HF.

5 Conclusion and Outlook

A multitude of regenerative approaches have been evolved over the last decades with the purpose to encourage the damaged myocardial tissue to regenerate instead of remodelling to non-contractile collagenous scar tissue [59-65, 77-83, 93, 94, 133, 138, 139]. Especially stem cell technologies have drawn considerable attention, as exogenously administered cells may be capable to potentially compensate the massive loss of CMs post-MI. But currently employed administration strategies of hydrogels and patches used as cellular scaffolds to improve retention and survival of the cells are still associated with several issues [63, 66, 89]. These application-related issues are supposed to impair the therapeutic efficacy of the cells and thus hamper their translation into clinical routine motivating the need for novel advanced delivery strategies for hydrogel- and patch-based biomaterials loadable with exogenous stem cells as presented in this PhD thesis. Within this PhD thesis, two novel devices were developed aiming to enable targeted delivery of either hydrogels or patches, theoretically loadable with stem cells but also with gene- or protein-based regenerative therapeutics, to the epicardial heart surface in a minimal-invasive approach ensuring their sustained contact to the epicardium without employing any surgical aids.

Implementation of a carrier device for hydrogel-based biomaterials

The developed bioresorbable carrier device for hydrogel-based biomaterials SPREADS has successfully shown its capacity to accomplish the atraumatic site-specific administration of a fluid, *in situ* curing hydrogel to the epicardial heart surface. Prior challenges [90, 106, 107] associated with the defined application of a hydrogel in its fluid pre-curing state to a well-defined region on a dynamic surface such as the epicardium are effectively resolved by SPREADS [76]. Its unique structure provides a defined space into which the hydrogel can be injected, while preventing undefined dispersion of the injected hydrogel until completely cured. Besides, results obtained by *in vivo* pre-clinical efficacy trials suggest that the hydrogel reservoir defining components of SPREADS facilitated sufficient interaction of the encapsulated hydrogel with the surrounding tissue *in vivo*. No residues of the encapsulated hydrogel were found four weeks after delivering SPREADS loaded

with a degradable HA-based hydrogel to the epicardium. Similar results were obtained by Whyte *et al.* [133], but with a device made from non-degradable materials. To my knowledge SPREADS is the first bioresorbable cargo device facilitating potential epicardial treatment of patients with *in situ* curing hydrogels in a single-stage procedure. SPREADS also successfully tolerated the required folding procedure to get minimally-invasively implanted into the pericardial cavity via a subxiphoidal access and expanded inherently without losing its initial geometrical shape. The unique structure of SPREADS with two half-circumferential grooves represents the essential feature ensuring sustained contact of SPREADS and thus also of intrinsically non-adhesive hydrogels with the epicardial heart surface without the need of any surgical aids. Avoiding of surgical fixation of SPREADS prevents in turn the need of a surgical access to the epicardial surface. No invasive surgical procedure is consequently needed for treatment of patients with SPREADS, facilitating its rapid clinical translation by being applied in combination with commonly carried out interventions such as PCI in the cardiac catheterization laboratory [15, 16, 20]. In case of employing hydrogel-based biomaterials characterised by sufficient adhesive strength to wet tissue surfaces such as BioGlue®, targeted hydrogel administration to the epicardial heart surface can be also accomplished by SPREADS design generation 1.

Exemplary assessment of SPREADS' pre-clinical efficacy loaded with either a HA-PH-RGD hydrogel alone or additionally with 40 million c-ADSCs/animal compared to the GS treatment group revealed a significant improvement of cardiac function in terms of increasing %LVEF, respectively. However, the exact mechanism of action involved in the improvement of the cardiac function could not be clearly elucidated. Comparing analyses of infarct quality as shown by directionality and coherency of collagen fibres, and vascularisation as evaluated by CD31 positive blood vessels revealed no statistical differences between any of the treatment groups. The comparable improvement of cardiac function by both the acellular and cellular treatment group compared to GS indicate that the observed therapeutic benefit may be attributed to the passive mechanical stabilisation of the weakened myocardium provided by SPREADS and the HA-PH-RGD hydrogel. A similar positive effect of mechanically stabilizing patches [78-83] or hydrogels [77, 84-87, 130] has already been described in literature. To better evaluate the therapeutic effect of the

encapsulated hydrogel alone, further chronic *in vivo* studies are needed with applying the empty SPREADS device alone.

The *de facto* reasons for the missing additional therapeutic effect by the applied stem cells could not be clarified within the framework of this PhD thesis, motivating the need for further studies for clarification. A more detailed characterisation and tracking of the delivered stem cells could help to elucidate potential reasons why the cardiac function was not further improved compared to the acellular approach of SPREADS with encapsulated HA-PH-RGD hydrogel alone. Future studies are consequently needed to gain more insight into the potential benefit of the applied materials and cells. Still, shown compatibility of SPREADS with both Contipro's *in situ* fast-curing hydrogel and Celyad's stem cells provide evidence of SPREADS' capacity to effectively carry living cells to the heart surface and ensure their adequate retention. Hence, SPREADS provides an attractive opportunity to deliver a myriad of potent cell sources but also gene- or protein-based therapeutics suspended in hydrogel-based biomaterials in an always uniform, minimal-invasive way to the epicardial heart surface independently of the hydrogel and therapeutics to be applied. SPREADS may represent an important step towards carrying out efficacy evaluation of different hydrogel-based biomaterials and regenerative therapeutics at comparable conditions. Thus, SPREADS is able to determine the most effective treatment approach for patients with impaired cardiac function post-MI. Additionally, SPREADS offers the unique opportunity to investigate the potential therapeutic benefit of exogenously delivered cells by adjusting the porosity of SPREADS' PEU fleece more precisely, so that potential migration of the cells to the weakened myocardial tissue *in vivo* is once prohibited and once permitted. In conclusion, SPREADS successfully addressed current limitations for the targeted local delivery of fluid *in situ* curing hydrogels in a minimal-invasive approach to the epicardial heart surface achieving the first aim for the PhD thesis specified in section 1.5.

Implementation of a concept device enabling delivery of patch-based biomaterials and potentially provide active mechanical support

The developed concept device EpiPAD for patch-based biomaterials has effectively proven its capacity to facilitate the targeted local administration of a preformed textile-like scaffold as exemplary cardiac patch to the epicardial heart surface in a minimal-invasive, closed chest intervention. The elaborated concept to connect the patch to EpiPAD via a detachable patch carrier that is intended to be inserted into a pocket represents a conveniently operable procedure but also a sufficiently stable linkage, being suitable for minimal-invasive application of EpiPAD and capable to retain the patch in its intended position after implantation. Correct alignment of a patch relative to the treatment target is effectively addressed by EpiPAD's patient-specific sleeve and support frame, providing adequate circumferential orientation and axial stabilisation of EpiPAD and thus also of the accommodated patch. The patch carrier additionally facilitates complete spreading of the textile-like patch after implanting the crimped EpiPAD into the pericardial cavity without any additional aids, even though Contipro's Pal-HA mesh is characterised by its insufficient intrinsic expansion force. Autonomous alignment and expansion of the patch with the aid of EpiPAD requires no longer a large access to the epicardial surface, that is commonly accomplished surgically. EpiPAD's capability to tolerate crimping to a diameter of 20 mm and subsequently expanding without losing its initial geometrical shape has been also successfully proven as further prerequisite to be minimally-invasively implantable.

Motivated by previous studies, which have shown the effect of mechanical cues on the cell fate [6, 146] and thus the potential to impact their regenerative capacity, an inflatable pad was incorporated in EpiPAD's sleeve beneath the pocket for the patch carrier. The inflatable pad is additionally envisaged to provide active mechanical augmentation to the weakened myocardium. Hence, EpiPAD may play a dual role in heart regeneration by serving as cargo device for patch-based materials, facilitating biological support on the one hand, but also as DCC device aiming to relieve the heart from increased workload by providing active mechanical support on the other hand. However, further studies are necessary to evaluate EpiPAD's capability to effectively serve as DCC device similar as AdjuCor's previously developed BEAT device [55]. Moreover, chronic *in vivo* studies need to be

carried out to assess the long-term *in vivo* compatibility of EpiPAD first of all, but also to determine the therapeutic effect of patches delivered by EpiPAD on the cardiac function as well as to evaluate the potential impact of mechanical cues on the fate of immobilised cells. In conclusion, EpiPAD successfully provided evidence of enabling targeted local delivery of a textile-like patch in a minimal-invasive approach to the epicardial heart surface, fulfilling the cargo function specified in the context of the second aim for the PhD thesis as mentioned in section 1.5. By consideration of an inflatable pad EpiPAD moreover fulfils all necessary requirements to possibly provide additional mechanical support to the weakened myocardium in a multimodal approach, thus achieving completely the second main objective of this PhD thesis mentioned in section 1.5.

Overall thesis conclusion

In summary, both developed devices SPREADS and EpiPAD represent promising delivery options for hydrogel- and patch-based biomaterials to the epicardial heart surface that successfully address previous limitations associated with the site-specific biomaterial administration to the dynamic heart surface in a minimal-invasive approach, respectively. The elaborated concepts avoid known major risks associated with intravascular administration procedures of biomaterials including thrombus formation or bleeding for instance. Last, the epicardium has been identified as region with vast regenerative potential, as cardiac progenitors participating in cardiac homeostasis at basal levels and potentially capable to replace lost CMs have been localised at the epicardial heart surface [105]. Hence, the epicardium is supposed to represent a reasonable target for regenerative therapeutics, which can be successfully delivered either by SPREADS or EpiPAD depending on the type of employed biomaterial.

6 References

1. Cabin, H.S. and S. Henry, *The heart and circulation.* The heart book, 1992: p. 3-10.
2. Marieb, E.N. and S.M. Keller, *Essentials of Human Anatomy and Physiology*. 12th ed. 2018: Pearson Education, Inc.
3. Sun, X. and S.S. Nunes, *Overview of hydrogel-based strategies for application in cardiac tissue regeneration.* Biomedical Materials, 2015. **10**(3): p. 034005.
4. Kennedy, J., *Clinical anatomy series: cardiac anatomy.* Scottish Univ. Med. J, 2012. **1**: p. 76-80.
5. Barclay, T. *Bones of the Chest and Upper Back*. 2018 3th July 2018 [cited 2019 15th May]; Available from: https://www.innerbody.com/anatomy/skeletal/upper-torso.
6. Sepantafar, M., et al., *Stem cells and injectable hydrogels: synergistic therapeutics in myocardial repair.* Biotechnology advances, 2016. **34**(4): p. 362-379.
7. Freytes, D.O., et al., *8 - Biomaterial scaffolds for cardiac regeneration and repair derived from native heart matrix*, in *Cardiac Regeneration and Repair*, R.-K. Li and R.D. Weisel, Editors. 2014, Woodhead Publishing. p. 201-224.
8. Venugopal, J.R., et al., *Biomaterial strategies for alleviation of myocardial infarction.* J R Soc Interface, 2012. **9**(66): p. 1-19.
9. Organizsation, W.H. *Cardiovascular diseases (CVDs)*. 2017 [cited 2019 20th May]; Available from: https://www.who.int/news-room/fact-sheets/detail/cardiovascular-diseases-(cvds).
10. Organization, W.H., *International statistical classification of diseases and related health problems*. Vol. 1. 2004: World Health Organization.
11. Benjamin, E.J., et al., *Heart disease and stroke statistics-2018 update: a report from the American Heart Association.* Circulation, 2018. **137**(12): p. e67.
12. Flammer, A., J. Steffel, and T. Lüscher, *Epidemiologie der Herz-Kreislauf-Erkrankungen–Prävalenz, Risikofaktoren und Prävention*, in *Herz-Kreislauf*. 2014, Springer. p. 29-34.
13. Wilkins, E., et al., *European cardiovascular disease statistics 2017.* 2017.
14. Davies, M.J., *The pathophysiology of acute coronary syndromes.* Heart, 2000. **83**(3): p. 361-366.
15. Reed, G.W., J.E. Rossi, and C.P. Cannon, *Acute myocardial infarction.* The Lancet, 2017. **389**(10065): p. 197-210.
16. Boateng, S. and T. Sanborn, *Acute myocardial infarction.* Disease-a-Month, 2013. **59**(3): p. 83-96.
17. Thygesen, K., et al., *Third universal definition of myocardial infarction.* Circulation, 2012. **126**(16): p. 2020-2035.
18. Yu, X.-H., et al., *Foam cells in atherosclerosis.* Clinica Chimica Acta, 2013. **424**: p. 245-252.
19. Shinde, A.V. and N.G. Frangogiannis, *Fibroblasts in myocardial infarction: A role in inflammation and repair.* Journal of Molecular and Cellular Cardiology, 2014. **70**: p. 74-82.

20. Steg, P.G. and J.M. Juliard, *Primary percutaneous coronary intervention in acute myocardial infarction: time, time, and time!* Heart (British Cardiac Society), 2005. **91**(8): p. 993-994.
21. Prabhu, S.D. and N.G. Frangogiannis, *The biological basis for cardiac repair after myocardial infarction: from inflammation to fibrosis.* Circulation research, 2016. **119**(1): p. 91-112.
22. Talman, V. and H. Ruskoaho, *Cardiac fibrosis in myocardial infarction—from repair and remodeling to regeneration.* Cell and tissue research, 2016. **365**(3): p. 563-581.
23. Kemp, C.D. and J.V. Conte, *The pathophysiology of heart failure.* Cardiovascular Pathology, 2012. **21**(5): p. 365-371.
24. Gabriel-Costa, D., *The pathophysiology of myocardial infarction-induced heart failure.* Pathophysiology, 2018. **25**(4): p. 277-284.
25. Sutton, M.G.S.J. and N. Sharpe, *Left ventricular remodeling after myocardial infarction: pathophysiology and therapy.* Circulation, 2000. **101**(25): p. 2981-2988.
26. Jessup, M. and S. Brozena, *Heart failure.* N Engl J Med, 2003. **348**(20): p. 2007-18.
27. Yancy, C.W., et al., *2013 ACCF/AHA guideline for the management of heart failure: a report of the American College of Cardiology Foundation/American Heart Association Task Force on Practice Guidelines.* Journal of the American College of Cardiology, 2013. **62**(16): p. e147-e239.
28. Ponikowski, P., et al., *2016 ESC Guidelines for the diagnosis and treatment of acute and chronic heart failure: The Task Force for the diagnosis and treatment of acute and chronic heart failure of the European Society of Cardiology (ESC). Developed with the special contribution of the Heart Failure Association (HFA) of the ESC.* European journal of heart failure, 2016. **18**(8): p. 891-975.
29. Pearse, S.G. and M.R. Cowie, *Heart failure: classification and pathophysiology.* Medicine, 2014. **42**(10): p. 556-561.
30. Association, N.Y.H., C. Committee, and M. Dolgin, *Nomenclature and criteria for diagnosis of diseases of the heart and great vessels*. 1994: Little, Brown.
31. Benjamin, E.J., P. Muntner, and M.S. Bittencourt, *Heart disease and stroke statistics-2019 update: A report from the American Heart Association.* Circulation, 2019. **139**(10): p. e56-e528.
32. Savarese, G. and L.H. Lund, *Global Public Health Burden of Heart Failure.* Cardiac failure review, 2017. **3**(1): p. 7-11.
33. Gardner, R.S. and T.A. McDonagh, *Chronic heart failure: epidemiology, investigation and management.* Medicine, 2014. **42**(10): p. 562-567.
34. Francis, G.S., *Pathophysiology of chronic heart failure.* The American Journal of Medicine, 2001. **110**(7, Supplement 1): p. 37-46.
35. Mukherjee, S., et al., *Multimodal biomaterial strategies for regeneration of infarcted myocardium.* Journal of Materials Chemistry, 2010. **20**(40): p. 8819-8831.
36. Molina, E.J. and S.W. Boyce, *Current Status of Left Ventricular Assist Device Technology.* Seminars in Thoracic and Cardiovascular Surgery, 2013. **25**(1): p. 56-63.
37. Ensminger, S.M., et al., *Mechanical circulatory support: heart failure therapy "in motion".* Innovations, 2016. **11**(5): p. 305-314.

38. Sánchez-Enrique, C., U.P. Jorde, and J. González-Costello, *Heart Transplant and Mechanical Circulatory Support in Patients With Advanced Heart Failure.* Revista Española de Cardiología (English Edition), 2017. **70**(05): p. 371-381.
39. Slaughter, M.S., et al., *Advanced heart failure treated with continuous-flow left ventricular assist device.* New England Journal of Medicine, 2009. **361**(23): p. 2241-2251.
40. Aaronson, K.D., et al., *Use of an Intrapericardial, Continuous-Flow, Centrifugal Pump in Patients Awaiting Heart Transplantation.* Circulation, 2012. **125**(25): p. 3191-3200.
41. Pagani, F.D., et al., *Improved Mechanical Reliability of the HeartMate XVE Left Ventricular Assist System.* The Annals of Thoracic Surgery, 2006. **82**(4): p. 1413-1418.
42. Seitz, T., et al., *Berlin Heart EXCOR-System*, in *Synopsis der biologischen und mechanischen Kreislaufunterstützung*. 2003, Springer. p. 77-82.
43. Griffith, B.P., et al., *HeartMate II left ventricular assist system: from concept to first clinical use.* The Annals of thoracic surgery, 2001. **71**(3): p. S116-S120.
44. Westaby, S., et al., *First permanent implant of the Jarvik 2000 Heart.* The Lancet, 2000. **356**(9233): p. 900-903.
45. D'Alessandro, D., et al., *First reported use of the heartware HVAD in the US as bridge to transplant in an adolescent.* Pediatric transplantation, 2012. **16**(8): p. E356-E359.
46. Hetzer, R., et al., *First experiences with a novel magnetically suspended axial flow left ventricular assist device.* European Journal of cardio-thoracic surgery, 2004. **25**(6): p. 964-970.
47. Schmitto, J.D., et al., *First implantation in man of a new magnetically levitated left ventricular assist device (HeartMate III).* The Journal of Heart and Lung Transplantation, 2015. **34**(6): p. 858-860.
48. Hakami, L., S. Ensminger, and R. Feyrer, *AbioCor® IRH*, in *Synopsis der biologischen und mechanischen Kreislaufunterstützung*. 2003, Springer. p. 141-147.
49. Copeland, J.G., *SynCardia Total Artificial Heart: update and future.* Texas Heart Institute journal, 2013. **40**(5): p. 587-588.
50. Laumen, M., et al., *A novel total artificial heart for destination therapy: in-vitro and in-vivo study.* Biomedical Engineering/Biomedizinische Technik, 2013.
51. Pelletier, B., et al., *System overview of the fully implantable destination therapy—ReinHeart-total artificial heart.* European Journal of Cardio-Thoracic Surgery, 2014. **47**(1): p. 80-86.
52. Anstadt, G.L., *A new instrument for prolonged mechanical massage.* Circulation, 1965. **32**.
53. Roche, E.T., et al., *Soft robotic sleeve supports heart function.* Science Translational Medicine, 2017. **9**(373): p. eaaf3925.
54. Hord, E.C., et al., *Evaluation of the CorInnova Heart Assist Device in an Acute Heart Failure Model.* Journal of Cardiovascular Translational Research, 2019. **12**(2): p. 155-163.
55. Jagschies, L., et al., *Individualized Biventricular Epicardial Augmentation Technology in a Drug-Induced Porcine Failing Heart Model.* ASAIO journal (American Society for Artificial Internal Organs: 1992), 2017.

56. Naveed, M., et al., *Cardio-supportive devices (VRD & DCC device) and patches for advanced heart failure: A review, summary of state of the art and future directions.* Biomedicine & Pharmacotherapy, 2018. **102**: p. 41-54.
57. Han, J. and D.R. Trumble, *Cardiac Assist Devices: Early Concepts, Current Technologies, and Future Innovations.* Bioengineering, 2019. **6**(1): p. 18.
58. AdjuCor. [cited 2019 16th June]; Available from: https://www.adjucor.com/.
59. Ghiroldi, A., et al., *Cell-based therapies for cardiac regeneration: A comprehensive review of past and ongoing strategies.* International journal of molecular sciences, 2018. **19**(10): p. 3194.
60. Christman, K.L. and R.J. Lee, *Biomaterials for the treatment of myocardial infarction.* Journal of the American College of Cardiology, 2006. **48**(5): p. 907-913.
61. Rane, A.A. and K.L. Christman, *Biomaterials for the treatment of myocardial infarction: a 5-year update.* Journal of the American College of Cardiology, 2011. **58**(25): p. 2615-2629.
62. Radhakrishnan, J., U.M. Krishnan, and S. Sethuraman, *Hydrogel based injectable scaffolds for cardiac tissue regeneration.* Biotechnology advances, 2014. **32**(2): p. 449-461.
63. Hastings, C.L., et al., *Drug and cell delivery for cardiac regeneration.* Advanced Drug Delivery Reviews, 2015. **84**: p. 85-106.
64. Awada, H.K., M.P. Hwang, and Y. Wang, *Towards comprehensive cardiac repair and regeneration after myocardial infarction: aspects to consider and proteins to deliver.* Biomaterials, 2016. **82**: p. 94-112.
65. Peña, B., et al., *Injectable Hydrogels for Cardiac Tissue Engineering.* Macromolecular bioscience, 2018: p. 1800079.
66. O'Neill, H.S., et al., *Biomaterial-Enhanced Cell and Drug Delivery: Lessons Learned in the Cardiac Field and Future Perspectives.* Advanced Materials, 2016. **28**(27): p. 5648-5661.
67. Bertero, A. and C.E. Murry, *Hallmarks of cardiac regeneration.* Nature Reviews Cardiology, 2018: p. 1.
68. Doppler, S.A., et al., *Cardiac regeneration: current therapies—future concepts.* Journal of thoracic disease, 2013. **5**(5): p. 683.
69. Emmert, M.Y., *Cell-based cardiac regeneration.* European heart journal, 2017. **38**(15): p. 1095-1098.
70. Hinkel, R., T. Trenkwalder, and C. Kupatt, *Gene therapy for ischemic heart disease.* Expert opinion on biological therapy, 2011. **11**(6): p. 723-737.
71. Monaghan, M.G., et al., *Exogenous miR-29B Delivery Through a Hyaluronan-Based Injectable System Yields Functional Maintenance of the Infarcted Myocardium.* Tissue Eng Part A, 2018. **24**(1-2): p. 57-67.
72. Kwon, M.H., et al., *Ventricular restraint therapy for heart failure: A review, summary of state of the art, and future directions.* J Thorac Cardiovasc Surg, 2012. **144**(4): p. 771-777.e1.
73. Oz, M.C., et al., *Reverse remodeling of the failing ventricle: surgical intervention with the Acorn Cardiac Support Device.* Congestive Heart Failure, 2004. **10**(2): p. 96-104.
74. Oliveira, G.H., et al., *Left ventricular restoration devices.* Journal of cardiovascular translational research, 2014. **7**(3): p. 282-291.
75. Kitahara, M., et al., *Biodegradable vs Nonbiodegradable Cardiac Support Device for Treating Ischemic Cardiomyopathy in a Canine Heart.* Seminars in Thoracic and Cardiovascular Surgery, 2017. **29**(1): p. 51-61.

76. Dolan, E.B., et al., *A bioresorbable biomaterial carrier and passive stabilization device to improve heart function post-myocardial infarction.* Materials science and engineering: C, 2019. **103**: p. 109751.
77. Lee, L.C., et al., *Algisyl-LVR™ with coronary artery bypass grafting reduces left ventricular wall stress and improves function in the failing human heart.* International journal of cardiology, 2013. **168**(3): p. 2022-2028.
78. Serpooshan, V., et al., *The effect of bioengineered acellular collagen patch on cardiac remodeling and ventricular function post myocardial infarction.* Biomaterials, 2013. **34**(36): p. 9048-9055.
79. Fujimoto, K.L., et al., *An elastic, biodegradable cardiac patch induces contractile smooth muscle and improves cardiac remodeling and function in subacute myocardial infarction.* Journal of the American College of Cardiology, 2007. **49**(23): p. 2292-2300.
80. Hashizume, R., et al., *Biodegradable elastic patch plasty ameliorates left ventricular adverse remodeling after ischemia-reperfusion injury: A preclinical study of a porous polyurethane material in a porcine model.* Journal of Thoracic and Cardiovascular Surgery, 2013. **146**(2): p. 391-+.
81. Chi, N.-H., et al., *Cardiac repair using chitosan-hyaluronan/silk fibroin patches in a rat heart model with myocardial infarction.* Carbohydrate Polymers, 2013. **92**(1): p. 591-597.
82. D'Amore, A., et al., *Bi-layered polyurethane – Extracellular matrix cardiac patch improves ischemic ventricular wall remodeling in a rat model.* Biomaterials, 2016. **107**: p. 1-14.
83. Lin, X., et al., *A viscoelastic adhesive epicardial patch for treating myocardial infarction.* Nature Biomedical Engineering, 2019.
84. Hasan, A., et al., *Injectable Hydrogels for Cardiac Tissue Repair after Myocardial Infarction.* Advanced science (Weinheim, Baden-Wurttemberg, Germany), 2015. **2**(11): p. 1500122-1500122.
85. Tous, E., et al., *Injectable acellular hydrogels for cardiac repair.* Journal of cardiovascular translational research, 2011. **4**(5): p. 528-542.
86. Han, Y., et al., *Development of functional hydrogels for heart failure.* Journal of Materials Chemistry B, 2019. **7**(10): p. 1563-1580.
87. Grigore, M., *Hydrogels for cardiac tissue repair and regeneration.* J. Cardiovasc. Med. Cardiol, 2017. **4**.
88. Christman, K.L., et al., *Fibrin glue alone and skeletal myoblasts in a fibrin scaffold preserve cardiac function after myocardial infarction.* Tissue engineering, 2004. **10**(3-4): p. 403-409.
89. Russo, V., et al., *Mesenchymal stem cell delivery strategies to promote cardiac regeneration following ischemic injury.* Biomaterials, 2014. **35**(13): p. 3956-3974.
90. Martens, T.P., et al., *Percutaneous Cell Delivery Into the Heart Using Hydrogels Polymerizing In Situ.* Cell transplantation, 2009. **18**(3): p. 297-304.
91. O'Cearbhaill, E.D., K.S. Ng, and J.M. Karp. *Emerging medical devices for minimally invasive cell therapy*. in *Mayo Clinic Proceedings*. 2014. Elsevier.
92. Hafeman, A.E., et al., *Characterization of the degradation mechanisms of lysine-derived aliphatic poly(ester urethane) scaffolds.* Biomaterials, 2011. **32**(2): p. 419-29.
93. Liau, B., et al., *Pluripotent stem cell-derived cardiac tissue patch with advanced structure and function.* Biomaterials, 2011. **32**(35): p. 9180-9187.

94. Jang, J., et al., *3D printed complex tissue construct using stem cell-laden decellularized extracellular matrix bioinks for cardiac repair.* Biomaterials, 2017. **112**: p. 264-274.
95. Hou, D., et al., *Radiolabeled cell distribution after intramyocardial, intracoronary, and interstitial retrograde coronary venous delivery: implications for current clinical trials.* Circulation, 2005. **112**(9_supplement): p. I-150-I-156.
96. Roche, E.T., et al., *Comparison of biomaterial delivery vehicles for improving acute retention of stem cells in the infarcted heart.* Biomaterials, 2014. **35**(25): p. 6850-6858.
97. Ishikawa, K., et al., *Gene delivery methods in cardiac gene therapy.* The journal of gene medicine, 2011. **13**(10): p. 566-572.
98. Tilemann, L., et al., *Gene therapy for heart failure.* Circulation research, 2012. **110**(5): p. 777-793.
99. Yaniz-Galende, E. and R.J. Hajjar, *16 - Stem cell and gene therapy for cardiac regeneration*, in *Cardiac Regeneration and Repair*, R.-K. Li and R.D. Weisel, Editors. 2014, Woodhead Publishing. p. 347-379.
100. Wildhirt, S.M., et al. *Collapsible myocardial patch*. CN201811284156.1, 2018.
101. Wildhirt, S.M., et al. *Collapsible myocardial patch*. EP17198740.7, 2017.
102. Braunwald, E., *Cell-based therapy in cardiac regeneration: an overview.* Circulation research, 2018. **123**(2): p. 132-137.
103. Curley, C.J., et al., *An in vitro investigation to assess procedure parameters for injecting therapeutic hydrogels into the myocardium.* Journal of Biomedical Materials Research Part B: Applied Biomaterials, 2017. **105**(8): p. 2618-2629.
104. Dolan, E.B., et al., *A dvanced M aterial Cath eter (AMCath), a minimally invasive endocardial catheter for the delivery of fast-gelling covalently cross-linked hyaluronic acid hydrogels.* Journal of Biomaterials Applications, 2018. **33**(5): p. 681-692.
105. Burchfield, J.S., M. Xie, and J.A. Hill, *Pathological ventricular remodeling: mechanisms: part 1 of 2.* Circulation, 2013. **128**(4): p. 388-400.
106. Nelson, D.M., et al., *Intra-myocardial biomaterial injection therapy in the treatment of heart failure: Materials, outcomes and challenges.* Acta Biomater, 2011. **7**(1): p. 1-15.
107. Bouten, P.J.M., et al., *The chemistry of tissue adhesive materials.* Progress in Polymer Science, 2014. **39**(7): p. 1375-1405.
108. Rodell, C.B., et al., *Injectable Shear-Thinning Hydrogels for Minimally Invasive Delivery to Infarcted Myocardium to Limit Left-Ventricular Remodeling.* Circulation. Cardiovascular interventions, 2016. **9**(10): p. e004058.
109. Madden, L.R., et al., *Proangiogenic scaffolds as functional templates for cardiac tissue engineering.* Proceedings of the National Academy of Sciences, 2010. **107**(34): p. 15211-15216.
110. Laube, T., et al., *In situ foamable, degradable polyurethane as biomaterial for soft tissue repair.* Materials Science & Engineering C-Materials for Biological Applications, 2017. **78**: p. 163-174.
111. Gugerell, A., et al., *Electrospun poly(ester-Urethane)- and poly(ester-Urethane-Urea) fleeces as promising tissue engineering scaffolds for adipose-derived stem cells.* PLoS One, 2014. **9**(3): p. e90676.

112. Weems, A.C., et al., *Shape memory polyurethanes with oxidation-induced degradation: In vivo and in vitro correlations for endovascular material applications.* Acta biomaterialia, 2017. **59**: p. 33-44.
113. Dempsey, D.K., et al., *Comparative analysis of in vitro oxidative degradation of poly(carbonate urethanes) for biostability screening.* J Biomed Mater Res A, 2014. **102**(10): p. 3649-65.
114. Foltz, W., et al., *MRI relaxation fluctuations in acute reperfused hemorrhagic infarction.* Magnetic resonance in medicine, 2006. **56**(6): p. 1311-1319.
115. Graham, J.J., et al., *Long-term tracking of bone marrow progenitor cells following intracoronary injection post-myocardial infarction in swine using MRI.* American Journal of Physiology-Heart and Circulatory Physiology, 2010. **299**(1): p. H125-H133.
116. Lee, H.W., et al., *Effects of intracoronary administration of autologous adipose tissue-derived stem cells on acute myocardial infarction in a porcine model.* Yonsei medical journal, 2015. **56**(6): p. 1522-1529.
117. Albl, B., et al., *Tissue sampling guides for porcine biomedical models.* Toxicologic pathology, 2016. **44**(3): p. 414-420.
118. Horvath, M.A., et al., *Towards Alternative Approaches for Coupling of a Soft Robotic Sleeve to the Heart.* Annals of Biomedical Engineering, 2018.
119. Dolan, E.B., et al., *The development and mechanical characterisation of a novel reinforced venous conduit that mimics the mechanical properties of an arterial wall.* Journal of the Mechanical Behavior of Biomedical Materials, 2017. **71**: p. 23-31.
120. Coleman, R., *Picrosirius red staining revisited.* Acta Histochem, 2011. **113**(3): p. 231-3.
121. Rezakhaniha, R., et al., *Experimental investigation of collagen waviness and orientation in the arterial adventitia using confocal laser scanning microscopy.* Biomechanics and Modeling in Mechanobiology, 2012. **11**(3): p. 461-473.
122. FDA, U., *Guidance for FDA Reviewers and Sponsors. Content and Review of Chemistry, Manufacturing, and Control (CMC) Information for Human Somatic Cell Therapy Investigational New Drug Applications (INDs).* US Department of Health and Human Services, Rockville, MD, USA, 2008. **1**: p. 1-39.
123. Lee, L.S., et al., *Optimized ventricular restraint therapy: adjustable restraint is superior to standard restraint in an ovine model of ischemic cardiomyopathy.* J Thorac Cardiovasc Surg, 2013. **145**(3): p. 824-31.
124. Chitsaz, S., et al., *Material Properties of CorCap Passive Cardiac Support Device.* The Annals of thoracic surgery, 2013. **95**(1): p. 148-154.
125. Ifkovits, J.L., et al., *Injectable hydrogel properties influence infarct expansion and extent of postinfarction left ventricular remodeling in an ovine model.* Proceedings of the National Academy of Sciences, 2010. **107**(25): p. 11507-11512.
126. Gaffey, A.C., et al., *Injectable shear-thinning hydrogels used to deliver endothelial progenitor cells, enhance cell engraftment, and improve ischemic myocardium.* The Journal of Thoracic and Cardiovascular Surgery, 2015. **150**(5): p. 1268-1277.
127. Rodell, C.B., et al., *Injectable Shear-Thinning Hydrogels for Minimally Invasive Delivery to Infarcted Myocardium to Limit Left Ventricular Remodeling.* Circulation: Cardiovascular Interventions, 2016. **9**(10): p. e004058.

128. Christman, K.L., et al., *Injectable fibrin scaffold improves cell transplant survival, reduces infarct expansion, and induces neovasculature formation in ischemic myocardium.* J Am Coll Cardiol, 2004. **44**(3): p. 654-60.
129. Lee, L.C., et al., *Algisyl-LVR™ with coronary artery bypass grafting reduces left ventricular wall stress and improves function in the failing human heart.* International Journal of Cardiology, 2013. **168**(3): p. 2022-2028.
130. Mann, D.L., et al., *One-year follow-up results from AUGMENT-HF: a multicentre randomized controlled clinical trial of the efficacy of left ventricular augmentation with Algisyl in the treatment of heart failure.* European journal of heart failure, 2016. **18**(3): p. 314-325.
131. Domenech, M., et al., *Tissue Engineering Strategies for Myocardial Regeneration: Acellular Versus Cellular Scaffolds?* Tissue engineering. Part B, Reviews, 2016. **22**(6): p. 438-458.
132. Bartunek, J., et al., *Cardiopoietic stem cell therapy in heart failure: the C-CURE (Cardiopoietic stem Cell therapy in heart failURE) multicenter randomized trial with lineage-specified biologics.* Journal of the American College of Cardiology, 2013. **61**(23): p. 2329-2338.
133. Whyte, W., et al., *Sustained release of targeted cardiac therapy with a replenishable implanted epicardial reservoir.* Nature Biomedical Engineering, 2018. **2**(6): p. 416-428.
134. Zhao, X., et al., *Comparison of Non-human Primate versus Human Induced Pluripotent Stem Cell-Derived Cardiomyocytes for Treatment of Myocardial Infarction.* Stem Cell Reports, 2018. **10**(2): p. 422-435.
135. Hinderer, S. and K. Schenke-Layland, *Cardiac fibrosis – A short review of causes and therapeutic strategies.* Advanced Drug Delivery Reviews, 2019.
136. Yoshizumi, T., et al., *Timing effect of intramyocardial hydrogel injection for positively impacting left ventricular remodeling after myocardial infarction.* Biomaterials, 2016. **83**: p. 182-193.
137. Hayakawa, K., et al., *Inhibition of granulation tissue cell apoptosis during the subacute stage of myocardial infarction improves cardiac remodeling and dysfunction at the chronic stage.* Circulation, 2003. **108**(1): p. 104-109.
138. Gaetani, R., et al., *Epicardial application of cardiac progenitor cells in a 3D-printed gelatin/hyaluronic acid patch preserves cardiac function after myocardial infarction.* Biomaterials, 2015. **61**: p. 339-348.
139. Kapnisi, M., et al., *Auxetic cardiac patches with tunable mechanical and conductive properties toward treating myocardial infarction.* Advanced functional materials, 2018. **28**(21): p. 1800618.
140. Mewhort, H.E.M., et al., *Epicardial infarct repair with basic fibroblast growth factor–enhanced CorMatrix-ECM biomaterial attenuates postischemic cardiac remodeling.* The Journal of Thoracic and Cardiovascular Surgery, 2014. **147**(5): p. 1650-1659.
141. Suarez, S.L., et al., *Intramyocardial injection of hydrogel with high interstitial spread does not impact action potential propagation.* Acta biomaterialia, 2015. **26**: p. 13-22.
142. Bergmann, O., et al., *Evidence for cardiomyocyte renewal in humans.* Science (New York, N.Y.), 2009. **324**(5923): p. 98-102.
143. Ye, L., et al., *Cardiac Repair in a Porcine Model of Acute Myocardial Infarction with Human Induced Pluripotent Stem Cell-Derived Cardiovascular Cells.* Cell Stem Cell, 2014. **15**(6): p. 750-761.

144. Gao, L., et al., *Large Cardiac-Muscle Patches Engineered from Human Induced-Pluripotent Stem-Cell-Derived Cardiac Cells Improve Recovery from Myocardial Infarction in Swine.* Circulation, 2017.
145. Liu, B., et al., *Cardiac recovery via extended cell-free delivery of extracellular vesicles secreted by cardiomyocytes derived from induced pluripotent stem cells.* Nature Biomedical Engineering, 2018. **2**(5): p. 293-303.
146. Gwak, S.-J., et al., *The effect of cyclic strain on embryonic stem cell-derived cardiomyocytes.* Biomaterials, 2008. **29**(7): p. 844-856.
147. Canseco, D.C., et al., *Human ventricular unloading induces cardiomyocyte proliferation.* Journal of the American College of Cardiology, 2015. **65**(9): p. 892-900.
148. Puente, Bao N., et al., *The Oxygen-Rich Postnatal Environment Induces Cardiomyocyte Cell-Cycle Arrest through DNA Damage Response.* Cell, 2014. **157**(3): p. 565-579.
149. Wildhirt, S.M., et al. *Implantable device for precise supply and application of substances to the pericardial sac or the surface of the heart*. EP 3115023 B1, 2017.
150. Wildhirt, S.M., et al. *Implantable device for the locationally accurate delivery and administration of substances into the pericardium or onto the surface of the heart*. US 2017/0007403 A1, 2017.
151. Wildhirt, S.M., et al. *Implantierbare Vorrichtung zur ortsgenauen Zuführung und Applikation von Substanzen in das Perikard oder auf die Herzoberfläche*. EP 3348235 A1, 2018.
152. Wildhirt, S.M., et al. *Implantierbare Vorrichtung zur ortsgenauen Zuführung und Applikation von Substanzen in das Perikard oder auf die Herzoberfläche*. DE 10 2015 212 699 A1, 2017.
153. Zapotocky, V., et al., *Fabrication of biodegradable textile scaffold based on hydrophobized hyaluronic acid.* International journal of biological macromolecules, 2017. **95**: p. 903-909.
154. Abdelwahid, E., et al., *Stem cell death and survival in heart regeneration and repair.* Apoptosis : an international journal on programmed cell death, 2016. **21**(3): p. 252-268.

Declaration

I hereby declare that all the work presented in this PhD thesis is all my own original work, except where indicated by citations and references. No other sources or aids than those explicitly mentioned in the dissertation were used. All supportive contributions of third parties related to collaborative research programmes are distinctly mentioned and appropriately acknowledged. I declare that I abided by the guidelines for safeguarding good scientific practice (Richtlinien zur Sicherung guter Wissenschaftlicher Praxis) at the University of Tübingen (conclusion of Academic Senate 25th May 2000). I hereby make an affirmation in lieu of an oath (Eidesstattliche Versicherung) that all of the above-stated declarations are true and that I did not withhold or conceal anything. I am well aware that any deliberate false statement is punishable by a prison sentence up to three years or by a monetary penalty under German law.

Björn Hofmann

Forstinning, January 29th, 2020

Acknowledgements/Danksagung

The present work emerged from my activity at AdjuCor as external PhD student of the Eberhard-Karls Universität Tübingen from 2014 to 2019 in the context of the European Union's 'Seventh Framework' program AMCARE. This time has been an invaluable experience in my life broaden my professional but also my personal horizons. I have received great support and help from lots of people. Hence, I would like to take the chance to thank my supervisors, colleagues, friends and family, who accompanied me during this journey over the past years and helped me to finally make this PhD thesis possible.

First, I would like to express my sincere gratitude to my supervisors Prof. Dr. Katja Schenke-Layland and Prof. Dr. Garry Duffy for giving me the unique opportunity to complete my PhD thesis as external PhD student of the Eberhard-Karls Universität Tübingen. I would like to thank you both for all the great support, constructive discussions as well as your trust in my scientific work. I especially want to thank Katja for her offer to be my first supervisor from the beginning of my work at AdjuCor. I also want to thank Garry for initiating the AMCARE project, without the subject-matter of my work would have been not exist, and for your advice regarding the writing of the publication.

Mein besonderer aufrichtiger Dank gilt zudem Prof. Dr. Stephen Wildhirt, ohne den es das Thema für meine Arbeit ebenfalls nicht gegeben hätte. Vielen Dank für Dein entgegengebrachtes Vertrauen in die Fähigkeiten eines damals 25-jährigen Hochschulabsolventen mit der einzigartigen Möglichkeit für mich, als Teil der Firma AdjuCor GmbH an solch innovativen Fragestellungen mitarbeiten zu dürfen, ohne dessen Grundlage die Anfertigung meiner Dissertation nicht möglich gewesen wäre. Ich möchte Dir zudem herzlich für Dein stets offenes Ohr, Deine Ermutigungen, die ausführlichen Informationen zum medizinischen Hintergrund von Myokardinfarkt und Herzinsuffizienz, die für einen Ingenieur unheimlich aufschlussreichen Erkenntnisse aus dem OP sowie Deine stetige Unterstützung auch bei technischen Fragestellungen herzlich danken. Zuletzt möchte ich mich vielmals bei Dir für Deine hilfreichen Ratschläge zur Anfertigung dieser Dissertation bedanken.

Weiterhin möchte ich die Gelegenheit nutzen, mich herzlich bei Dr. Andreas Maier sowie Dr. Hamman de Vaal zu bedanken, die mir bei der Entwicklung der in dieser Arbeit beschriebenen Implantate ebenfalls stets mit Rat und Tat kompetent zur Seite gestanden haben. Ein besonderer Dank geht an Andi für das vermittelte konstruktive und mechanische Wissen während meiner Zeit bei AdjuCor sowie an Hamman für die Ratschläge zur Anfertigung der hier vorliegenden schriftlichen Arbeit. Vielen Dank Euch beiden auch für die stets spannenden außerfachlichen Diskussionen sowie die Ermutigung zur Anfertigung meiner Dissertation.

I would like to especially thank all the partners of the AMCARE project who I closely collaborated with and whose great support made the completion of this PhD thesis possible. First, I want to thank all members of Contipro and Celyad who kindly provided the hydrogel-/ patch-based materials and the stem cells, respectively. I would like to thank additionally all members of Explora Srl enrolled in the pre-clinical *in vivo* trials for carrying out the experiments and for assessing the cardiac function. Moreover, I would like to thank all collaborators at the Fraunhofer Institute for Interfacial Engineering and Biotechnology IGB, who kindly carried out the cytotoxicity assays. I also would like to acknowledge the facilities, scientific, and technical assistance of the Centre for Microscopy & Imaging at the National University of Ireland Galway for their help regarding the histological and immunohistochemical analyses as well as SEM analysis of SPREADS' PEU fleece. Finally, I would like to thank INNOVENT e.V. for the manufacturing of SPREADS' PEUU foam and PEU fleece.

I also would like to use this opportunity to express my sincere gratitude to certain collaborators of the AMCARE project. In no particular order:

- Dr. Eimear Dolan for the valuable discussions, her great support and useful advices regarding writing of the paper, for her help to gather all needed data for this PhD thesis.
- Dr. Michael Monaghan and Robert Greensmith for their help with the birefringence analysis.
- David Monaghan and Ruth Levey for the evaluation of the histological samples.
- Lenka Kovářová for her help to gather all data regarding kindly carried out hydrogel characterisations.

- Dr. Svenja Hinderer für die zahlreichen Diskussionen im Rahmen des AMCARE-Projektes sowie weiterer Kooperationsprojekte zwischen AdjuCor und der EKUT. Zudem möchte ich Svenja herzlich für ihre Ratschläge zur Anfertigung meiner Dissertation danken.

Des Weiteren möchte ich all meinen ehemaligen und aktuellen Kollegen bei AdjuCor herzlich danken. Vielen Dank für die angenehme Arbeitsatmosphäre sowie die Bereitschaft zur Übernahme meiner Aufgaben während meiner Schreibzeit, die sehr zum Gelingen meiner Arbeit beigetragen haben. Ein besonderer Dank gilt an Felix Steinbacher für die Ratschläge beim Verfassen dieser Arbeit. Auch meinen Studenten danke ich für ihre geleistete Arbeit, mit der sie durch ihre Studien- oder Abschlussarbeiten ebenso zum Erfolg meiner Arbeit beigetragen haben.

Ebenso möchte ich mich bei all meinen Freuden und meiner Familie bedanken, die mir während meiner Promotionszeit stets mit Rat und Tat zur Seite gestanden haben. Vielen Dank an Claudia Drescher und Dr. Marc Hirschvogel für die Vermittlung zu AdjuCor sowie für eure fachlichen als auch persönlichen Ratschläge zu meiner Promotion. Meiner Familie verdanke ich es, studiert haben zu können und somit überhaupt die Möglichkeit zu haben, meine Dissertation anfertigen zu können. Vielen Dank für all eure Unterstützung. Zuletzt möchte ich mich herzlichst bei meiner liebevollen Ehefrau Aline Hofmann bedanken, die mir seit mehr als 12 Jahren in jeder Situation helfend zur Seite steht. Ihre Geduld, Verständnis, Unterstützung und steter Glaube an meine Fähigkeit waren essenziell, um diese Arbeit erfolgreich fertigstellen zu können.

Curriculum Vitae

Personal information

Name	Björn Hofmann
Address	St.-Josef-Str. 14, 85661 Forstinning
Date/Place of birth	05.03.1989 in Gotha
Nationality	German
e-Mail	bjoern-hofmann@hotmail.de

Work and research experience

05/2014 – Present	AdjuCor GmbH, Munich Senior Research Engineer, R&D
10/2013 – 04/2014	TU München, Garching Master's Thesis Title: Metabolic analysis of *Escherichia coli* producing L-phenylalanine
04/2013 – 08/2013	Technical University of Denmark (DTU), Copenhagen Research internship Title: Mechanistic Modelling of Reaction Kinetics for liquid Lipase-mediated (trans-)esterification in Bio-diesel Production
06/2011 – 09/2011	TU München, Garching Bachelor's Thesis Title: Synthesis and Characterization of Metal-Oxide supported Platinum-Catalysts
03/2011 – 06/2012	TU München, Garching Research Assistant, Dept. of Chemistry

Education

10/2017 – 06/2020	Eberhard-Karls Universität Tübingen, Tübingen Ph.D. Candidate in Biology
10/2011 – 04/2014	TU München, Garching M.Sc. in Industrial Biotechnology, Munich School of Engineering
10/2008 – 09/2011	TU München, Garching B.Sc. in Chemical Engineering, Dept. of Chemistry
09/1999 – 06/2007	Staatliches Gymnasium Ernestinum, Gotha

Publications

1. Eimear B. Dolan* and **Björn Hofmann***, M. Hamman de Vaal, Gabriella Bellavia, Stefania Straino, Lenka Kovarova, …, Katja Schenke-Layland, Peter Dockery, Bruce P. Murphy, Helena M. Kelly, Stephen Wildhirt, Garry P. Duffy. *A bioresorbable biomaterial carrier and passive stabilization device to improve heart function post-myocardial infarction.* Materials science and engineering: C, 2019. **103**: p. 109751. **(Accepted 14th May 2019)**

   *both authors contributed equally to this work and are co-first authors

2. Jason Price, **Björn Hofmann**, Vanessa T. L. Silva, Mathias Nordblad, John M. Woodley, Jakob K. Huusom. *Mechanistic modeling of Biodiesel production using a liquid lipase Formulation.* Biotechnology progress, 2014. **30**(6): p. 1277-1290.

7 Appendices

7.1 Appendix I – Supplementary information regarding Section 3

7.1.1 Technical drawings of PTFE moulds employed for preparation of the outer SPREADS layer

The following Figure 7.1 to Figure 7.4 show the technical drawings of the PTFE moulds employed to manufacture the respective outer PEUU foam layer to the corresponding design generation of SPREADS. Each mould consists of an upper and lower part.

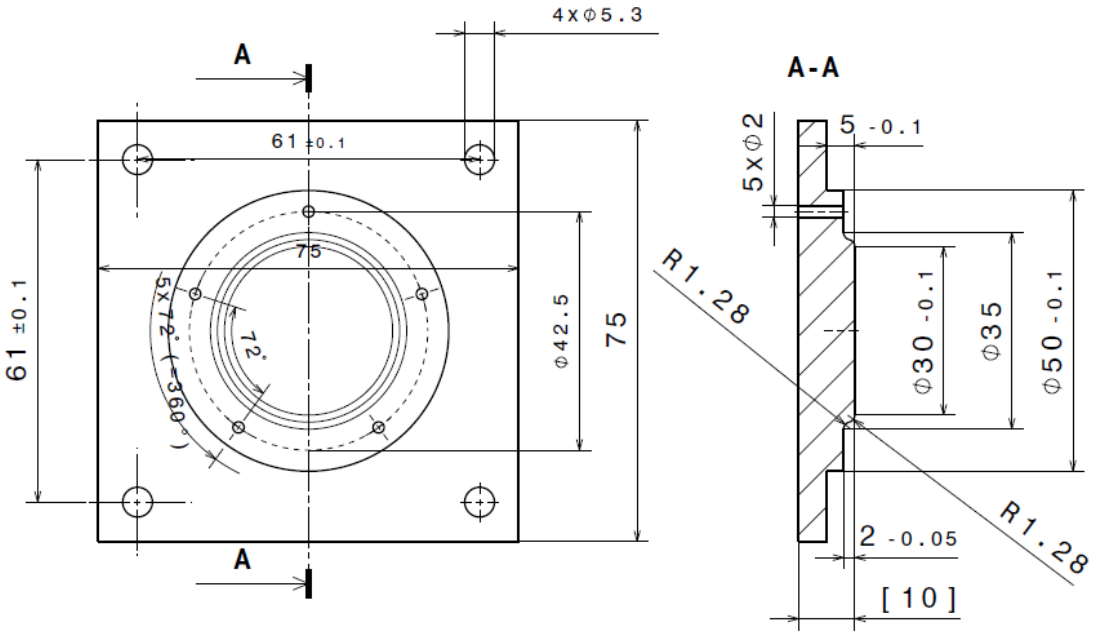

Figure 7.1: Essential production dimensions and tolerances according to DIN ISO 2768-1m of the upper casting mould employed to manufacture the outer PEUU foam layer belonging to SPREADS design generation 1.

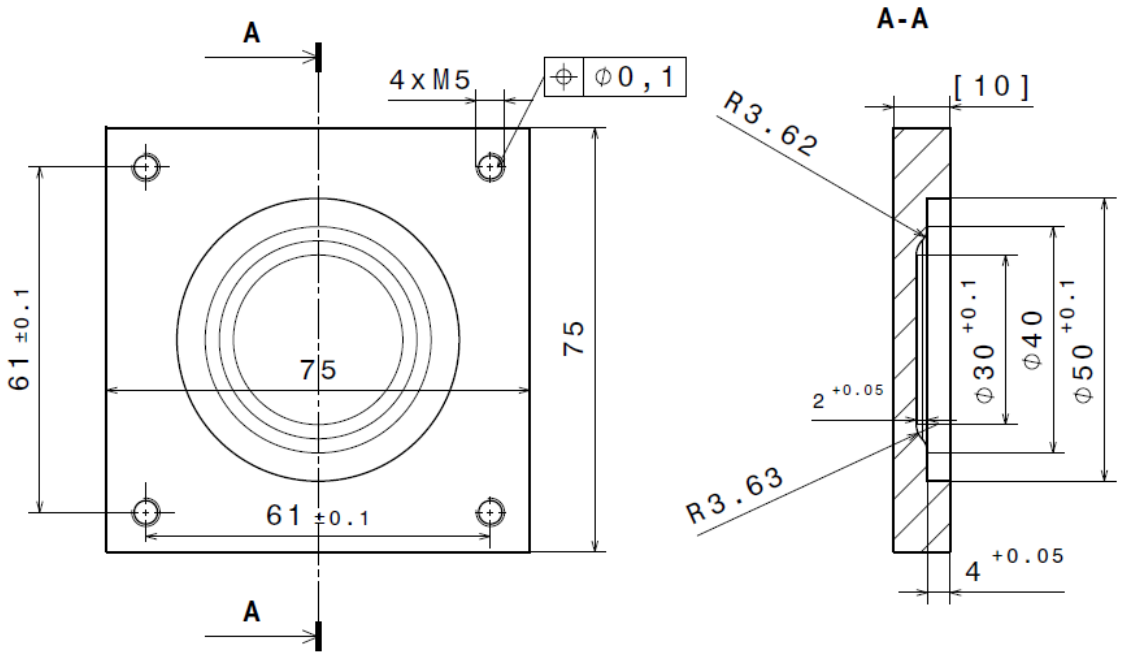

Figure 7.2: Essential production dimensions and tolerances according to DIN ISO 2768-1m of the lower casting mould employed to manufacture the outer PEUU foam layer belonging to SPREADS design generation 1.

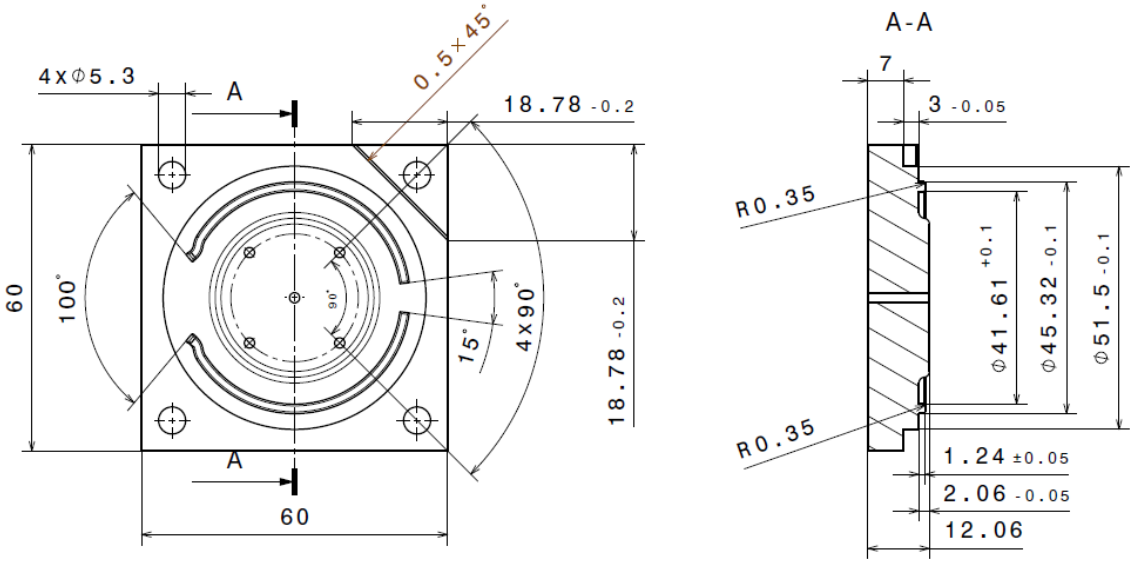

Figure 7.3: Essential production dimensions and tolerances according to DIN ISO 2768-1m of the upper casting mould employed to manufacture the outer PEUU foam layer belonging to SPREADS design generation 2.

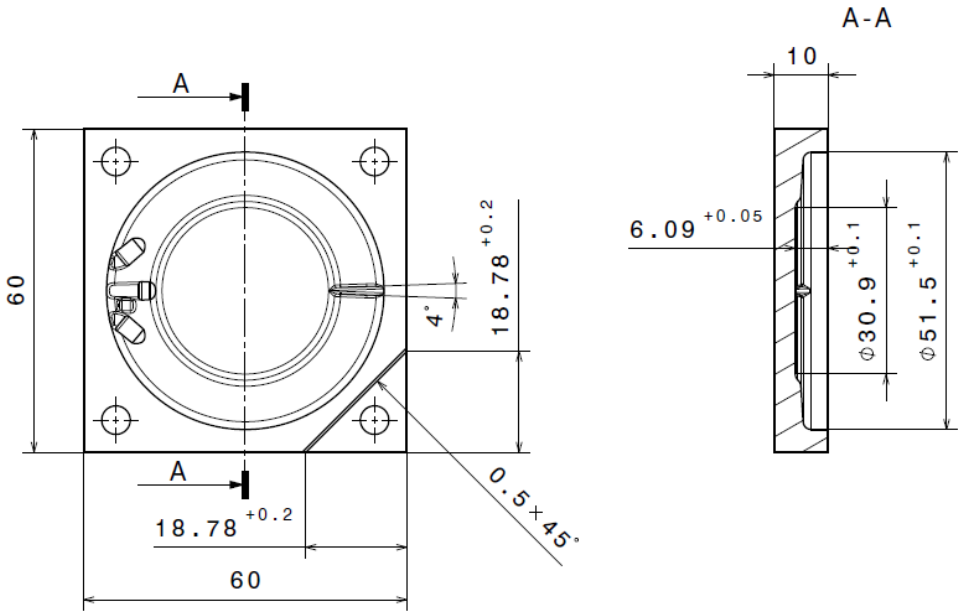

Figure 7.4: Essential production dimensions and tolerances according to DIN ISO 2768-1m of the lower casting mould employed to manufacture the outer PEUU foam layer belonging to SPREADS design generation 2.

7.1.2 Technical drawings of aids employed for thermal joining of both layers and defined perforation of the PEU fleece

The following Figure 7.5 to Figure 7.7 show the technical drawings of the respective aids employed to thermally join both layers of SPREADS' second design generation.

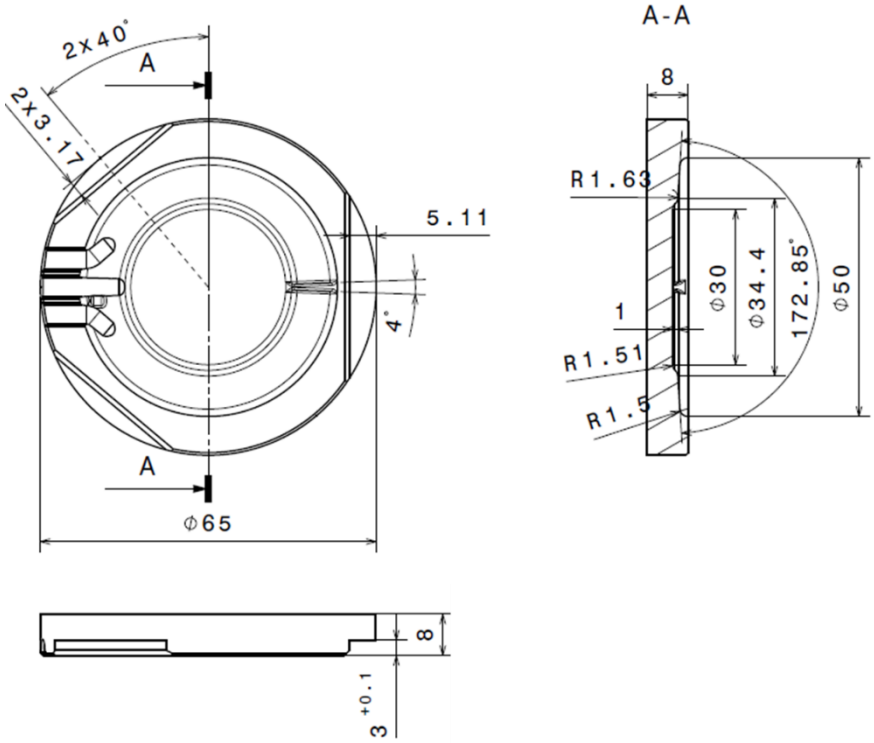

Figure 7.5: Essential production dimensions and tolerances according to DIN ISO 2768-1m of the positioning mould employed in case of SPREADS design generation 2 to arrange both layers for thermal joining.

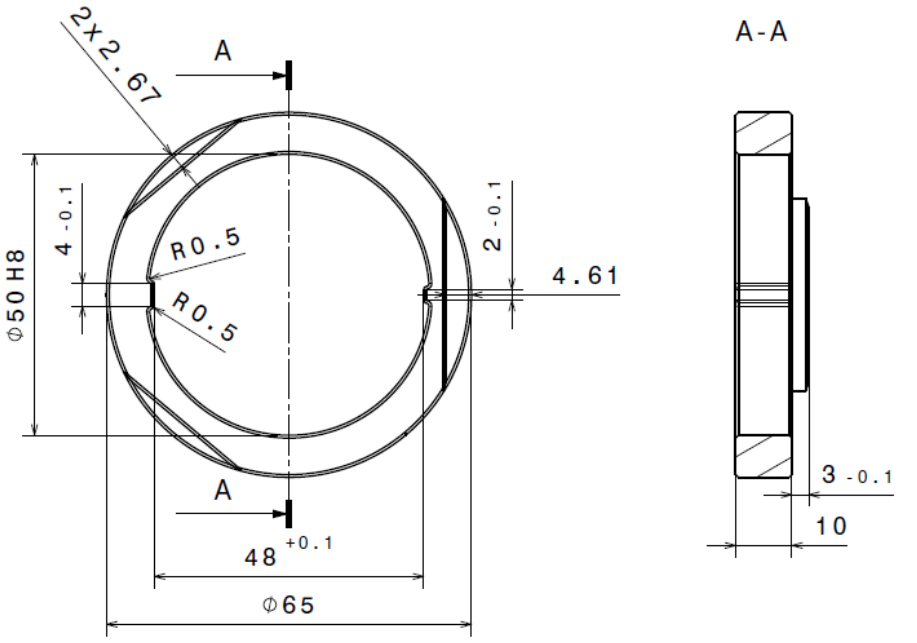

Figure 7.6: Essential production dimensions and tolerances according to DIN ISO 2768-1m of the aid employed in case of SPREADS design generation 2 to guide the respective stamp for thermal joining.

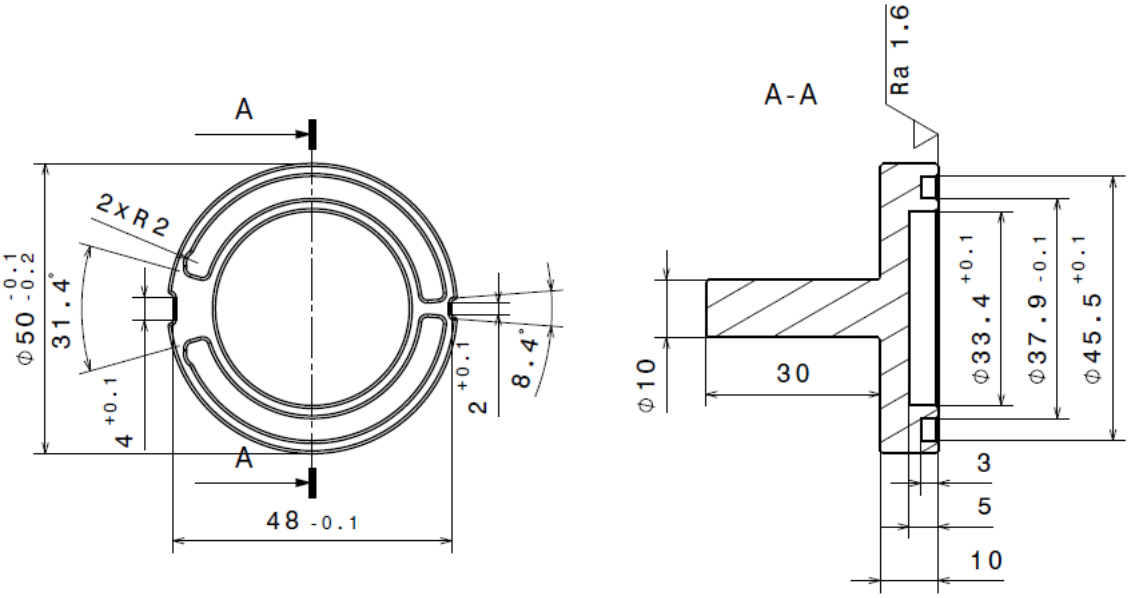

Figure 7.7: Essential production dimensions and tolerances according to DIN ISO 2768-1m of the respective stamps employed in case of SPREADS design generation 2 to thermally join the PEUU foam and PEU fleece in well-defined regions.

The following Figure 7.8 shows the plate employed as aid to perforate the PEU fleece along each circumferential bioadhesive reservoir.

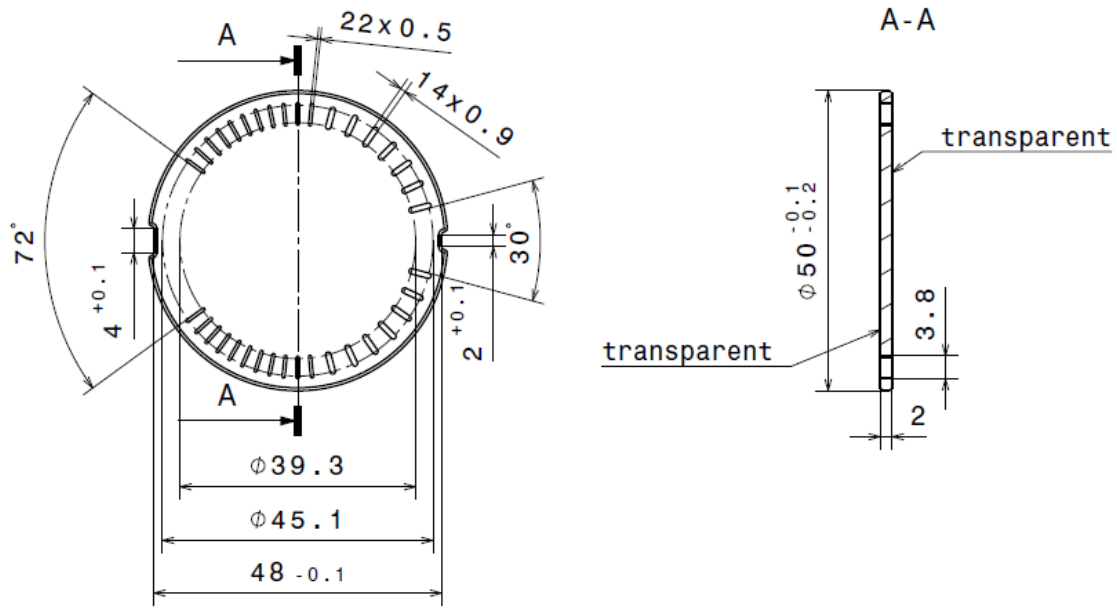

Figure 7.8: Essential production dimensions and tolerances according to DIN ISO 2768-1m of the transparent PMMA plate employed in case of SPREADS design generation 2 to facilitate defined perforation of the PEU fleece along both circumferential bioadhesive reservoirs.

7.1.3 Viscosity dependence on shear rate

The following Figure 7.9 shows the dependence of the viscosity on the shear rate for an acellular 2 % HA-PH-RGD hydrogel (60-90 kDa) at crosslinking concentration 1 (see Table 3.1).

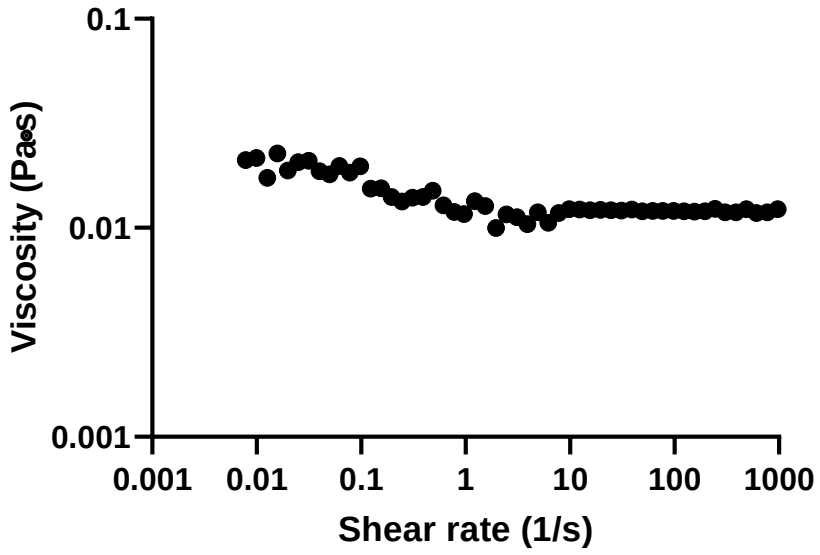

Figure 7.9: Dependence of the viscosity on the shear rate in case of an acellular 2 % HA-PH-RGD hydrogel (60-90 kDa) at crosslinking concentration 1 (see Table 3.1). Adapted from Dolan *et al.* [76] with permission from Elsevier.

7.1.4 *In vivo* pre-clinical assessment of SPREADS

The following Figure 7.10 shows exemplary angiographic pictures during and after induction of acute MI carried out at Explora Biotech Srl (Italy).

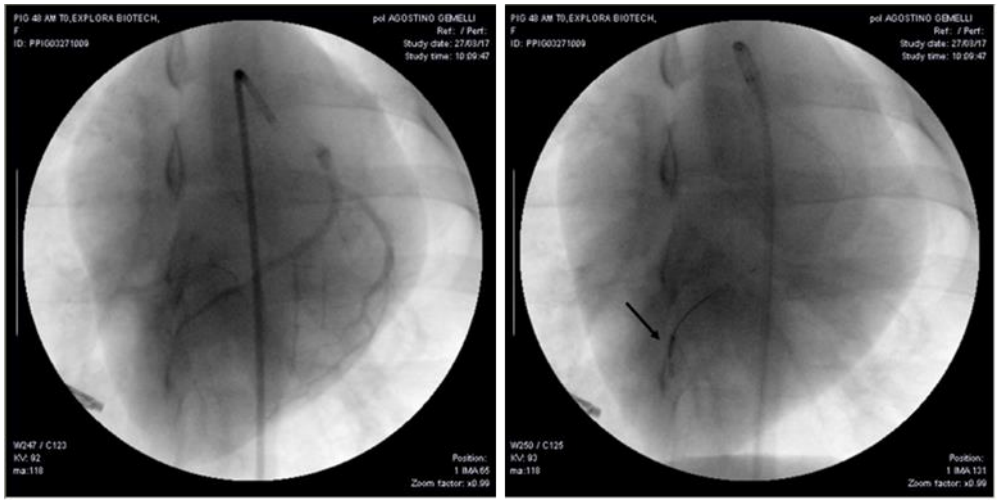

Figure 7.10: Angiograms of LAD catheterisation (left) and balloon placement (right). The balloon inflation is indicated by an arrow. Reprinted from Dolan *et al.* [76] with permission from Elsevier.

The following Figure 7.11 shows an exemplary echocardiographic image employed for determination of LVEF.

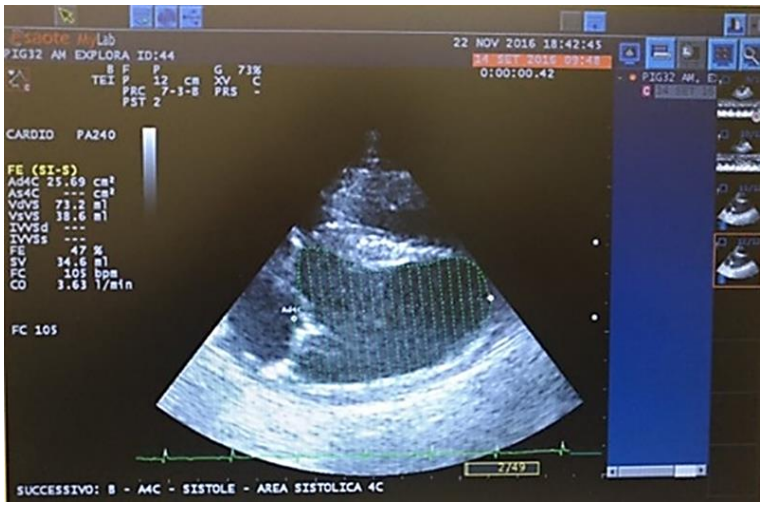

Figure 7.11: Exemplary image obtained from echocardiography showing representatively LVEF determination in the parasternal long axis view. Reprinted from Dolan *et al.* [76] with permission from Elsevier.

The following image sequence in Figure 7.12 shows representative ECG traces of all leads to confirm myocardial injury.

Figure 7.12: Exemplary ECG recordings of all leads at the day of inducing acute MI showing the ECG (A) before, (B) 20 minutes after LAD occlusion and (C) 20 minutes after reperfusion. The ST-elevation in the V-lead is indicated by a red arrow. Reprinted from Dolan *et al.* [76] with permission from Elsevier.

The following Figure 7.13 shows the vital signs during the implantation procedure of SPREADS at D14.

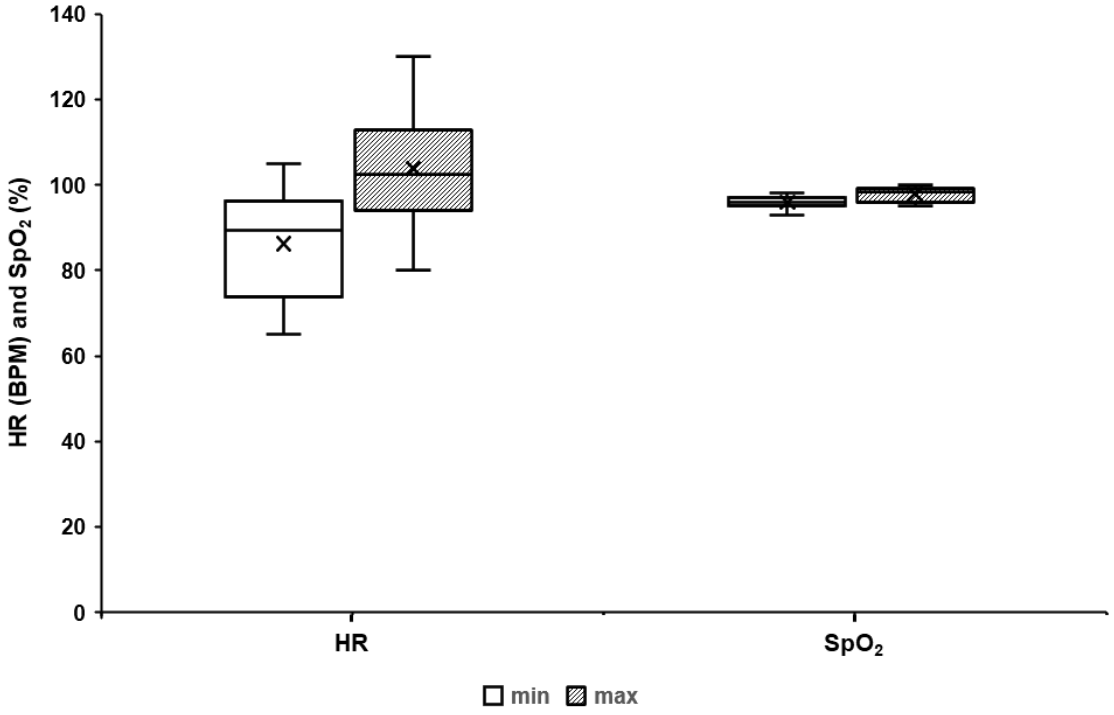

Figure 7.13: Vital signs during the implantation procedure at D14 showing the respective upper and lower limits of heart rate (HR) and oxygen saturation, respectively. Reprinted from Dolan *et al.* [76] with permission from Elsevier.

The following Figure 7.14. shows the growth curve of animals enrolled in the pre-clinical efficacy study of SPREADS.

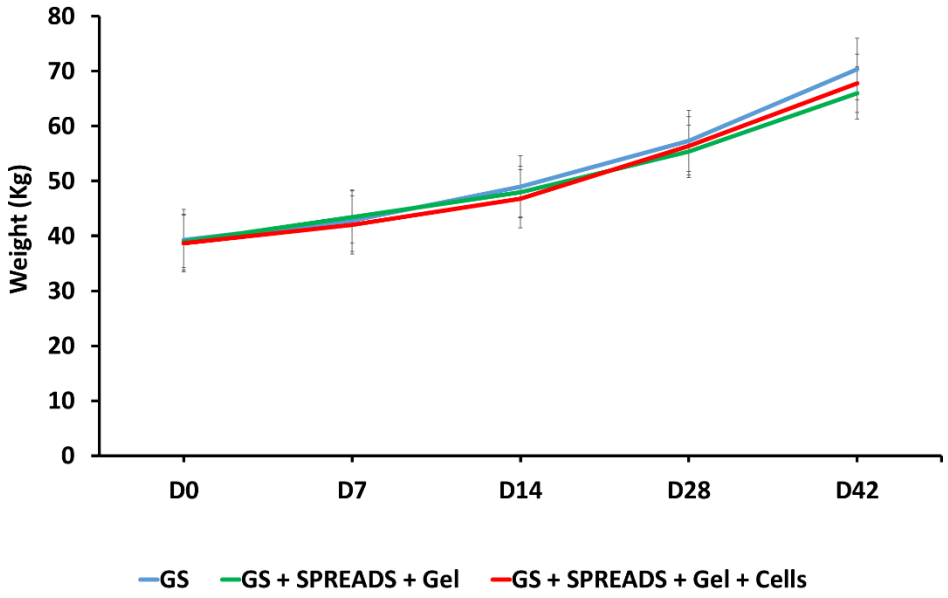

Figure 7.14: Growth curves of pigs enrolled in treatment groups I – III, respectively, to assess pre-clinical efficacy of SPREADS + HA-PH-RGD hydrogel with/without c-ADSCs. Reprinted from Dolan *et al.* [76] with permission from Elsevier.

The following Figure 7.15 shows both surfaces of SPREADS 28 days after implantation.

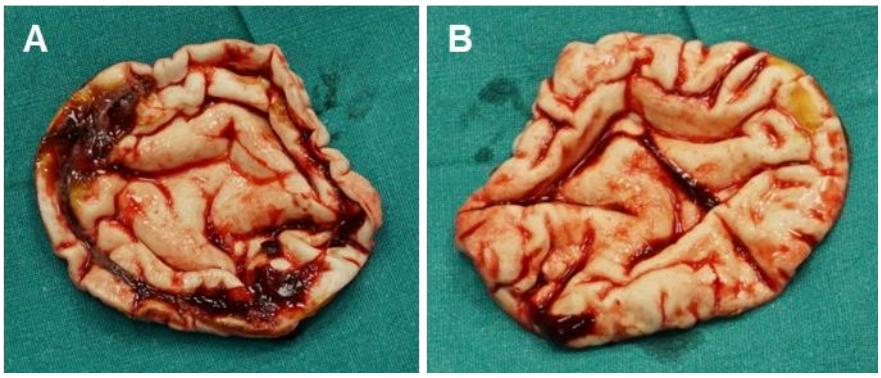

Figure 7.15: View to the epicardium (A) and pericardium (B) facing surfaces of SPREADS after 28 days *in vivo*. Reprinted from Dolan *et al.* [76] with permission from Elsevier.

7.2 Appendix II – Supplementary information regarding Section 4

The following Figure 7.16 shows the technical drawings of a tube with angled abutting face employed for minimal-invasive implantation of EpiPAD crimped to a diameter of 20 mm. The tube was manufactured from a polyamide (PA-6) round bar.

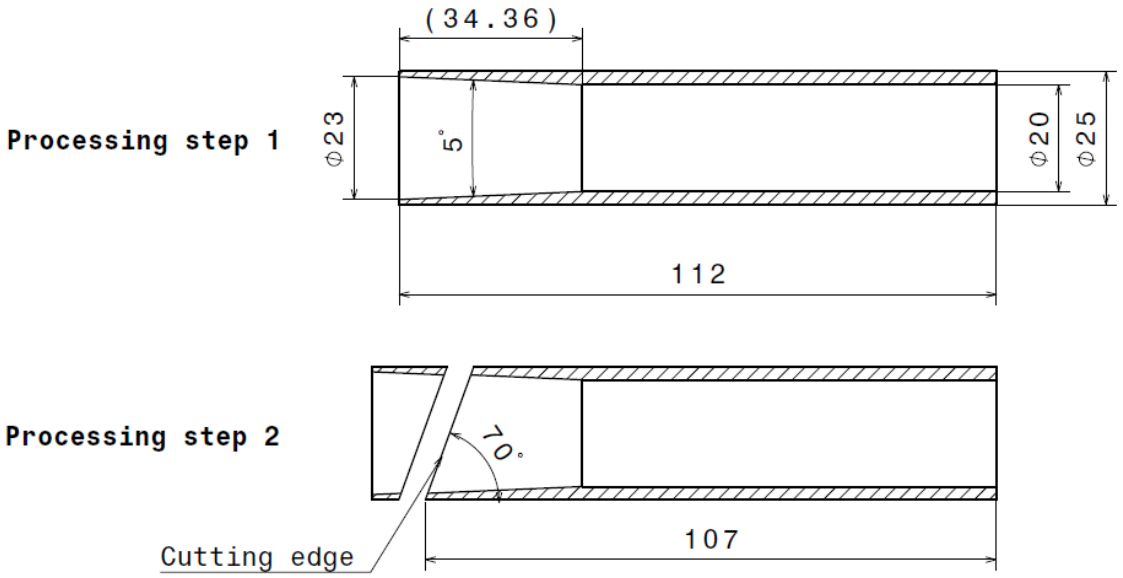

Figure 7.16: Essential production dimensions and tolerances according to DIN ISO 2768-1m of the tube with angled abutting face employed for minimal-invasive implantation of EpiPAD crimped to a diameter of 20 mm.

The following Table 7.1 lists the vital signs that were controlled during the entire implantation procedure of EpiPAD in an acute porcine *in vivo* trial.

Table 7.1: Vital signs before, during and after the implantation procedure of EpiPAD, respectively.

Vital parameter	Pre-implantation procedure	During implantation procedure	Post-implantation procedure
Systolic/diastolic BP [mmHG]	118/83	98/74	114/74
O_2 saturation [%]	99	99	99
Heart rate [min^{-1}]	67	54	57